RICE UNIVERSITY

Graphite Oxide: Structure, Reduction and Applications

by

Wei GAO

A THESIS SUBMITTED
IN PARTIAL FULFILLMENT OF THE
REQUIREMENTS FOR THE DEGREE

Doctor of Philosophy

APPROVED, THESIS COMMITTEE

Pulickel M. Ajayan, Chair
Benjamin M. and Mary Greenwood Anderson Professor, Mechanical Engineering and Material Science & Chemistry

R. Bruce Weisman
Professor of Chemistry

Enrique V. Barrera
Professor of Mechanical Engineering and Material Science

HOUSTON, TEXAS
March 2012

ABSTRACT

Graphite Oxide: Structure, Reduction and Applications

by

Wei GAO

This thesis proposes a modified structure model for graphite oxide (GO), an important precursor in graphene chemistry, develops a new strategy to convert GO back to graphene-like structure, and demonstrates its possible applications in both water purification and supercapacitor technologies. GO, a nontraditional compound first obtained from graphite oxidation over 150 years ago, is now becoming an important player in the production of graphene-based materials, which has high technological relevance. GO structure and reduction have been vigorously investigated, but its precise chemical structure still remains obscure, and the complete restoration of the sp^2 carbon lattice has not yet been achieved. In our work, solid state ^{13}C NMR (MAS) analysis offered a piece of evidence for five or six-membered ring lactol structure existing in GO that had never been assigned before, leading to a modified Lerf-Klinowski model for GO. A three-step reduction strategy, involving sodium borohydride ($NaBH_4$), sulfuric acid, and high temperature thermal annealing, described in the thesis, successfully reduced GO back to chemically converted graphene (CCG) with the lowest heteroatom abundance among all those previously reported. In addition to the chemical significance of graphene/CCG production, GO and its derivatives were used as novel adsorbents in water

purification. GO-coated sand showed higher retention than ordinary sand for both Rhodamine B and mercuric ion (Hg^{2+}) contaminants in water. Further functionalization of GO with thiophenol resulted in better adsorption capacity toward Hg^{2+} than that of activated carbon. In addition, free-standing films of GO were treated and reduced with a CO_2 laser beam into different conductive reduced GO (RGO) patterns, and directly used as supercapacitor devices which showed good cyclic stability and energy storage capacities comparable to that of existing thin film ultracapacitors. GO turned out to be a solid electrolyte with anisotropic proton conductivity similar to Nafion, while the large amount of trapped water in GO played an important role.

Acknowledgments

Here I express my sincere gratitude to my PhD advisor, Professor Pulickel M. Ajayan, for his visionary guidance, insightful advices and genuine supports in my PhD program, without which this thesis would not have been accomplished to its least content. Additionally I appreciate the funding support from IFC and Nano holdings. I would also like to thank our lab manager Dr Robert Vajtai, senior research scientist Dr. Lawrence Alemany, senior postdoctoral researcher Dr Lijie Ci, Dr Mainak, Majumder, Dr Li Song, Dr Zheng Liu, Dr Aditya Mohite, and Dr T N Narayanan, our collaborator Professor Bingqing Wei, and Dr Bipin Kumar Gupta, close labmates Dr Brent Cary, Neelam Singh, Charudatta Galande, Akshay Mathkar, Dr Yongjie Li, Dr Changru Rong, Dr Changyu Tang, Dr Hui GAO, Juan Peng and Guanhui GAO, SEA research scientist Dr Wenhua Guo, Dr Bo Chen and Dr Angelo Francis Benedetto, and Dr. Liang Gang, all of whom have been always so supportive, helpful and collaborative to the research work demonstrated here. In addition, I really appreciate the kindness, care and joyful experience offered by OISS officers including Adria Baker, Cory Owen and Agnes Vajtai, which made my life in Rice interesting and colorful. Finally, I would like to thank my parents and sisters for their consistent supporting of my oversea studies at Rice, and all those lovely close friends that I have made here in Houston, including Chanjuan Sun, Qiong Wu, just to name a few. Thanks for all their generous supports whenever and wherever I needed. I feel so blessed to meet all of them in my first five years exploration in American.

Contents

List of Figures

List of Tables

List of Schemes

Nomenclature

GO	Graphite Oxide or Graphene Oxide
RGO	Reduced Graphite Oxide or Reduce Graphene Oxide
CCG	Chemically Converted Graphene
CMG	Chemically Modified Graphene
gm	gram
FTIR	Fourier-Transformed Infra-Red
SAED	Small Angle Electron Diffraction
XRD	X-ray Diffraction
XPS	X-ray Photoelectron Spectroscopy
SEM	Scanning Electron Microscopy
TEM	Transmission Electron Microscopy
HOMO	Highest Occupied Molecular Orbital
LUMO	Lowest Unoccupied Molecular Orbital
H-bond	hydrogen bonding
DI water	deionized water

Chapter 1 **An Overview of Graphite Oxide**

This chapter introduces a peculiar carbon compound previously named as graphitic acid, graphite oxide (GO), or more recently, graphene oxide (GO). It is basically a wrinkled two-dimensional carbon sheet with various oxygenated functional groups on its basal plane and peripheries, with the thickness around 1 nm and lateral dimensions varying between a few nanometers and several microns. It was first prepared by the British chemist B. C. Brodie in 1859, and became very popular in the scientific community during the last half decade, simply because it was believed to be an important precursor to graphene (a single atomic layer of graphite, the discovery of which won Andre Geim and Konstantin Novoselov the 2010 Nobel Prize in Physics). Several strategies have been introduced to reduce GO back to graphene; however, in this chapter we will mainly focus on GO itself, and more relevantly, its synthesis, chemical structure, physical and chemical properties, and possible applications. We would like to emphasize here, despite its strong relevance to graphene, GO itself also has its own scientific significance as a basic form of oxidized carbon and technological importance as a platform for all kinds of derivatives and composites, which have already demonstrated various interesting applications.

Two-dimensional nanomaterials typically refer to flat or slightly corrugated sheets with nanometer thicknesses and extended lateral dimensions, such as graphene, single layer boron nitride (BN), molybdenum disulfide (MoS_2) and so on. The quantum confinement on the thickness direction results in exotic electronic properties and highlighted surface effects that can be useful in sensing, catalysis and energy storage applications.[1] They have attracted tremendous attention recently, since they are one of the major categories in nanoscience that were predicted thermodynamically unstable in the free state and have not been well explored. In 2005, Professor Andre Geim's group first reported the experimentally observed room temperature quantum hall effect on a real piece of graphene, which was obtained by mechanical exfoliation of Highly Oriented Pyrolytic Graphite (HOPG)[2, 3], and soon after that, a storm of graphene research dominated the world of carbon nanomaterial science. The term graphene has then become a new super star after carbon nanotube (CNT) in the carbon world. One of the biggest challenges in graphene research by then was the large scale production of graphene, since the first method Geim's group adapted was both time consuming and extremely low in yield. Different strategies have been introduced, including metal ion intercalation[4], liquid phase exfoliation of graphite[1, 5], Chemical Vapor Deposition (CVD) growth[6], vacuum graphitization of silicon carbide (SiC)[7], bottom up organic synthesis of large polycyclic aromatic hydrocarbons(PAHs)[8-10], and of course, chemical reduction of GO[11, 12]. Each strategy has its own advantages and disadvantages; nevertheless, GO was believed to be one of the most

promising pathways to graphene, mainly due to its wet chemical processability and large scale availability to monolayers.

GO is not a naturally occurring compound; the history of GO research can be dated back to over one hundred and fifty years ago. When it was first made by chemical treatments of graphite with potassium chlorate ($KClO_3$) and fuming nitric acid (HNO_3), British chemist Brodie named it graphitic acid or graphite oxide[13], and after graphene research emerged in 2004, people started calling it graphene oxide. From the chemistry point of view, there is barely any difference between the two. If there has to be, we would refer to a single atomic layer of graphite oxide as graphene oxide. Since most of the experiments on GO were done in wet chemical processes, and people are generally dealing with large amount of GO flakes in solution, we believe that when GO is dispersed in certain solvents, it is at least partially exfoliated by the solvent molecules, and thus can be referred to as graphene oxide. Otherwise, in solid state, GO powder or GO film is basically graphite oxide. In the following content, we will generally abbreviate both graphite oxide and graphene oxide as GO, since there is really no big difference between them, even in the context of electronic structures and properties (the case is different for graphite and graphene).

In terms of chemistry, GO is a new type of non-stoichiometric macromolecule that is chemically labile and hygroscopic in ambient condition. However, the synthesis of GO has evolved and been modified several times with different chemicals such as potassium permanganate, concentrated sulfuric acid[14] and

even phosphoric acid[15]; the resulted compounds differ a little bit in their chemical compositions depending on the protocols used.

Over the past 150 years, research in GO has been quite limited. Without recent popularity of graphene, researcher would still be confused about its detailed chemical structure. In the past few years, extensive research has been done to elucidate its chemical composition[16, 17], which turns out to be a corrugated carbon sheet with over half of the carbon atoms functionalized with hydroxyl and epoxy groups, and edges partially occupied by hydroxyl, carboxyl, ketone, ester and even lactol structures. Even with those clarifications, the distribution of these groups and the spatial connectivity is still obscure today. The chemical reduction of GO to graphene is one of the hottest topics in GO research, and the most commonly accepted reagent is hydrazine, as firstly introduced by Professor Rodney Ruoff in UT Austin[12]. Pristine GO is an electrical insulator, and after reduction, it becomes electrically conductive. Several orders of magnitude increase in conductivity are usually observed during reduction processes; however, so far all the graphene materials derived from GO are much poorer in crystallinity[18] and carrier mobility than their mechanically cleaved counterpart[2, 3]. Thus researchers would rather name them Reduced GO (RGO), Chemically Modified Graphene (CMG) or Chemically Converted Graphene (CCG). For convenience, we will stick to the term RGO for these materials in the following discussions. The harsh chemical oxidation environment in GO synthesis actually creates lots of defects and vacancies within the sp^2 carbon lattice, which are almost impossible to recover by subsequent chemical treatments.[18, 19] On this aspect, GO researchers have switched their interests

toward GO and RGO applications. Despite its poor crystallinity, GO, RGOs and their derivatives have shown several promising applications in energy storage, sensing, water purification, electronics, and so on. We would like to enunciate that in literature, some researchers tend to ignore the differences between RGO and high quality graphene, and announce their results as graphene properties and applications, while we think it is necessary to put GO and RGOs into different categories and summarize RGO results into a separated topic isolated from graphene research.

1.1. Synthesis

In this section we introduce four different recipes for GO preparation in the chronological order, and discuss and compare their chemical processes and product structures in detail. The recipes include 1.1.1 Brodie Method and Staudenmaier Method, 1.1.2 Hummers Method and Its Modification 1.1.3 Tour Method and Discussions.

1.1.1. Brodie Method and Staudenmaier Method

B.C. Brodie, a British chemist in nineteenth century, prepared the first batch of GO when he was investigating the chemistry of graphite in 1859. [13] When he added $KClO_3$ into slurry of graphite in fuming HNO_3, he got a new batch of compound which later on was determined to contain carbon, oxygen and hydrogen. He washed the batch free from the salts produced in the reaction, dried it at 100 °C and again put it under oxidation environment. The batch product underwent an appearance change in the following three repeated treatments, and finally resulted in a substance with a "light yellow color" which would not change with any additional oxidation treatment. He emphasized that the product could not be produced by one prolonged treatment, and one had to promote the oxidation process with the restoration of the original conditions each time.

According to his elemental analysis, the molecular formula for the final product was $C_{11}H_4O_5$. Weak acidity and mild dispersibility in basic solution was

observed, however, the reflective goniometry characterization failed due to the small size, limited thickness and imperfect structure. He also reacted the final product with “protochloride of copper and protochloride of tin” to get GO salts, and followed up with detailed analysis in composition and thermal decomposition. Nonetheless, his observations and conclusions were limited by the theories and characterization techniques by then, which left us a huge space to work and improve today.

One of the earliest improvements on Brodie’s work happened in 1898 by L. Staudenmaier[20, 21]. Two major changes were introduced: 1) adding concentrated sulfuric acid to increase the acidity of the mixture; 2) adding multiple aliquots of potassium chlorate solution into the reaction mixture over the course of reaction. These changes led to a highly oxidized GO product (composition same as the final product that Brodie got) in a single reaction vessel, thus largely simplified GO synthesis process.

However, Staudenmaier’s method was both time consuming and hazardous: the addition of potassium chlorate typically lasted over a week, and the chlorine dioxide evolved needed to be removed by an inert gas, while explosion was a constant hazard. Therefore, further modification or development of this oxidation process was still worth investigation.

1.1.2. Hummers Method and Its Modifications

Almost 60 years after Staudenmaier's strategy, chemists Hummers and Offeman in Mellon Institution of Industrial Research developed a different recipe for making GO.[14] A water-free mixture of concentrated sulfuric acid, sodium nitrate and potassium permanganate was prepared and maintained below 45 °C for graphite oxidation. According to their description, the whole oxidation process finished within two hours, and led to a final product with higher degree of oxidation than Staudenmaier's product (Table 1.1).

Table 1.1 Comparison of Staudenmaier GO and Hummers GO in chemical compositions (adapted from ref. [14]).

Method	Carbon (wt %)	Oxygen (wt %)	Water (wt %)	Ash (wt %)	C/O atomic ratio
Acid-permanganate-nitrate	47.06	27.92	22.99	1.98	2.25
Staudenmaier	52.11	23.99	22.22	1.90	2.89

However, people found that Hummers' product usually has an incompletely oxidized graphite core with GO shells, and a pre-expansion process is helpful to achieve higher degree of oxidation. First introduced by Kovtyukhova in 1999[22], a pretreatment of graphite with an 80 °C mixture of concentrated H_2SO_4, $K_2S_2O_8$, and

P_2O_5 for several hours was widely adopted afterwards. The pretreated mixture was diluted, filtered, washed and dried before the real Hummers oxidation step took place. Other reported modifications also include the increase of the potassium permanganate amount, etc.[11] Nowadays, this modified Hummers method is the most common recipe for GO preparation (as described in Figure 1.1). A typical GO product in this method consists of thin flakes of GO with 1 nm thickness (which corresponds to a single layer), and around 1 micron in lateral dimensions by average; meanwhile the chemical composition was determined to be C:O:H = 4:2.95:2.5.[22] The oxidation degree and yield of GO have been extensively improved when compared with the very first product by Brodie. However, the separation and purification processes in the modified Hummers method are still quite tedious and time consuming.

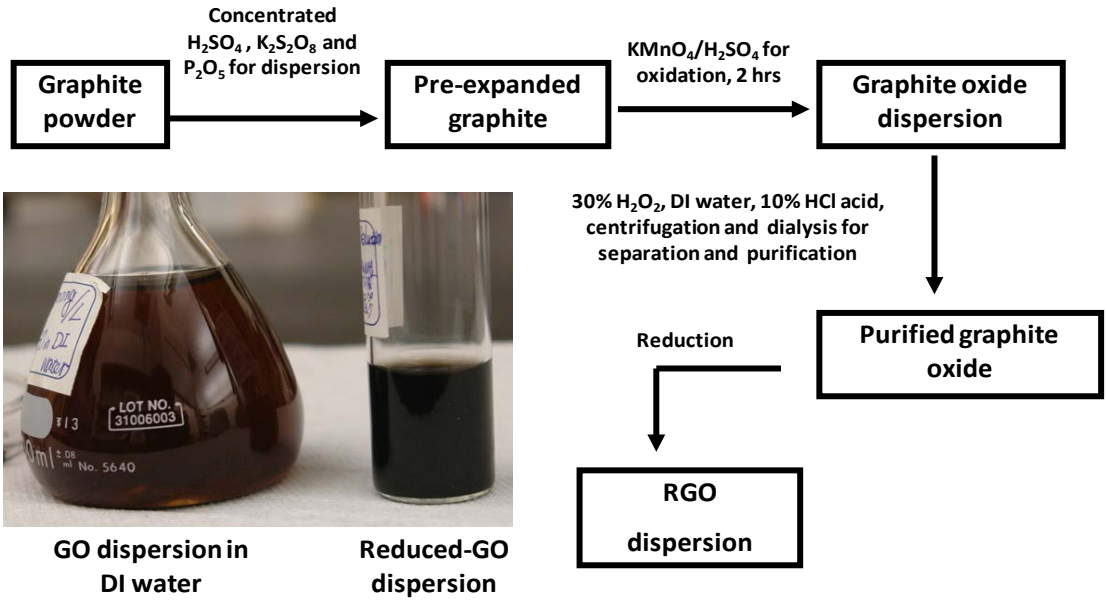

Figure 1.1 A Schematic of modified Hummers method for GO preparation[11]. Lower left: photographic images of the final product GO in deionized (DI) water (left) and the dispersion after hydrazine reduction with ammonia (right).

1.1.3. Tour Method and Discussions

1.1.3.1. Tour Method

As the gold rush of graphene research started in 2004, GO has jumped into the center of the carbon material research, and lots of publications have emerged talking about its structure, reduction and applications. In 2010, a new recipe was introduced by Professor Tour's group in Rice University, which has got rid of sodium nitrate and increased the amount of potassium permanganate, and also introduced a new acid into the reaction vessel: phosphoric acid.[15] They reported a GO product with higher degree of oxidation by reacting graphite with six

equivalents of $KMnO_4$ in a 9:1 mixture of H_2SO_4/H_3PO_4. One of the biggest advantages of this protocol is the absence of $NaNO_3$, thus no generation of toxic gases such as NO_2, N_2O_4 or ClO_2 in the reaction, and making it more environmentally friendly. Furthermore, phosphoric acid is believed to offer more intact graphitic basal planes and the final yield is much higher than Hummers method. A comparison among these protocols are adapted from ref [15] and shown in Figure 1.2.

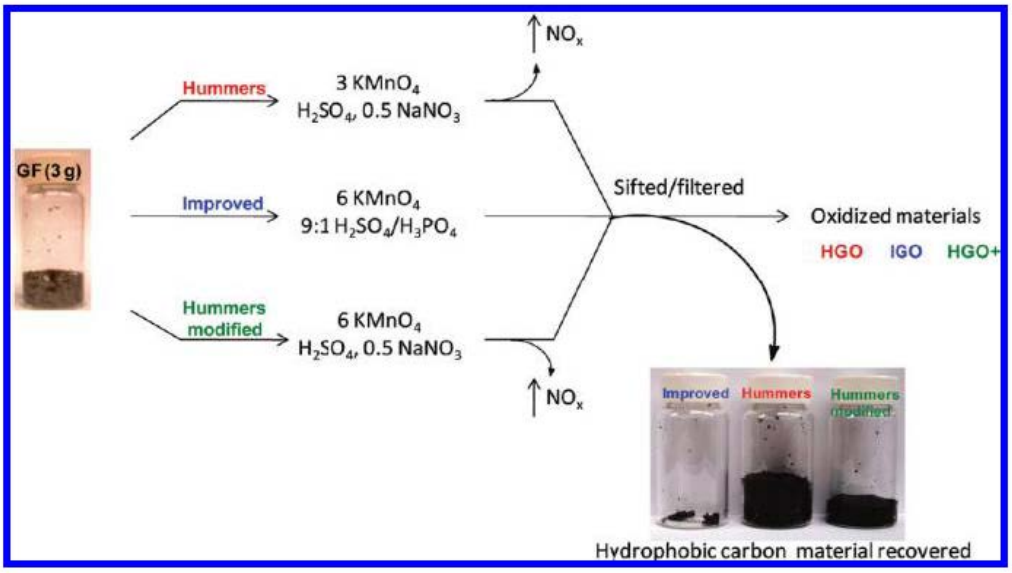

Figure 1.2 A comparison of procedures and yields among different GO preparation recipes (adapted from ref [15]).

1.1.3.2. Discussion

Graphite source is also an important factor in GO fabrication. The most common source of graphite is a naturally occurring mineral which has been purified

to remove heteroatomic contaminations such as sulfur and iron. As a result, there must be certain defects in the crystalline structure which could serve as starting sites for chemical oxidation. However, also due to the inherent defects and complexity of the structure, the precise oxidation mechanism in those reactions are hard to elucidate. Besides that, graphite nanofibers have also been used as starting material to make GO, and resulted GO nanosheets are more uniform in size distribution. The coin-stacked graphene planes along the length of the fibers are believed to play an important role here, and tunability of the GO size upon oxidation time was also observed.[23]

So far, two different combinations of oxidation reagents have been used to oxidize graphite into GO, including potassium chlorate with nitric acid, and potassium permanganate with sulfuric acid (both acids are in the most concentrated state). In literature, nitric acid has been reported to react with aromatic carbon surfaces such as carbon nanotubes[24] and fullerenes[25], which resulted in various oxygenated functional groups such as carboxyls, lactones, ketones, and meanwhile, releasing of toxic gases like NO_2 and N_2O_4. Similarly, potassium chlorate provides its oxidation capability by in situ generating dioxygen that is very reactive[26]. When Brodie method and Staudenmaier method was introduced for GO synthesis, these chemicals were believed to be the strongest oxidizers available at that time. As for the second combination $KMnO_4$ and H_2SO_4, permanganate ion is also a typical oxidation reagent. The reactivity of MnO_4^- can only be activated in acidic solution, mainly described as the following reaction[27]:

$$KMnO_4 + 3H_2SO_4 \rightarrow K^+ + MnO_3^+ + H_3O^+ + 3HSO_4^-$$

$$MnO_3^+ + MnO_4^- \rightarrow Mn_2O_7$$

Scheme 1.1 Formation of dimanganeseheptoxide from $KMnO_4$ in the presence of strong acid (adapted from ref. [27])

The transformation of MnO_4^- into a more reactive form Mn_2O_7, will certainly help oxidize graphite, but the bimetallic form of manganese oxide has been reported to detonate when heated up to 55 °C or when reacted with organic compounds.[27, 28]

The final acid that has been introduced into the GO synthesis is phosphoric acid, which is also believed to have an advantage of offering more intact 6-membered rings in the basal planes of the final product[29]. Figure 1.3 shows a possible explanation for this advantage, as adapted from Ref. [29]. The formation of the 5-membered phosphor ring helps prevent the further oxidation of the diols.

Purification is another important but tedious step in GO fabrication, since all of these protocols require long washing, filtration, centrifugation and dialysis. It has been reported that GO contaminated with potassium salts is highly flammable which poses a fire hazard. The volume expansion and gelation observed during water wash of GO significantly slows down the purification process, and a substitution with HCl acid and acetone has been introduced by Kim *et al.*.[30]

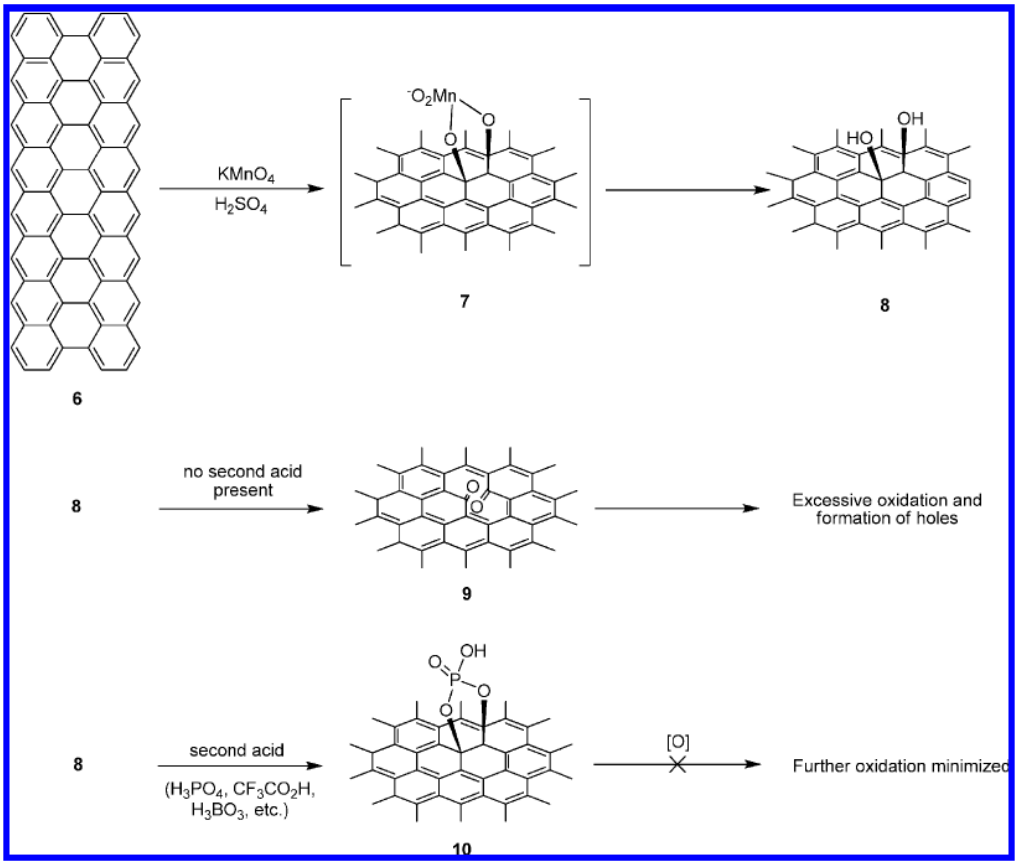

Figure 1.3 Proposed mechanisms for the effect of the second acid in prevention of over-oxidation of the sp^2 carbon network once they have formed the vicinal diols (adapted from ref [29]).

In summary, at least four different recipes have been introduced in the history of GO synthesis, and improvements in oxidation, simplicity, yield and the product qualities have been demonstrated. Today, making a batch of GO is no longer a problem, which thus has facilitated the rush of GO research; however, we still lack basic understanding of the oxidation processes and detailed mechanisms, which is preventing us from chemically engineering and manipulating the reaction to tackle

critical technology issues, such as band gap tuning, size distribution control, edge structure selectivity, and *etc*.

1.2. Characterizations, Chemical Structure and Properties

As a unique form of oxidized carbon, GO lies beyond the scope of organic compounds and large polycyclic aromatic hydrocarbons (PAHs), thus making it quite interesting and challenging to characterize this peculiar structure. In this section, we will start with a variety of characterization results shown in literature on GO and then try to clarify its molecular structure, electronic states and chemical reactivity.

1.2.1. Characterizations

1.2.1.1. Solid State ^{13}C Nuclear Magnetic Resonance (SSNMR) Spectroscopy

GO sheets are gigantic molecules that fall into colloids' category. GO dispersion in water is much too concentrated to be analyzed by liquid phase NMR. In literature, the most powerful and precise technique to characterize GO is solid state ^{13}C NMR.[31] Due to the low natural abundance of ^{13}C (1.1%), the signal to noise ratio in the measurement of regular samples is quite low, and long acquisition time is usually required for good quality data. Therefore, in 2008, professor Ruoff's group prepared a ^{13}C-enriched GO sample and pushed the structure characterization to a new stage.[16] According to their analysis, cross polarization/magic angle spinning (CP/MAS) experiments displayed three broad resonances at 60, 70 and 130 ppm in the ^{13}C NMR spectrum of GO. Figure 1.4 shows typical 1D and 2D ^{13}C pulse spectra in the ^{13}C labeled sample (adapted from ref. [16]), clearly

demonstrated both the chemical structure assignments of major peaks, and the spatial vicinity between sp^2 carbon, epoxy carbon and hydroxyl carbon atoms (as indicated by the green, blue and red circles in Fig. 1.4 B).

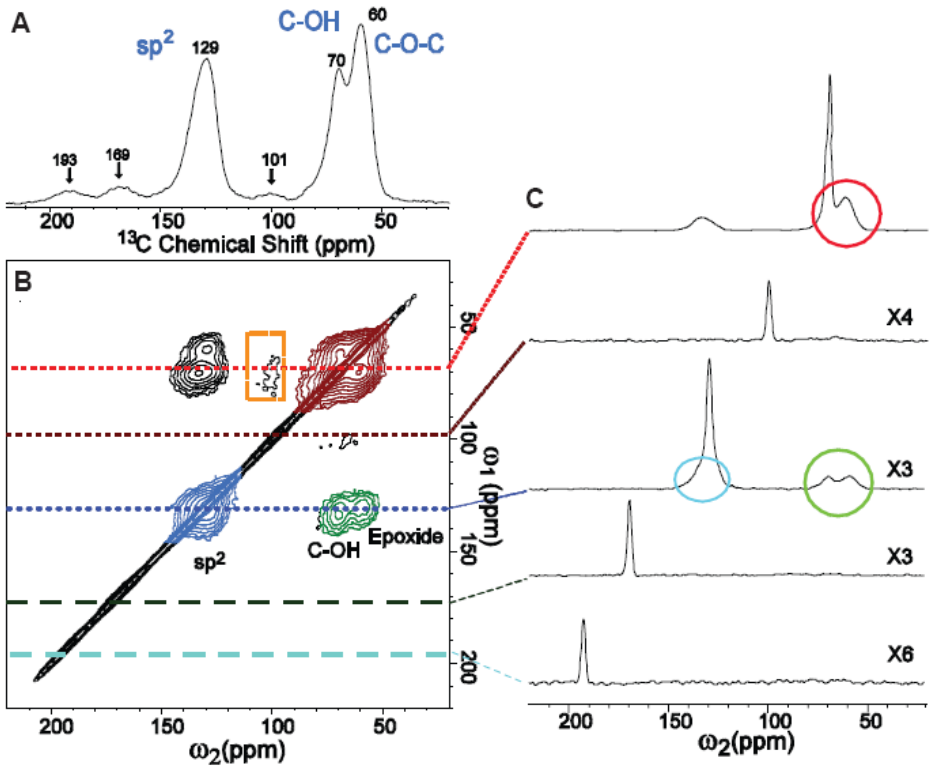

Figure 1.4 (A) 1D ^{13}C MAS and (B) 2D $^{13}C/^{13}C$ chemical-shift correlation solid-state NMR spectra of ^{13}C-labeled graphite oxide with (C) slices selected from the 2D spectrum at the indicated positions (70, 101, 130, 169 and 193 ppm) in the ω1 dimension. All the spectra were obtained at a ^{13}C NMR frequency of 100.643 MHz with 90 kHz ^{1}H decoupling and 20 kHz MAS for 12 mg of the sample. In (A), the ^{13}C MAS spectrum was obtained with direct ^{13}C excitation by a π/2-pulse. The recycle delay was 180 s, and the experimental time was 96 min for 32 scans. In (B), the 2D spectrum was obtained with cross polarization and fpRFDR ^{13}C-^{13}C dipolar recoupling sequence. The experimental time is 12.9 hours with recycle delays of 1.5 s and 64 scans for each real or imaginary t1 point. A Gaussian broadening of 150 Hz was applied. The green, red, and blue areas in (B) and circles in (C) represent cross peaks between sp^2 and C-OH/epoxide (green), those between C-OH and epoxide (red), and those within sp^2 groups (blue), respectively (adapted from ref [16]).

Interestingly, although the isotopic labeling of GO greatly improved the SSNMR analysis resolution, there still remained some unassigned peaks in this work. Later on, further reports came out with more detailed assignments of those peaks, such as a new identification of the 101 ppm peak, which has long been ignored by previous researcher. The 101 ppm peak is probably coming from the five or six-membered ring lactol structure as shown in Scheme 1.2. Figure 1.5 show a typical comparison of ^{1}H-^{13}C cross polarization spectrum and direct ^{13}C pulse spectrum obtained on unlabeled GO, with quantitative data on the relative ratio of all these functionalities to be 115 (hydroxyl and epoxy): 3(lactol O–C–O): 63 (graphitic sp^2 carbon): 10 (lactol+ester+acid carbonyl): 9 (ketone carbonyl).[17]

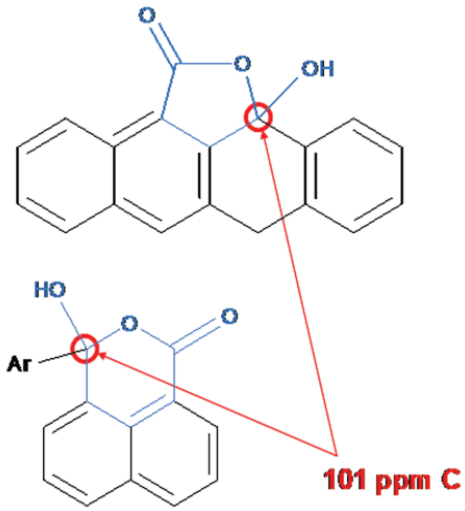

Scheme 1.2 Structure of the five- and six-membered lactol rings. The carbons circled in red are those that give ^{13}C NMR signals at 101 ppm (adapted from ref [17]).

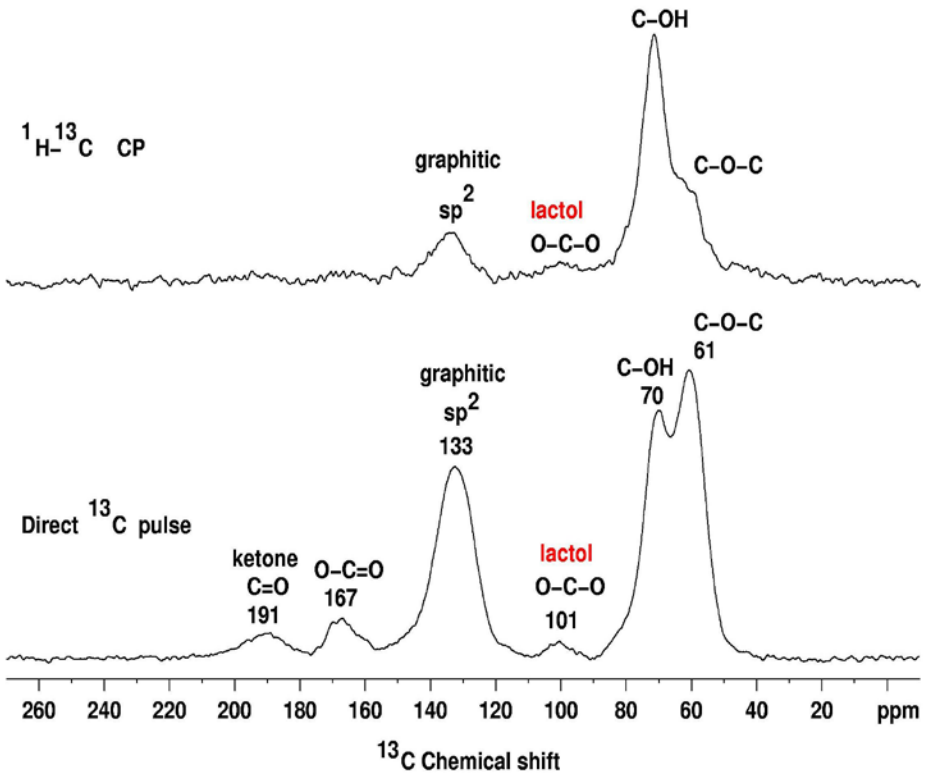

Figure 1.5 A ^{1}H–^{13}C cross polarization (CP) spectrum of GO obtained with 7.6 kHz MAS and a contact time of 1 ms (67,000 scans, top), and a direct ^{13}C pulse spectrum obtained with 12 kHz MAS and a 90° ^{13}C pulse (10,000 scans). The peak at 101 ppm is caused by the carbons of five- and six-membered-ring lactols (adapted from ref [17]).

More advanced SSNMR techniques have been used in GO characterization later on, including 2D ^{13}C double-quantum/single-quantum (2Q/SQ) correlation SSNMR, 2D ^{13}C chemical shift anisotropy (CSA)/isotropic shift correlation SSNMR, and 2D triple-quantum/ single-quantum (3Q/SQ) correlation SSNMR.[32] The 2Q/SQ spectrum eliminates diagonal signals in 2D spectrum, offering clearer correlation signal between ^{13}C-OH carbon and ^{13}C-O-^{13}C carbon (Figure 1.6); 3Q/SQ spectrum offers coherence correlation between three different carbons, thus

supports large amount of information regarding the connectivity between differently functionalized carbon atoms, and furthermore the distribution of those functional groups on GO surfaces. Interestingly, theoretical simulation was used simultaneously to fit these data with simplified GO structure model, and satisfying fitting was obtained by *ab* initio calculations with the structure model A (with only 1, 2-ether) shown in Figure 1.6d).

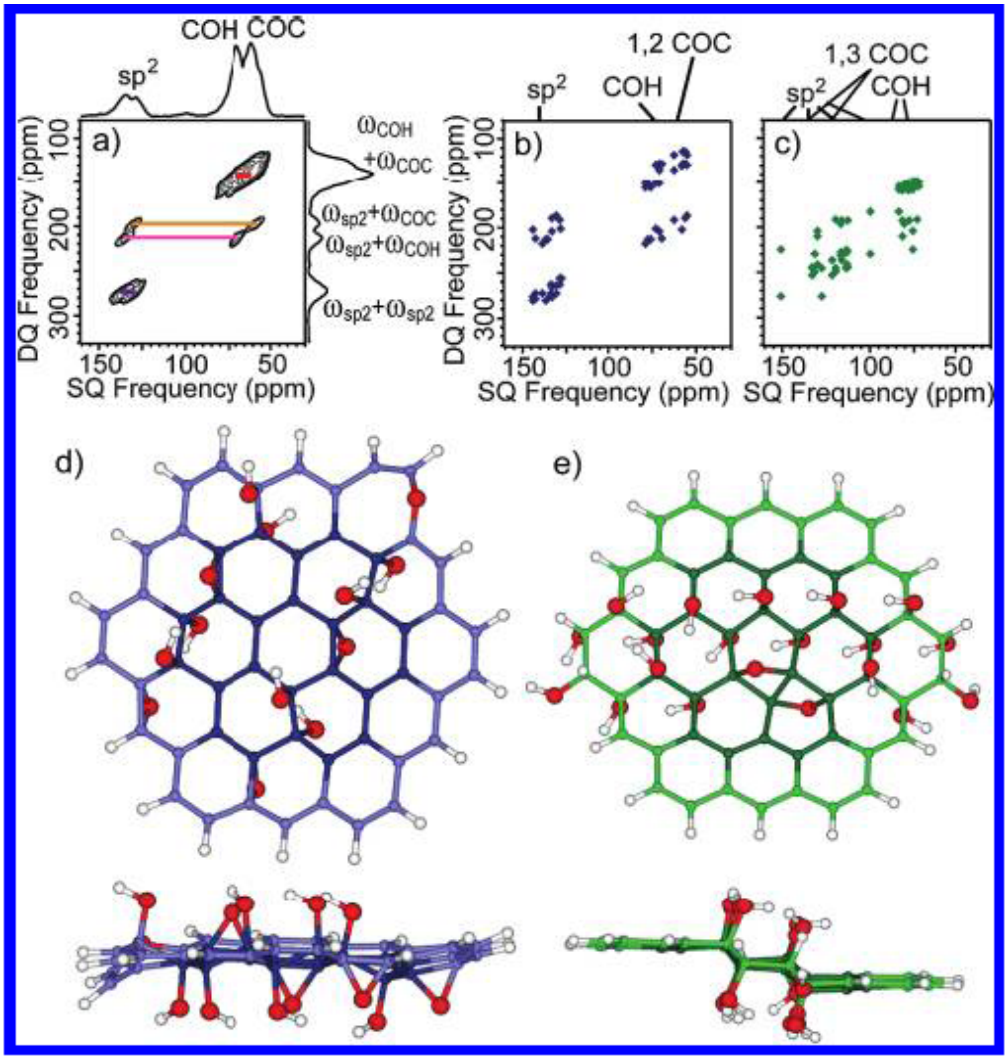

Figure 1.6 (a) Experimental 2D ^{13}C DQ/SQ correlation SSNMR spectrum of uniformly ^{13}C-labeled GO using ^{13}C-^{13}C *J* coherence transfer. Fast recycling with short recycle delays of 0.3 s and low power (7 kHz) decoupling was used. Signal assignments in (a) are those made in ref [16] and confirmed here. The carrier frequency was set at 211.17 ppm. (b, c) Predicted DQ/SQ correlation spectra based on isotropic chemical shifts calculated for (b) model A and (c) model B. (d, e) Structural models for (d) model A and (e) model B from the (top) top and (bottom) side views. Carbons in (d, e) are color coded to match the spectra in (b, c). Red and white spheres denote O and H, respectively. ^{13}C at the edge of the models (light blue or green) were not included in (b, c). The calculated spectrum (b) based on model A well reproduced the experimental spectrum (a) (adapted from ref. [32]).

All these analysis significantly helped identify GO's chemical structure, leading to improved clarity in its chemical composition. However, it is also noteworthy to point out that all those SSNMR characterizations were done on GO samples made from modified Hummers method, and GO products from other methods do differ in the relative ratio of those functionalities.[15]

1.2.1.2. Diffuse Reflectance Infrared Fourier Transform (DRIFT) Spectroscopy

Besides SSNMR, DRIFT is another powerful tool to detect chemical functionalities in oxidized carbons.[33] As for GO sample, since it is hygroscopic, large amount of water molecules adsorbed in the structure have become the biggest obstacle in FTIR analysis. Therefore, in 2005, Décány's group reported a detailed DRIFT analysis of deuterated GO samples prepared with Brodie method, and they were able to assign most of the peaks observed in the spectra and distinguish the signals of hydroxyl groups from that of others, thus provided a strong clarification of

all the previous debated assignments in GO FTIR spectrum (Figure 1.7 and Table 1.2). Deuterium exchange over GO imposes red shifts of all hydroxyl related bands, thus one can easily distinguish between the $\nu_{(OH)}$ of structural hydroxyl groups and adsorbed water, and a new band was also uncovered around 1384 cm^{-1}, which hidden in the spectrum of air-dry GO and was attributed to organic carbonates. The possible functional moieties in GO includes carboxyl, lactone, phenol, lactol, chromene, ketone, etheric rings, organic carbonate, but definitely no pyrones.[33]

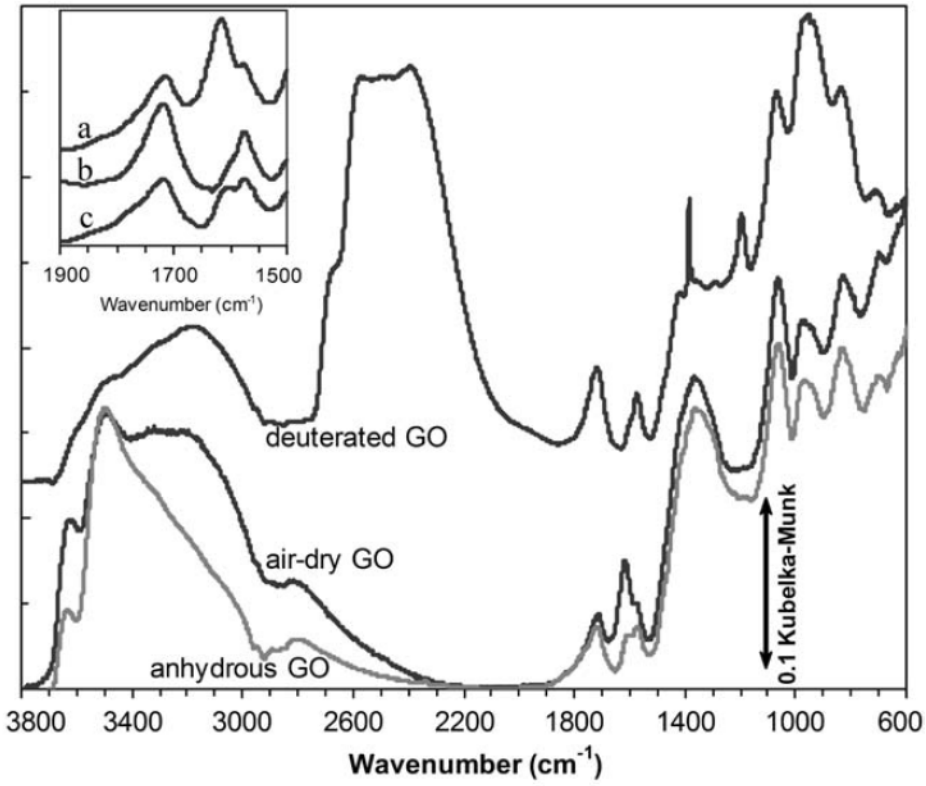

Figure 1.7 DRIFT spectra of graphite oxide samples. Spectrum of deuterated GO is offset by 0.12 Kubelka – Munk units. The inset shows the enlarged 1900–1500 cm^{-1} region of (a) air-dry GO, (b) deuterated GO and (c) anhydrous GO spectra (adapted from ref [33])

Table 1.2 IR peak positions (in cm^{-1}) of air-dry GO (GO/H_2O) and deuterated GO (GO/D_2O) and their assignments. Asterisks (in the same row) designate the isotopomer peak pairs. Band intensities and widths are classified as: w (weak), m (medium), s (strong), vs (very strong) and sh (shoulder), vsp (very sharp), sp (sharp), br (broad), respectively (adapted from ref [33]).

GO/H_2O	GO/D_2O	Assignment	D/H
–	3210 *m, br*	ν_{OH} in HDO	–
3630* *m, sp*	2680* *m, sh*	ν_{OH} in C–OH/ν_{OD} in C–OD	0.738
3490* *s, sp*	2568* *vs, br*	ν_{OH} in C–OH/ν_{OD} in C–OD	0.736
3210* *s, br*	2396* *vs, br*	ν_{OH} in H_2O/ν_{OD} in D_2O	0.746
2814 *w, br*	–	ν_{OH} in dimeric COOH	–
1714 *m, sp*	1716 *m, sp*	$\nu_{C=O}$	–
1616* *m, sp*	1196* *m, sp*	β_{OH} in H_2O/β_{OD} in D_2O	0.740
1574 *w, sh*	1574 *m, sp*	Aromatic $\nu_{C=C}$	–
1368* *s, br*	968* *s, br*	β_{OH} in C–OH/β_{OD} in C–OD	0.708
–	1384 *m, vsp*	Organic carbonate	–
1064	1064	Skeletal modes of ν_{C-C} and ν_{C-O} bonds (*m, sp*)	–
968	968		–
828	828		–
698	698		–

1.2.1.3. Other Characterizations

As a pseudo-ordered structure, the surface of GO is covered non-uniformly with those oxygenated groups, leaving 2~3 nm sp^2 carbon clusters isolated within the sp^3 carbon matrix, which can be easily verified by Raman spectroscopy[18, 34], Scanning tunneling microscopy[35, 36], high resolution transmission electron microscopy[19, 37, 38] and transport[39, 40] studies.

Raman spectrum of GO basically consists of a broad D peak (~ 1350 cm^{-1}, corresponding to structural defects), G peak (~1594 cm^{-1}, corresponding to graphitic domain vibration), and a wide weak bump extended from 2681 cm^{-1} to 3050 cm^{-1}. The D/G is around 0.95, indicating large amount of defects within the crystal lattice. However, upon chemical reduction, an increase in D/G is usually observed, and the explanation for this is still ambiguous.

UV-Vis spectrum of GO in water has two featured peaks around 233 nm due to π to π^* transition of C=C bonds, and broad shoulder between 290~300 nm assigned as n to π^* transition of C=O bonds.[41] Upon reduction, red shift of the first peak and disappearance of the second one are usually observed.

X-ray diffraction (XRD) analysis of GO powder shows a prominent but somewhat broad peak around 11 degrees and the position can be easily influenced by oxidation and hydration level of GO sample. The reported interlayer distance of GO samples varies from 5.97 Å[33] to 9.5 Å[15].

X-ray photoelectron spectroscopy (XPS) analysis of GO powder also offers two broadened and overlapped peaks centered around 284 and 286 eV, corresponding to sp^2 carbon and oxidized carbon respectively. Some workers try to deconvolute these peaks into different oxidation functionalities, while we think XPS is at most a semi-quantitative analyzing technique, and this kind of analysis is beyond the resolution limit of the instrument.

Atomic Force Microscopy (AFM) and Transmission Electron Microscopy (TEM) could easily confirm the 2D nature of GO sheets when they are spin coated

onto a pretreated silicon wafer. The thickness of a GO sheet is typically around 1~ 2 nanometers, and the lateral dimensions vary between several nanometers and microns. Based on the AFM studies, it is believed that sonication results in near-complete exfoliation of GO.[42] The wrinkled surface and occasionally holes can be observed in both AFM and TEM images of GO (Figure 1.8).

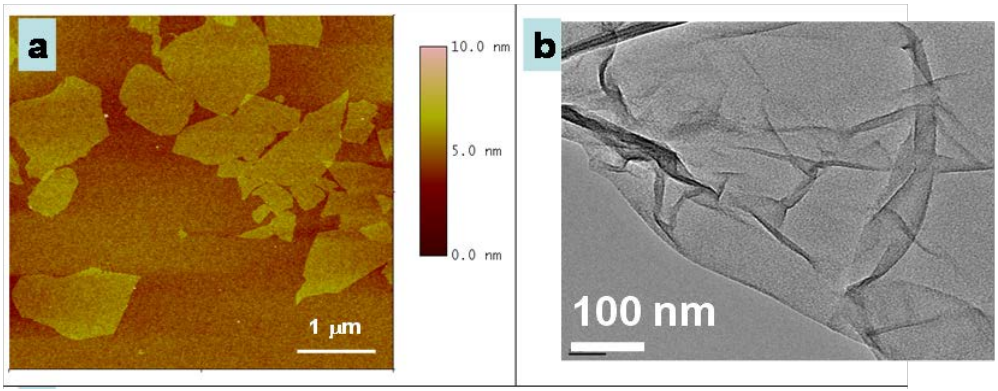

Figure 1.8 a) AFM and b) TEM images of GO sheets.

Thermal gravimetric analysis (TGA) offers information on thermal stability of GO. Unfortunately GO is thermally unstable, when heated in Ar, GO starts decomposing slowly above 60-80 °C, and loses up to 60 % of its total weight when heated up to 950 °C. The loss of adsorbed water will also occur during this process. It is important to mention that, for GO TGA analysis, the temperature ramping rate is usually set to be very low (around 1 °C/min), to avoid making the rapidly evolved gases explode and cause problems.

1.2.2. Chemical Structure

Based on the characterizations listed above (mainly SSNMR and DRIFT analysis data), people have suggested at least six different structure models for GO as shown following (Figure 1.9 [43], and the precise chemical structure of GO is still controversial.

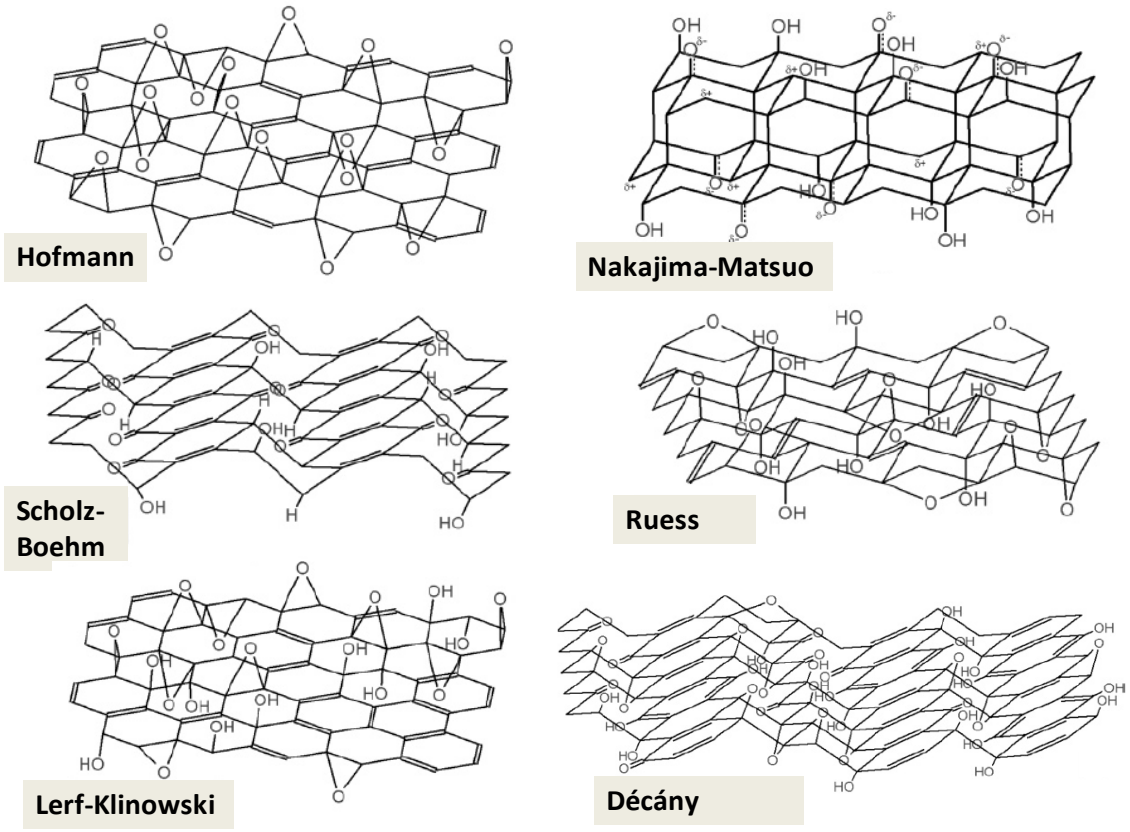

Figure 1.9 Proposed structure models for GO.

The earliest model by Hofmann and Holst in 1939 consisted of epoxy groups spreading across the basal planes of graphene, with C/O equals two.[44] The model was modified by Ruess in 1946 with the introduction of hydroxyl groups into the

lattice and also the corrugating of the basal plane.[45] Different from the Hofmann model, Ruess model prefer 1, 3-ether on a cyclohexane ring with the 4 position hydroxylated, and also stoichiometrically regular. Ruess's suggestion was supported by the observed structure of poly(carbon monofluoride), $(CF)_n$[46] later by Mermoux in 1991. The existence of hydroxyl groups in this model accounts for the hydrogen content in GO for the first time; in 1957, Clauss and Boehm supplemented this contribution with C=C bonds, ketone and enolic groups, as well as the carboxylic groups around the edges.[47] More than a decade later, Scholz and Boehm reconsidered the stereochemistry of this model, and modified it into a corrugated carbon layers consisting of alternately linked ribbons of quinoidal structure and opened cyclohexane rings in chair conformation.[48] They completely removed epoxy and ether structure in this model, and put hydroxyl groups on 4 position of 1, 2 oxidized cyclohexane rings. On the other hand, the Ruess model was still a possibility; in 1988, Nakajima and Matsuo proposed a stage II type model $(C_2F)_n$ in graphite fluorinated product, and tried to make the oxide analog for GO.[49]

Yet most of the above models have been supplanted by the two most recent models named by Lerf-Klinowski[31, 50, 51]and Décány[43], respectively. In Lerf-Klinowski model, the periodicity in the structure was rejected, and substituted with a nonstoichiometric amorphous alternative. In their studies, SSNMR technique was for the first time introduced into GO structure characterization, while all the previous reports were simply based on elemental analysis, reactivity observations and XRD data. Obviously this is an important milestone in GO structure debate, and

as discussed in the previous section, the assignments of all those CP/MAS signals in SSNMR spectra soon helped clarify the basic structure information in GO.

Lerf and coworkers have actually done lots of detailed discussions and analysis on GO structure with not only SSNMR analysis, but also GO reactivity with a variety of compounds and infrared spectroscopic data. First of all, they tried to have a Diels-Alder type cycloaddition reactions (4+2) on GO (conjugated double bonds should react) with maleic anhydride, however no reaction was observed.[50] In the context of the distribution of the alkenes on GO basal plane, the result they got is definitely inconclusive, since the lack of reactivity of GO with dienophile could be due to the complexity on the GO local environment such as the steric effect of epoxy and hydroxyl groups. Later on they suggested that alkenes (C=C) in GO are probably either aromatic or conjugated with the logic of isolated double bonds could not survive the harsh oxidation environment when making GO.[31] Secondly, in combine with the interpretation on FTIR data earlier, they proposed that keto groups are more favored at the periphery of GO than carboxylic acids.[52] The acidity in GO were further explained by them with a keto-enol tautomerization and the proton exchange on the enol site. The keto form is supposed to be thermodynamically more favored, however, α,β-unsaturated ketones that are present in aromatic regions would favor phenoxide product and allow proton exchange (also known as phenol-quinone exchange, shown in Scheme 1.3) Thirdly, they observed strong hydrogen bonding between GO flakes themselves and water molecules, as indicated by the constant full width at half maximum height of the water peak in the ^{1}H NMR spectrum.[51]

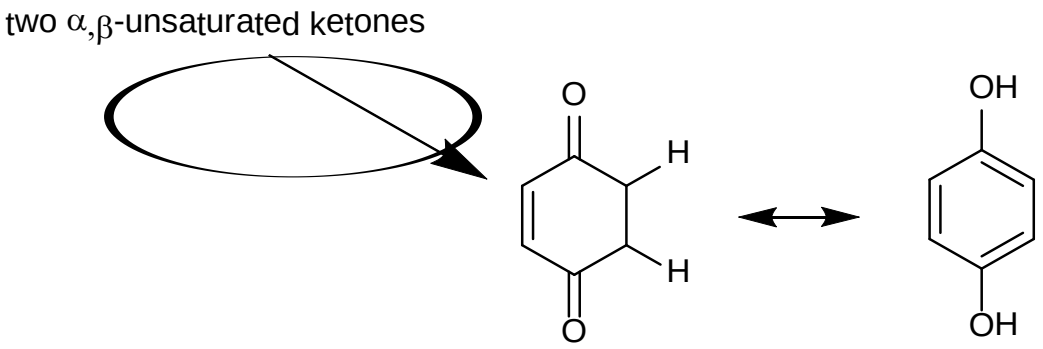

Scheme 1.3 Schematics of phenol-quinone exchange, favoring the forward direction due to the aromaticity in phenol structure.

Décány model was another well-recognized structure for GO, which adopted the logic in Ruess and Scholz-Boehm models, and stuck to the corrugating nature of the carbon network. It followed the basic framework in Scholz-Boehm model, while adding 1, 3-ethers into the structure and extending the trans-linked cyclohexyl networks.[43] In 2008, Cai *et al.* prepared ^{13}C labeled GO sample, and conducted 1D and 2D SSNMR analysis on it. According to their conclusion, only Lerf-Klinowski model and Décány model are possible.[16]

Later on, *ab* initio chemical shift calculations were used to simulate the SSNMR signals in GO by Professor Ruoff's group[32], and an experimental 2D ^{13}C double-quantum/single-quantum correlation SSNMR spectrum of ^{13}C-labeled GO was compared with spectra simulated for different structural models using *ab* initio geometry optimization and chemical shift calculations. According to their conclusion, only Lerf-Klinowski model fits the best with the experimental data; furthermore, all the previous proposed models were excluded. This is definitely another big step

forward to clarify GO structure; however, we need to point out that due to the size limitation in theoretical modeling, the Lerf-Klinowski model used to simulate NMR spectrum in this paper is quite simplified, and thus trivial details of the structure on the edges as well as the precise distributions of those functional groups are still unclear.

Unfortunately, until today the precise structure of GO still remains elusive. Major reasons include sample-to-sample variability due to different synthesis method and degree of oxidations, amorphous, nonstoichiometric nature of GO, and limited resolution in the major characterization techniques such as SSNMR and FTIR. In this case, the term “graphite oxide” may refer to a family of different compounds with certain discrepancies in the functional group distribution and relative content.

1.2.3. Reactivity and Physical Properties

1.2.3.1. Dispersibility

The most common reaction media for GO is water, and there are different ways to disperse GO into water, including sonication and mechanical stirring. Sonication has been reported to create defects and decrease sheet size of GO from several microns to few hundreds of nanometers, and also widen the size distribution, thus are less favorable than mechanical stirring in many applications.[42, 53, 54] The dispersibility of GO in water are typically on the order of 1-4 mg/mL. [55] On the other hand, GO can also be dispersed in organic solvents such as DMF, NMP, THF and *etc.*[56, 57], thus is also believed to be amphiphilic with the core more hydrophobic and edges more hydrophilic[56, 57], acting just like a surfactant.[58] As a giant molecule with amphiphilicity, GO can be assembled into continuous single-layer films by Langmuir-Blodgett method.[59-61]

1.2.3.2. Toxicity

GO and RGO were reported to be toxic to bacteria (Escherichia and Staphylococcus) due to the cell membrane damage of the bacteria in contact with the sharp edges in GO and RGO by Akhaven *et al*, and hydrazine reduced GO was more toxic than pristine GO[62]; their inhibition toward bacteria growth with minimal toxicity to human alveolar epithelial A549 cells were also shown by Hu et al.[63] Wang *et al.* demonstrated that GO has dose-dependent toxicity to human fibroblast cells when obvious toxicity was observed at doses higher than 50

μg/mL.[64] GO toxicity and blood compatibility were also reported to be dependent on dose, extent of exfoliation and sheet size.[65-67] RGO was demonstrated to be less toxic than carbon nanotubes to PC12 cells at high concentrations by Zhang *et al.*[68] Pegylated nano-sized GO only exhibited mild toxicity toward Raji cells at concentrations as high as 100 mg/L.[69] Paradoxically, other recent reports showed the high biocompatibility of GO or RGO.[70-74] To address these discrepancies, Ruiz *et al.* reported the non-specific enhancement of cellular growth of GO, thus verifying that GO is non-toxic to both bacteria and mammalian cells, and attributing the previous reported toxicity as effects from carryon impurities in GO.[75] However, Incorporating Ag nanoparticles onto GO matrix significantly activated its antibacterial activity.[76, 77]

1.2.3.3. Hygroscopicity (Interaction with water)

The hydroxyl, epoxy, and carboxyl groups on GO make it very hydrophilic, and adsorbed water molecules tend to present in the interlayer voids even after prolonged drying.[78] Therefore, GO turns out to be quite hygroscopic, with water content strongly depending on the humidity level of the environment.[79] When large amount of interlamellar water is present in stacked GO films, a network of hydrogen bonds (H-bonds) forms between water molecules and those oxygenated groups on GO, thus significantly influencing its structural, mechanical and electronic properties.[78-81] For example, as the humidity level rises, GO film swells in volume[79, 81] and tensile modulus decreases.[78] Some theoretical simulation predicted that the interlayer distance between GO flakes arises from 5.1 Å to 9.0 Å

when water content increases from nearly zero to 26 wt%, and that as the water content exceeds 15 wt%, the H-bond network is dominated by water-water H-bonds while functional groups are indirectly connected via a chain of water molecules.[82] The dynamics of the interlamellar water has also been studied by neutron scattering, and a "two-site" jump motion mechanism has been proposed.[79] Interestingly, when water is replaced by D_2O, a lower interlayer distance was observed, probably due to the lower solubility, lower reactivity and stronger bonding of D_2O compared with H_2O.[79] The presence of water has also been accounted for the carbonyl formation and hole formation during GO reduction processes.[79]

1.2.3.4. Reactivity

No matter what the dispersion media is, a stable colloidal dispersion of GO is readily reactive with a variety of chemicals, most of which have been reducing reagents. The first example would be hydrogen sulphide reduction introduced by Hofmann in 1934.[83] No report on lithium aluminium hydride ($LiAlH_4$) reduction has come out, probably due to the strong reactivity of $LiAlH_4$ with the common dispersion media water. Although $NaBH_4$ is slowly reactive with water, the reaction is kinetically slow enough to allow GO reduction to happen. Meanwhile, the most popular reductant so far has been hydrazine.[12] The reduction mechanism was proposed at least for one of the major functional groups on GO, as shown in Scheme 1.4.[12] Besides these, GO was believed to be one of the most important precursors to graphene, thus in literature, lots of chemical reduction protocols have been demonstrated, and to compare their effectiveness, characterizations of products

with electrical measurement, elemental analysis, SS^{13}CNMR, XPS, FTIR, Raman, XRD, TEM, TGA, Near-edge X-ray absorption fine structure (NEXAFS) spectroscopy and *et al.* have been widely reported. Here we summarize those chemical or thermal treatments and their product characterizations in Table 1.3

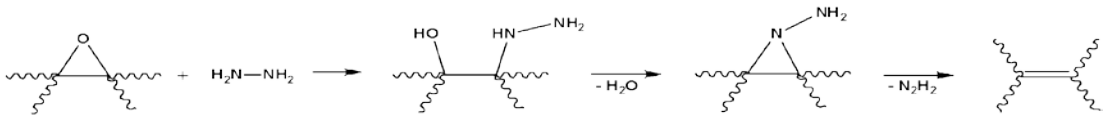

Scheme 1.4 A proposed reaction pathway for epoxide reduction by hydrazine (adapted from ref. [12]).

Table 1.3 Comparison in Reduction Protocols of GO

	Electrical Conductivity (Siemens/cm)	C/O (elemental analysis)	XPS (eV)	Raman (cm^{-1})	XRD (nm)	FTIR (cm^{-1})	$SS^{13}CNMR$ (ppm)	UV (nm)
GO	5.3×10^{-6} to 4×10^{-3} [17, 84]	2.7 [12] 2.44 [17]	284.8 (C-C) 286.2(C-O) 287.8(C=O) 289.0(C(O)-O) [12, 84]	1594(G) 1363(D) [12]	0.63-1.2 [12]	1060(C-O) 1220(phenolic) 1370 (OH bending) 1620 (H_2O bending) 1720 (C=O) [17]	57 (C-O-C) 68 (C-OH) 130 (sp^2) 188 (C=O) [12]	230 [85]
Hydrazine monohydrate [12] ($NH_2NH_2{\cdot}H_2O$)	2	10.3	284.5 with tails	1584(G) 1352(D)	NA	NA	117 (sp^2)	
Pure Hydrazine [86]	10^8-fold higher than GO	NA	284.5 dominant 532 (O) 533 (O) after thermal annealing	1600 (G) 1350 (D) 2700 (2D) 2950 (D+G) D/G increase	NA	NA	NA	NA
Vapor phase hydrazine [11]	4 orders increase	NA	NA	Changes observed	NA	NA	NA	NA
Dimethylhydrazine [87]	1×10^{-3} with 1 vol.% in PS	NA	NA	NA	0.426 0.245	NA	NA	NA
p -toluenesulfonyl hydrazide [88]	1.64	NA	285.89 C-N	NA	NA	1052,1226,1727, 3400 decreased	NA	268
Trioctylphosphine [89]	2.5	NA	C/O=9.09 284.6 with tails	1608 (G) 1312 (D)	0.385	1574 (C=C)	NA	268
hydriodic acid with acetic acid [90]	3.04×10^2 7.85×10^3 (vapor phase)	15.27	C/O=6.67 284.6 with tails	1581 (G) 1350 (D) D/G=1.10	0.362	Absent of obvious peaks	110.1 (sp^2)	Flat absorbance up to 900 nm
Hydrogen iodide (HI) [91]	NA	NA	NA	NA	NA	1710 (C=O) disappeared	NA	NA
Melatonin [92]	NA	NA	284.5 with tails	1583 (G) 2D/G=0.23 D/G=1.07	NA	NA	NA	269
Aqueous only[93]	5 orders of magnitude decrease	6	284.4 with tails	NA	None	Reduction in C=C, C=O, and C-O-C	NA	NA
Hydrothermal Steam Etching [94]	Increase observed	NA	287 peak decrease					
SO_2 [95]	NA	NA	C/O=4.49	1583 (G) 1349 (D) D/G=1.01	0.395	NA	NA	272.5
hydrazine with NH_3 (NH)/HI in acetic acid (HI); (HI/NH) [96]	4.88; 24.5	15.06; 16.58	67.9% (sp^2); 75.6% (sp^2)	NA	0.368; 0.368	NA	NA	NA
microwave[97-99]	2	4.5	284.5 with tails, p-p* bump	1591 (G) 1348 (D) D/G=0.96	0.355/no peak	1562/1577 appear 1724 decrease 1622 absent	NA	260
Sodium hydrosulfite ($Na_2S_2O_4$) [100]	13.77	NA	79% (C-C, C-H)	D/G=1 1570.7 (G) 1347.3(D)	0.377	NA	NA	NA
Polyphenol[101]	4.33×10^1	NA	284.6 with tails	D/G=1.18	0.43	NA	NA	278
$NaBH_4$[85]	1.5×10^{-6} ~4.5×10^1	2.6~8.6	284 with tails p-p* bump	D/G increase upon C_{NaBH4} increase	0.380 to 0.373	NA	~120 (sp^2)	260
Variable-valence metal assisted $NaBH_4$ [102]	3×10^2	1.81~4.99	284.6 with lower tails	D/G: 1.39~1.48 1595 (G) 1360 (D)	0.356~0.366	All disappear except for 1220 (C-OH)	NA	NA
Thermal reduction[103]	0.009~2.75	NA	NA	D/G increase	NA	NA	NA	NA

Single large sheet Thermal annealing[104]	760	NA	Decrease of oxygenated carbon peaks 89% C-C	D/G decrease 1586 (G)	NA	NA	NA	NA
Solvent thermal reduction[105-107]	2.3/52.30	NA	C/O=4.70/ C/O=6.8~8.3	1586 (G) 1347 (D)	0.41/ 0.36	1573 exists/ Most peaks disappeared	NA	NA
Hydrothermal dehydration[108]	NA	NA	Sp^2/sp^3=5.6	1593 (G) 1352 (D) D/G=0.90	NA	NA	Broad 94-160	254
Sulfur containing compounds ($NaHSO_3$, Na_2SO_3, $Na_2S_2O_3$, $Na_2S{\cdot}9H_2O$, $SOCl_2$, and SO_2) [109]	6.5×10^1 ($NaHSO_3$)	6.48~7.89 ($NaHSO_3$) 2.32(Na_2SO_3) 3.88($Na_2S_2O_3$) 5.61(Na_2S) 6.49(SO_2) 6.75-8.48($SOCl_2$)	284.7 (C=C) 285.5 (C-C)	1352 (D) D/G: 0.95~1.22	NA	NA	1577 (C=C, aromatic)	NA
Vitamin C[110-114]	8/ 7.7×10^1/ 0.141/ 15	12.5	284.5 with tails/ 284.6 (C-C) fwhm 0.8-1.1/ N content observed/ 284.5 with tails	D/G increase/ D/G=1.752	0.37	1726, 3395, 1410, 1226, 1025 decrease dramatically/ 1300-1350	NA	264/ 268
KOH/NaOH[115]	NA	NA	291.5 (p-p*)	NA	NA	NA	90-150	NA
Reducing sugar[116]	NA	NA	Oxygen binding peaks decrease	1584 (G) 1354 (D) D/G increase	No peaks	Peaks from oxide groups decrease	NA	261
bovine serum albumin[117]	NA	NA	284.6 with tails	NA	NA	NA	NA	268
H_3PO_4/H_2SO_4[118]	69	NA	C/O=8.5-11.7 291.5 (p-p*)	D/G:0.85	NA	C-H (2950) C=C (1600)	NA	270
$NaBH_4$+H_2SO_4+thermal annealing[17]	2.02×10^2	>246	284.5 with tails	1582(G) 1346(D)	0.337	No signal	119 (CCG2) 105 (CCG3)	
Electrochemical reduction[108, 119-125]	35 85[125]	23.9[125]	NA	1595 (G) 1360 (D) 2D observed	0.335	C-O remains	NA	NA
Al powder[126]	2.1×10^1	18.6	284.6 with tails	D/G=1.81	0.375	NA	NA	NA
Hydroquinone[127]	NA	NA	NA	1595 (G) 1350 (D)	NA	NA	NA	NA
Hydrogen(H2) [128]	1×10^3	NA	284.3 with tails C/O:10.8~14.9	NA	NA	NA	NA	NA
UV irradiation[129, 130]	NA/ One order decrease	NA	C/O=10	D/G decrease	NA	NA	NA	Red-shift of adsorption peak
Flash light[131]	10	4.23	NA	NA	22.5 degree	Decrease of major peaks	NA	NA

The restoration of π conjugation can be verified by changes between GO and RGO in UV-Vis spectra, XPS data and electrical conductivities. The red shifts of UV absorption peaks suggested the extension of π-π conjugation according to Hückel's rule. The appearance of the π-π satellite peak in XPS was also a good indication. Electrical conductivity would be another good criterion to judge the degree of the

restoration. As shown in Table 1.3, more than twenty chemicals have been reported as reducing reagent for GO, and so far the product with highest electrical conductivity is produced by hydriodic acid with acetic acid treatment.[90] As mentioned before, we need to emphasize that all these chemical treatments worked as reduction protocols to GO, but their products were far from HOPG graphene in their crystallinities, and the carrier mobility in these products is at least three orders of magnitude lower than that of graphene. In this case, we would like to conclude that GO as a chemically active compound is prone to be reduced very easily, but the defects and disordered structure in GO are very hard to eliminate. This can also be verified by Raman data in Table 1.3. All of those Raman spectra reported on RGOs have prominent D peaks, and most of them have higher D/G than that of GO, indicating highly defective structures in RGOs.

On the other hand, the reduction processes usually come with the heteroatom incorporation into the final product, further complicating the structure and pushing RGOs further away from pristine graphene. As shown in table 1.3, both elemental analysis and XPS data show the existence of heteroatoms in the final product, including oxygen, nitrogen, sulfur, boron, and hydrogen etc. Thus, people also tried to compare the purity of their products by comparing the ratio of C/O, C/(O+N) and *etc*. These heteroatoms do influence the electrical conductivity as well, such as residual C-N groups can act as n-type dopants.[132]

In order to elucidate the reduction mechanism as well as we can, we have summarized how those functional groups on GO would react with various chemicals, as shown in Table 1.4. Most of these reactions are explained based on fundamental organic chemistry on the aspect of reactivity of individual functional groups. As we can see from the table, even the most popular reagent "hydrazine" would still leave some functional groups intact. Therefore, though the sp^2 carbon lattice structure is thermodynamically favored over GO, the complete restoration of π conjugation is really hard, let alone the carbon vacancies that have been created in the oxidation process.

Table 1.4 Reactivity of Functional Groups on GO with Different Chemical Reagents

	NH_2NH_2	$NaBH_4$	$LiAlH_4$	KOH/NaOH[115]	H_2SO_4(Conc.) [17]	H_3PO_4[118]	HI and AcOH[90]	Diazonium Salts[133]
Epoxy (C-O-C) [134]	C=C/$C_2N_2H_2$	CH-COH (low)	CH-COH	COH-COH	NA	COH-CH_2PO_4	CI-COH	NA
Hydroxyl (C-OH)	$CNHNH_2$	NA	NA	NA	C=C	NA	C-I	NA
Ketone (C=O)	$C=NNH_2$	C-OH	CHOH	COH-COH	NA	COH-CH_2PO_4	CICOH	NA
Carboxyl(-COOH)	inert[12, 135]	-NA	-CHOH	-COONa	NA	NA	NA	NA
sp^2 Carbon	-NA	-NA	NA	-NA	-NA	NA	NA	C(sp^3)-Ph-
Ester(-O-C=O)	$O-C=NNH_2$	NA	-O-CHOH	-COOH	-NA	-COOH	NA	NA
Lactol(-O-C-OH)	$O-C-NHNH_2$	NA	-O-CHOH	NA	-NA	NA	NA	NA

1.2.3.5. Electronic Structure and Fluorescence

If we recall GO chemical structure, it is basically composed of 2~3 nm sp^2 carbon clusters surrounded by a heterogeneous sp^3 carbon matrix. In a carbon material with a mixture of sp^2 and sp^3 carbon atoms, the photoluminescence behavior is determined by the π states of the sp^2 clusters.[136] This is simply due to the π and π^* electronic levels lie within the band gap of the σ and σ^* states (typically around 6 eV [136]) of the sp^3 domains.[137, 138] π-electrons are highly localized in sp^2 domains, and the radiative recombination of the electron-hole pairs in those sp^2 clusters can give rise to fluorescence.[138-140] Therefore, the size, shape, and even the interface structure of sp^2 carbon clusters can determine the local band gap and thus the energy of the fluorescence.

Since those oxygenated functional groups are randomly distributed on GO surface, the corresponding sp^2 carbon clusters have a wide size distribution; hence no signature features could be assigned in the electronic structure. The size dependent band gap of sp^2 carbon clusters has been calculated, as shown in Figure 1.10.[141] Just as expected, larger clusters come with lower energy band gaps, varying from ~7eV for a single benzene ring to ~2 eV for about 40 fused rings, though it is necessary to point out that the structure model adapted in this simulation was quite simplified (with only zigzag edges and ordered hexagonal shapes) and that it did not take into account of the electro-negativity effect of the nearby connected sp^3 carbons. When only sizes of the clusters are taken into account, the ensemble band diagram corollary are shown in Figure 1.11.[141]

Interestingly, in this figure, the authors also depicted a photoluminescence process from a finite sized sp^2 cluster (composed of several conjugated repeating alkene units that were populated at the initial stage of the vapor hydrazine reduction), corresponding to the enhanced blue luminescence (~390 nm, 3.18 eV) they observed in the first three minutes of reduction.

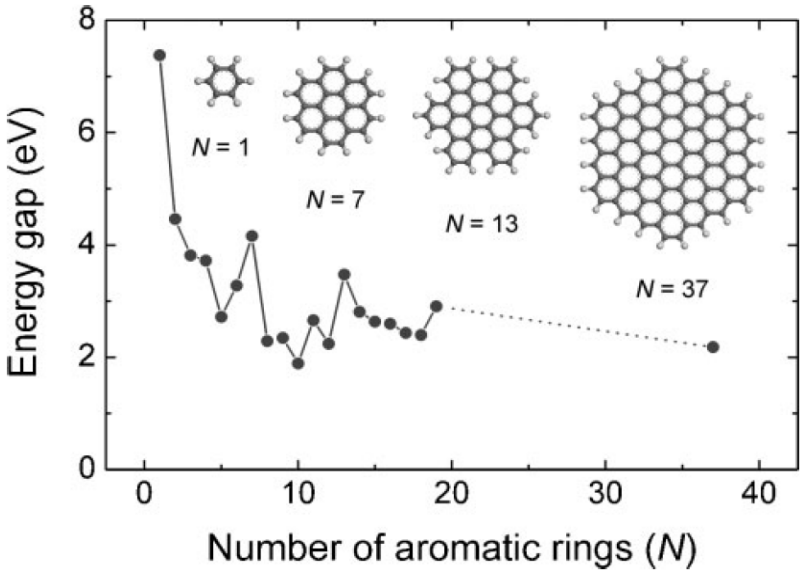

Figure 1.10 Energy gap of π–π* transitions calculated based on DFT as a function of the number of fused aromatic rings (N). The inset shows the structures of the graphene molecules used for calculation. (Adapted from ref [141])

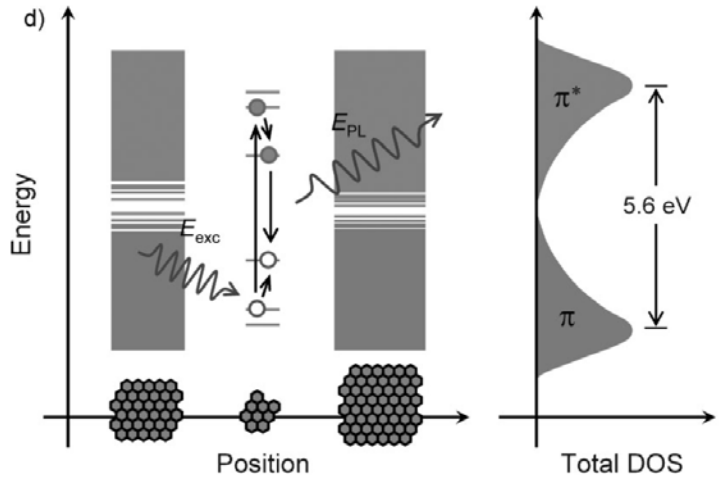

Figure 1.11 Representative band structure of GO. The energy levels are quantized with large energy gap for small fragments due to confinement. A photogenerated e–h pair recombining radiatively is depicted. (Adapted from ref [141])

On the other hand, some researchers suggested that edge structures can also be accounted for the opto-electronic properties of GO/RGO, or preferably, GO/RGO quantum dots.[142] When the size of GO/RGO sheets decrease down to nanometer scale, the peripheries start playing a major role in its electronic structure. As proposed earlier[143], instead of the commonly assumed H-termination or σ-type dangling bonds, the armchair edges are actually of carbyne (*o*-benzyne) type, whereas the zigzag edges are of carbene type, as shown in Figure 1.12. This means the non-bonding electron on the edge carbon is no longer in its free state, but couples with another electron on the adjacent carbon (the armchair case), or interacts with the π electron on the same carbon atom (the zigzag case). Therefore, the activity of an unsaturated valence has not been seen in this case, and the stabilization is achieved by the localization of the itinerant π electrons through σ-π

coupling in the zigzag case.[144] Based on both theoretical calculations and experimental data, Radovic *et al.* strongly suggested that this type of edge structure tends to be stable in the ambient conditions, and the stability increases when the number of conjugated aromatic rings goes higher. Carbenes have two electronic configurations in the ground state, the triplet ($\sigma^1\pi^1$) and singlet (σ^2) state, with triplet configuration typically lower in energy.[143] In the case of carbyne, the situation is exactly the opposite. Regardless of its detailed configurations, the strong blue luminescence observed in RGO quantum dots has been assigned to the HOMO-LUMO transition in the triplet state of carbenes at zigzag edges.[142]

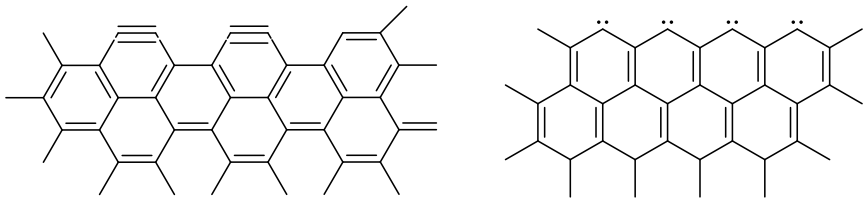

Figure 1.12 Carbyne (left) and carbene (right) structures on graphene edges, corresponding to armchair and zigzag edges, respectively.

As for GO, the peripheries are partially occupied by oxygenated groups; however, some researchers tend to exclude these groups as the origin of observed luminescence, because the luminescence was reported to be enhanced with reduction[141]. This inference seems to be questionable, since at the initial stage of GO reduction with hydrazine, some edge groups such as carboxyl groups still remain intact in the structure (Table 1.4). Interestingly, Galande *et al.* have reported a pH-dependent fluorescence from GO dispersions.[145] They suggest that the observed

fluorescence signals are originated from the –COOH groups electronically coupled with nearby graphitic carbon atoms. The resulted quasi-molecular fluorophores are similar to those polycyclic aromatic compounds. In strong basic conditions, G-COO^- groups get excited to the excited state (G-COO^-)*, and relax back to the ground state with sharp, structured emission at shorter wavelengths. When pH value goes below 8, the excited-state structure gets reprotonated, and results in broad, red-shifted emission, which can be attributed to both the strong interaction of the protonated acid with the polar solvent and the geometric changes of the fluorophore during excitation and emission.

Although the exact mechanism for the observed visible and ultraviolet fluorescence in GO remains to be reconciled, GO as a unique carbon platform, together with its chemically activity, tunability and solution processability, has already shown its technological significance. The photoluminescence from GO derivatives varies from near-infrared to ultraviolet region,[16, 118, 141, 142, 146-149] and further demonstrations of its application have been widely reported, such as in drug delivery, live cell imaging[16, 147], fluorescence quenching[150-155], biosensing[156, 157] and nonlinear optics[158-160].

1.3. Applications

In the beginning of this section, we would like to distinguish the applications of RGOs from that of GO. There are numerous reports in literature suggesting possible applications of RGOs and their derivatives (such as metal oxides/RGO and polymer/RGO composites), as vital components in conductive polymer composites[87], transparent conductors[42, 161-164], molecular, electrochemical, or biochemical sensors[11, 94, 111, 157, 165-187], electrochemical or photo catalysts[64, 109, 173, 174, 188-208], lithium storage materials[5, 6, 65, 209-224], electron field emission electrodes[225], supercapacitor electrodes[154, 176, 226-241], electronic transistors[242], artificial muscles[209], electroluminescence electrodes[110, 243], solid-phase microextraction materials[244], water purification adsorbents[241, 245-252], organic photovoltaic components[152, 253-257], electromechanical actuators[258] and *et al*. RGOs here either act as major functioning components themselves, or as matrix supports for those active nanoparticles and/or metal oxides in the composites. However, as we stated before, the direct use of unreduced GO is relatively few. When it comes to GO applications, we would like to summarize them into three different categories: 1) an important platform for RGOs and GO derivatives/composites (1.3.1); 2) an anisotropic proton conductor (1.3.2); 3) others such as a catalyst and an electron transparent window (1.3.3).

1.3.1. A platform for RGOs and GO Derivatives/Composites

1.3.1.1. For RGOs

We have discussed and compared reduction of GO in previous sections (table 1.3). RGOs derived from GO differ in their electrical conductivities, micro-morphologies, BET surface areas, optical activities *etc.*, thus leading to a variety of applications as mentioned above. Despite being referred to as graphene or RGO applications, these results actually take advantage of the large scale, wet chemical processability, high surface area, tunable conductivity[259] of GO. In order to focus on GO itself, we just skip this RGO part here.

1.3.1.2. For GO Derivatives

The addition of other functional groups directly onto GO, to form either covalent or non-covalent attachments, falls into another big category of GO chemistry. According to the widely accepted *Lerf-Klinowski* model, reactive functional groups on GO are epoxy, hydroxyl, carbonyl, carboxyl and ester moieties. It would be nice if one can selectively react with one of these groups and keep others intact; however, so far such kind of orthogonal reactions have not been demonstrated. Most of the functionalization occurred on more than one type of oxygenated groups and resulted in very complicated products with separation and purification almost impossible. Regardless of vague chemical characterizations, most of these products showed interesting applications in various aspects.

For instance, carboxyl acid groups, after being activated by thionyl chloride ($SOCl_2$)[260-262], 1-ethyl-3-(3-dimethylaminopropyl)-carbodiimide(EDC)[147], N,N'-dicyclohexylcarbodiimide(DCC)[263], or 2-(7-aza-1H-benzotriazole-l-yl)-1,1,3,3,-tetramethyluronium hexafluorophosphate (HATU)[264], are attacked by nucleophiles such as amines or hydroxyl groups forming covalent attachments. The resulted amides have shown possible applications in optoelectronics[260, 262, 265], biodevices[264], drug-delivery vehicles[147], and polymer composites[263, 266]. A more complicated case involves the attachment of diamine, further covalent binding with bromide terminated initiators, and subsequent polymerization on GO surface.[267, 268] The resulted GO/polymer composites usually offer better dispersibility in many solvents. Besides that, isocyanate derivatives have also been shown to react with carboxyl and hydroxyl groups leading to amide and carbamate esters.[269] The products here can be well-dispersed in polar aprotic organic solvents. Chitosan chains also reacted with the carboxyl groups on GO forming amino bonds with only microwave assistance, offering possible biomedical applications.[270]

Epoxy group is another major functionality on GO. The epoxy rings can be easily opened under acidic conditions or by nucleophilic attack. For example, octadecylamine was used to react with GO and offered a colloidal dispersion of functionalized GO (FGO) in organic solvents.[271] Hexylamine was also used to attack the epoxy rings on GO to form alkylated GO which can further be reduced into alkylated conductive graphene paper.[272] Ethylenediamino-β-cyclodextrin was also introduced to attach cyclodextrin on to GO surface via amine-epoxy

reaction.[147] An ionic liquid (1-(3-aminopropyl)-3-methylmidazolium bromide, RNH_2) was attached to GO via the end amine group in a nucleophilic attack of the epoxy groups.[273] Another example involved 3-aminopropultriethoxysilane (APTS) attachment onto epoxy via a S_N2 reaction and of course ring opening of epoxy groups, while reinforcement in the mechanical properties of the resulted silica composite was demonstrated.[274] Interestingly, inspired by the synthetic polymer chemistry or biochemical systems, crosslinking of GO with poly(allylamine) or sodium borate, via epoxy and hydroxyl groups, has also been investigated.[119, 275], and mechanical enhancement of the resulted GO film were observed in both cases. Unfortunately these crosslinking strategies cannot stabilize GO in solvents especially in water, unlike the case for polymers, cross-linked GO paper still breaks down when in contact with water, hence other chemical methodology to tackle this problem are of interest to GO chemists.

Hydroxyl groups on GO can act as nucleophiles to attack ketones. For instance, 2-bromo-2-methylpropanoyl bromide was used to react with hydroxyl groups on GO to form an initiator for atom transfer radical polymerization (ATRP), offering GO- polymethyl methacrylate (GO-PMMA) as the final product (see Scheme 1.5).[276]

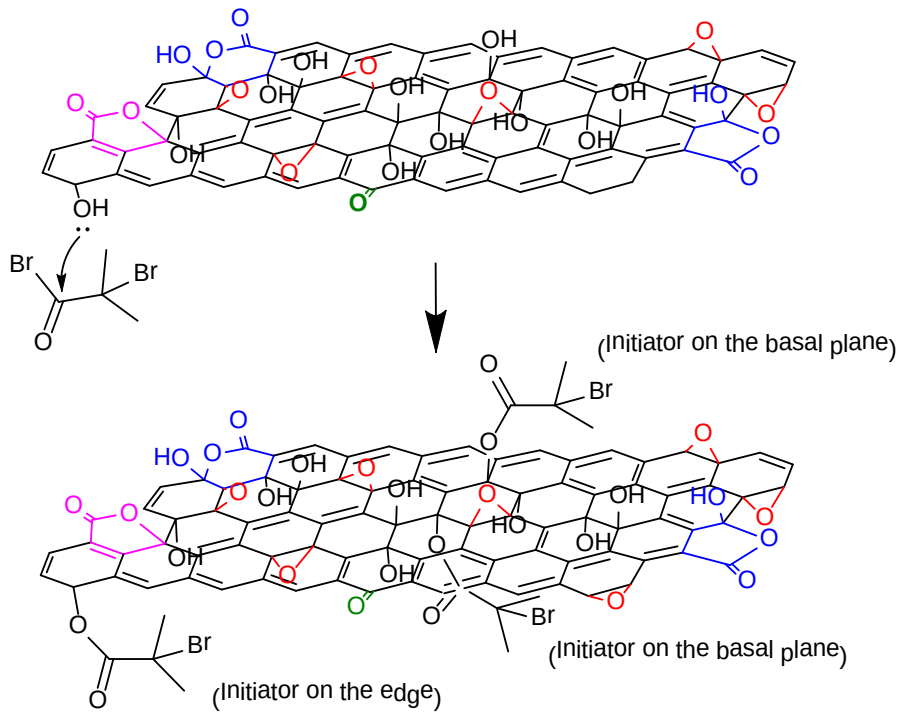

Scheme 1.5 Nucleophilic attack of hydroxyl groups on GO to 2-bromo-2-methylpropanoyl bromide, offering an initiator for ATRP.

It is also worthwhile to mention the covalent functionalization of RGOs with diazonium salts.[55, 133, 277] The aryl diazonium salt was believed to react with the sp^2 carbon domain in RGOs[278] and yield highly functionalized RGOs with superior dispersibility. Direct reacting diazonium salts with GO was also reported[245], rendering thiophenol functionalized GO with high mercuric ion adsorption capability. All these reactions mentioned above lead to strong covalent bonding between GO and the other chemical, and most of them happen with more than one functionality on GO, proving GO to be a very active compound.

Additionally, non-covalent functionalization of GO has also been demonstrated. Non-covalent interactions such as π-π stacking, cation-π, or van der

Waals interactions mainly happen on sp^2 carbon domains. For instance, a GO based biosensor has been demonstrated utilizing the GO-protein/DNA π-π interactions.[157] Doxorubicin hydrochloride was also reported to form hybrid with GO via non-covalent interactions.[279]

1.3.2. An Anisotropic Proton Conductor

As we revisit the chemical structure of GO, we find over half of the carbon atoms in GO are sp^3 hybridized, attached with oxygenated groups including hydroxyl, epoxy, and carboxyl moieties. These oxygen containing functionalization allow GO to be a unique substrate for hydrogen bonding network on its surface, and lead to its hygroscopicity, just like what we saw in the very first polymer electrolyte Nafion.

Protons in the H-bond network can hop from one to another, thus an ionic conductivity was observed in GO.[227] It is not hard to understand the humidity dependence of this observed ionic conductivity: as the humidity goes down, conductivity also decreases. The two-dimensional structure in GO renders it anisotropic, since the proton hopping should be facilitated on the lateral direction rather than the vertical direction. Around two orders of magnitude difference in vertical and in-plane conductivity was observed. Taking advantage of this attribute, both sandwich and in-plane supercapacitor devices, employing GO as the solid electrolyte and RGO as electrodes, have been reported to be the important complement to the existing thin-film ultracapacitors.[227]

The ionic (protonic) conductivity was also noticed by Cao *et al.*, and by incorporating only 5wt% of GO into poly(ethylene oxide) matrix, they were able to develop a solid electrolyte membrane for low temperature polymer fuel cells.[280] The authors attributed the observed ionic conductivity mainly to the carboxyl acid groups on GO edges, whereas we suggest other oxygenated groups also play

important roles. The composite film offered temperature dependent conductivity from 0.089 S/cm at 25 °C to 0.134 S/cm at 60 °C and 100% relative humidity, leading to a maximum powder density of 53 mW/cm^2 without optimizing the catalyst layer composition.

Interestingly, a relevant application of "unreduced" GO as a hole transport layer, substituting PEDOT:PSS in polymer solar cells, has also been demonstrated.[281, 282] Li *et al.* claimed that the sp^2 domain hopping at the Femi level does not contribute to the blocking of electron transport, and observed the injection of holes into the valence band of GO is much more favorable.[281] Murray *et al.* also showed that GO is an effective replacement of PEDOT:PSS in organic photovoltaic, and that it enhances the device durability by 20 times in humid ambient condition.[282]

1.3.3. Others Such as Catalysts and Electron Transparent Windows

Due to its extraordinary hygroscopicity, GO has been demonstrated as a dehydrative polymerization catalyst.[283] During the polymerization process, GO was substantially reduced by the thermal effect and further acted as a conductive carbon addictive in the polymer matrix. The elastic modulus was increased from 40 MPa to 320 MPa with only 0.1 wt% of GO loading. GO has also been used as a catalyst in Friedel-Crafts addition of indoles to α, β-unsaturated ketones, with recyclable activity up to five cycles.[284]

On the other hand, GO turns out to be transparent enough to photoelectrons (energy higher than 450 eV) that are captured and analyzed in XPS, Auger electron spectroscopy (AES), and electron energy loss spectroscopy (EELS), but not permeable to molecules.[285] Kolmakov *et al.* demonstrated the application of 100~1000 μm^2 GO sheets as transparent windows for in-situ environmental cell in XPS analysis. They obtained good quality XPS data from aqueous solutions and nanoparticles deposited on the back side of GO films.[285] Krueger *et al.* also applied self-assembled GO as SEM environmental cell membranes.[286]

1.4. Concluding Remarks

GO, a group of gigantic organic molecules first discovered over one and a half centuries ago, has reemerged as an important precursor to graphene during the last half decade, yet now has written its own history independent of its relationship with graphene.

In this chapter, we have summarized and discussed its synthesis, characterization, structures, chemical activities and physical features based on the fundamental understandings in chemistry and material science. The applications of GO and its derivatives have also been introduced and categorized. Starting from natural graphitic material, GO can be prepared in a large amount by strong chemical oxidation. Various characterizations proved GO to be an oxidized carbon compound with two dimensional structure, in other words a sheet of fused hexagonal rings attached with lots of oxygenated groups on both sides. The mixture of sp^2 and sp^3 carbon atoms in GO made it corrugated, amphiphilic, and fluorescent, while the oxygen-containing functionalization renders its hygroscopicity, dispersibility and chemical reactivity. Its two-dimensional nature leads to large scale availability of atomically thin, transparent GO films, which can be further reduced to form transparent, conductive membranes. Enormous amount of applications extended into more than ten categories have been demonstrated, and GO has become an important material in both fundamental science and contemporary technologies.

The salient feature in GO has made it hard to identify its precise chemical structure. Although many researchers have tried to tailor its molecular structure by various chemicals, the well-resolved control or manipulation of its sp^2/sp^3 domain, the location, density and type of chemical functionalization, and of course, the size, shape and edge structure of GO itself, is still far from realization. The development of better chemical processes to eliminate the oxygenated groups and to restore π conjugation is also of interest for technology applications. Water-proof crosslinking strategy would also be intriguing for its enhanced mechanical properties and wider technological applications.

Chapter 2 **Structure and Reduction of Graphite Oxide**

This chapter introduces one of my major contributions to GO research regarding its chemical structure and reduction. GO is one of the main precursors of graphene-based materials, highly promising for various technological applications because of their unusual electronic properties. But although epoxy and hydroxyl groups are widely accepted as its main functionalities, its complete structure has remained elusive. Interpreting spectroscopic data in the context of the major functional groups believed to be present in GO, we now show evidence for the presence of 5- and 6-membered-ring lactols. Based on this chemical composition, we devised a complete reduction process through chemical conversion by sodium borohydride and sulfuric acid treatment, followed by thermal annealing. Only small amounts of impurities are present in the final product (less than 0.5 wt% of sulphur and nitrogen, compared with about 3 wt% with other chemical reductions). This method is particularly effective in the restoration of the π conjugated structure, and leads to highly soluble and conductive RGO materials.

2.1. General Introduction

Graphene, the single layer graphite material, is now well known for its unusual electronic properties and possible applications in various fields. Nevertheless, several of these applications are still not feasible due to the challenges in the large scale production of pure graphene sheets. Chemical reduction of GO is one of the established procedures to make graphene in large volume. Many primary products with either high conductivity or good solubility have been made by chemical reduction, intercalation, or thermal annealing, but most of these procedures create either highly functionalized materials (~3% heteroatom except C and O)[55, 135] or materials with a surface polymer coating[287]. Liquid phase exfoliation of graphite turns out to be a facile way to make graphene, but the yield becomes quite low (~1 wt %)[5]. Above all, fabrication of single layer graphene with high conductivity, low functionality and high solubility has not yet been achieved on a large scale.

Among all the varied strategies pursued, the reduction of GO might be one of the most promising ways, although the reduction mechanism remains ambiguous and the detailed structure of GO unclear. Interest in the structure of GO has increased recently, and the most probable structural models are given by the Lerf-Klinowski model[31] and the Dékány model[43]. The final structure of GO obtained differs depending on the chemical oxidation process employed, and hence the two models differ considerably. We have used the oxidation protocol that results in the material that is typically described by the Lerf-Klinowski model, and hence we will consider this as our base structure model of GO here. However, even this model

cannot explain all the features observed in experiments, and some of the functionalities remain to be defined. Here we offer experimental support for a peripheral structure for GO containing 6- and 5-membered-ring lactols (Scheme 1.2) and possibly an occasional 2-hydroxynaphthalic anhydride or 1,3-dihydroxyxanthone (Scheme 2.1). GO produced by a modified Hummers method turns out to be quite hydrophilic. It is easily dispersed in water with the average sheet size around 1 μm and thickness around 1 nm (Figure 1.8, Figure 2.1).

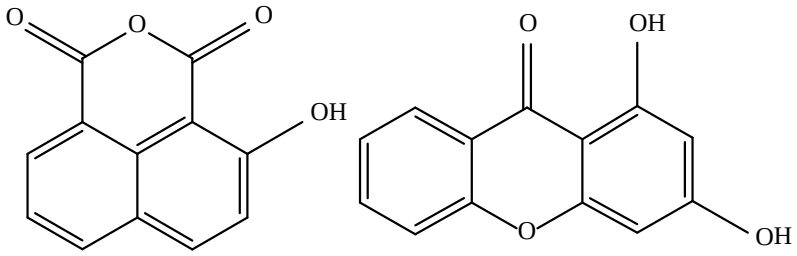

Scheme 2.1 Structure of 2-hydroxynaphthalic anhydride (left) and 1,3-dihydroxyxanthone.

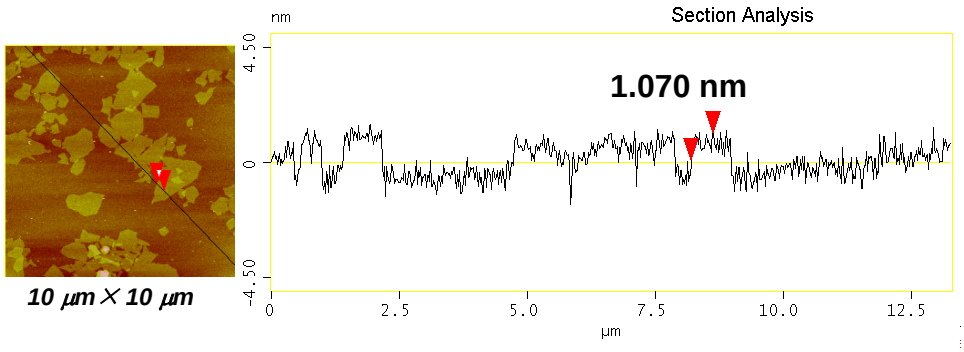

Figure 2.1 AFM analysis of GO sheets on Si substrate.

2.2. Method

2.2.1. Synthesis of GO and Its Reduction

The starting material is commercially available graphite powder (SP-1 graphite, purchased from Bay Carbon Corporation). GO was obtained by harsh oxidation of the graphite powder according to the modified Hummers method[14, 22]. After purification, the product was put in a vacuum desiccator over phosphorous pentoxide for a week. The dry GO sample was used for XRD, FTIR, AFM, Raman, NMR and XPS analysis. For the reduction procedure, dry GO was dispersed in DI water (18 MΩ, Purelab Classic Corp., USA) to get a 1.0 g/L colloidal solution. The pH of this solution was adjusted to 9~10 by 5 wt% sodium carbonate solution. 800 mg sodium borohydride ($NaBH_4$, reagent grade, 98.5%, Sigma-Aldrich) was directly added into 100 mL GO dispersion under magnetic stirring, and the mixture was kept at 80 °C for 1 h with constant stirring[55]. The reduction product was separated by filtration and washed with large amounts of water several times to remove most residual ions. This partially reduced GO was kept in a vacuum desiccators with phosphorous pentoxide for two days and re-dispersed in concentrated sulfuric acid (UN 1830, reagent grade, Fisher Scientific) and heated to 120 °C with stirring for 12 h. After cooling down, the dispersion was diluted with DI water. The final product was separated by filtration and thoroughly rinsed with water to remove most impurities. The product powder was compressed into a pellet and further annealed at 1100 °C under 1.3 slm (standard liter per minute) gas flow of Ar with 15 vol% H_2 for 15 minutes.

2.2.2. Analytical Instrumentation

Solid state ^{13}C MAS NMR spectra were acquired on a Bruker AVANCE-200 spectrometer (50.3 MHz ^{13}C, 200.1 MHz ^{1}H) using standard Bruker pulse programs, as described previously[288], as well as a modified pulse program in order to incorporate dipolar dephasing into the direct ^{13}C pulse experiment. Additional NMR details are given in the figure captions (Figure 2.2, Figure 2.3 and Figure 2.5). The powder samples are compressed into pellets under 4000 psi pressure (4350.L CARVER, FRED. S CARVER, INC.) with thickness around several hundred micrometers and a bulk density around 1.2 g/cm^3, and conductivity was measured by a fixed "film four-point probe" setup (Figure 2.6). Raman spectra (Figure 2.11) were recorded with a Renishaw InVia Raman microscope using a ×50 objective lens at room temperature, with 514.5 nm laser beam and 1800 lines/mm grating. The AFM image (Figure 2.1 and Figure 1.8) was obtained on a Digital Instrument Nanoscope IIIA Atomic Force Microscope. The TEM image (Figure 2.8) and the SAED pattern (Figure 2.8) were obtained on a JEOL 2100 Field Emission Gun Transmission Electron Microscope. XPS analyses (Figure 2.7) were carried out on a PHI Quantera X-Ray photoluminescence spectrometer with a chamber pressure of 5×10^{-9} torr and an Al cathode as the x-ray source. The source power was set at 100 W, and pass energy of 140.00 eV for survey scans and 26.00 eV for high resolution scans was used. XRD data (Figure 2.10) were collected on a Rigaku D/Max Ultima II Powder x-ray diffractometer. FTIR spectra (Figure 2.9) were obtained on a Nicolet FTIR Infrared Microscope with MCT/A detector, and for TGA-FTIR measurements,

MCT/B detector was used. TGA (Figure 2.12) was done on a SDT 2960 Simultaneous DSC-TGA, TA Instrument. For Raman, XPS, XRD and FTIR measurements, solid powder samples were used. Elemental analyses were performed by Galbraith Laboratories, Inc. Knoxville, TN.

2.3. Results and Discussion

2.3.1. Chemical Composition of GO Sheets

Various solid state ^{13}C NMR experiments were performed on our GO sample (Figure 2.2, Figure 2.3 and Figure 2.5). The direct ^{13}C pulse spectrum (Figure 2.2a) is very similar to the direct ^{13}C pulse spectrum recently reported by Cai *et al.*[16] in a preparation of highly ^{13}C-enriched GO. As in our work, Blumenfeld *et al.* detected noticeably stronger signals near about 100 and 170 ppm in a direct ^{13}C pulse spectrum than in a ^{1}H-^{13}C cross polarization (CP) spectrum[289]. These appear to be the only other studies of GO that have detected a signal near 100 ppm. Comparing the intensity of this signal in a CP spectrum against the intensity in a CP experiment with dipolar dephasing led Cai *et al*.[16] to conclude that this signal resulted from non-protonated carbons, but no further assignment has been indicated[16, 289].

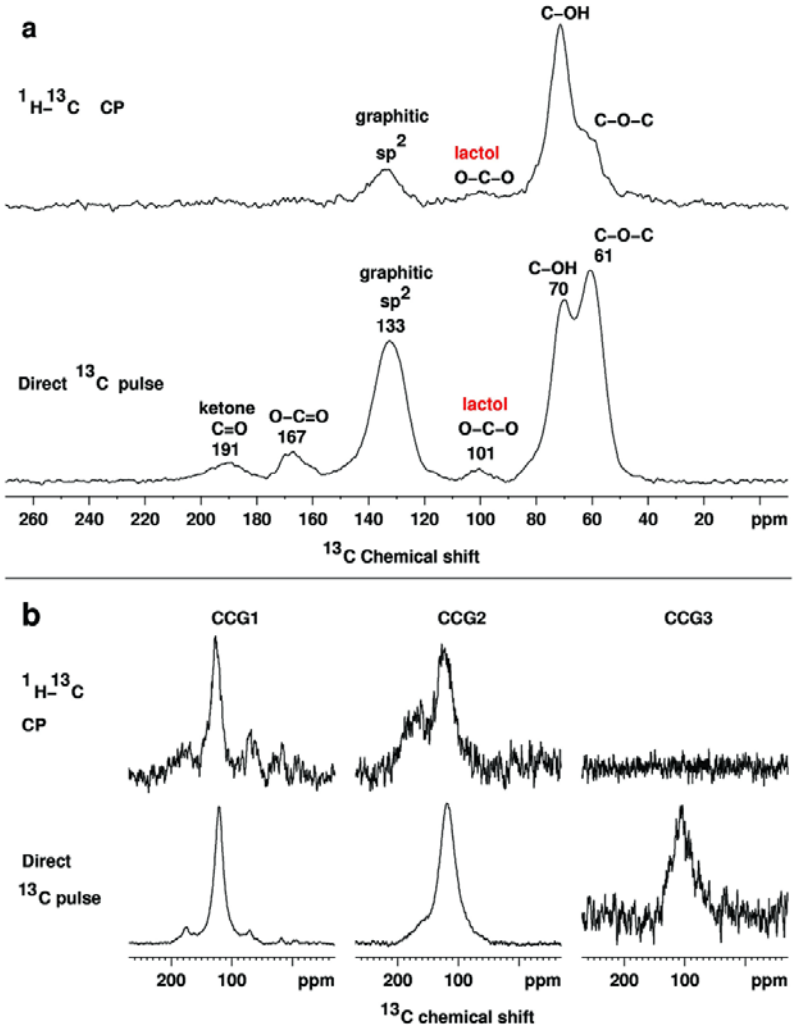

Figure 2.2 Solid state ^{13}C MAS NMR spectra of GO and its reduction products. a, GO: ^{1}H-^{13}C cross polarization (CP) spectrum obtained with 7.6 kHz MAS and a contact time of 1 ms (67,000 scans) and a direct ^{13}C pulse spectrum obtained with 12 kHz MAS and a 90° ^{13}C pulse (10,000 scans). The peak at 101 ppm is caused by the carbons of 5- and 6-membered rings lactols highlighted in red in Figure 1b. b, CPMAS and direct ^{13}C pulse MAS spectra of reduction products CCG1, CCG2 and CCG3 (with 25,320, 17,000, and 3,600 scans, respectively, in the CP spectra and 10,600, 24,000, and 6,800 scans, respectively, in the direct ^{13}C pulse spectra). Note that higher than normal drive pressure was required to spin sample CCG3 at 7.6 kHz for the CP experiment and that a drive pressure that would normally spin a sample at 12 kHz caused sample CCG3 to

spin at only 9.4 kHz. A series of processing steps removes the aliphatic functional groups and significantly broadens and shifts the aromatic signal of the extended graphitic sp^2 carbon network that is generated.

The corresponding comparisons of the CP spectra in Figure 2.3a and Figure 2.3c and of the direct ^{13}C pulse spectra in Figure 2.3d and Figure 2.3e also lead to the conclusion that the signal at 101 ppm results from non-protonated carbons. Appropriately substituted 6- and 5-membered-ring lactols along the periphery[290-292] appear to be the most likely structures in GO responsible for this signal, while 2-hydroxynaphthalic anhydrides or 1,3-dihydroxyxanthones might be minor contributing structures(Scheme 2.1). The lactol moieties have previously been considered as possible structural elements in acidic carbon surface oxides[290-292], with only indirect evidence for their presence[290].

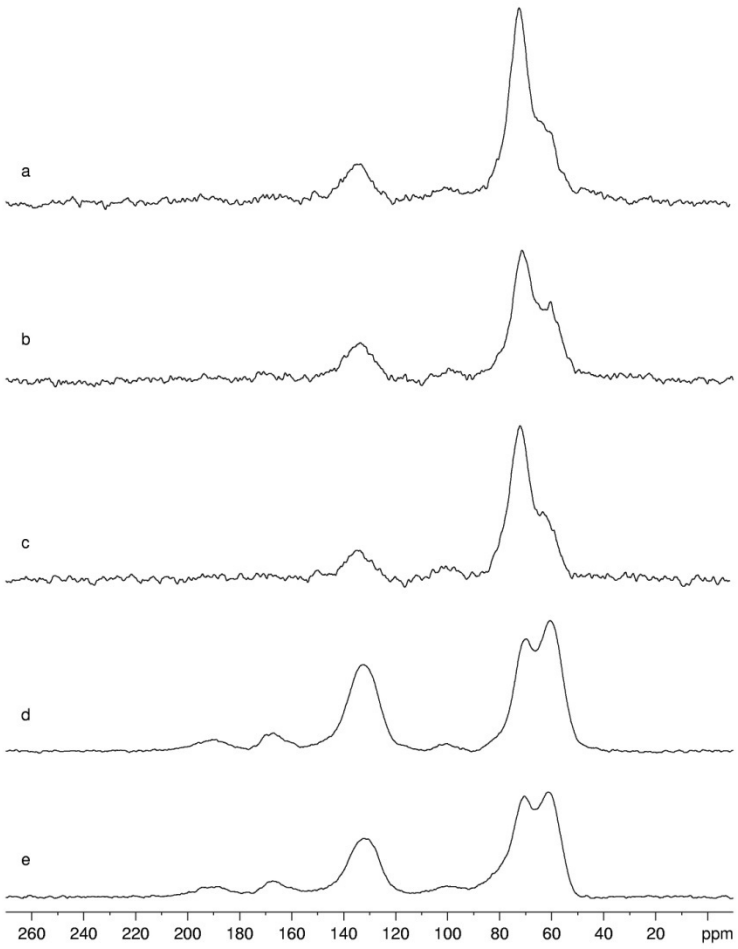

Figure 2.3 MAS ^{13}C NMR spectra of GO. (a) ^{1}H-^{13}C CP, t_{cp} = 1 ms, 67,000 scans. (b) Same as (a), except for t_{cp} = 3 ms. (c) Same as (a) but with a 50-μs dephasing interval prior to FID acquisition. These three spectra are plotted at the same noise level to facilitate comparing signal intensities among the spectra. (d) Direct ^{13}C pulse, 10,000 scans. (e) Same as (d) but with a 50-μs dephasing interval prior to FID acquisition. These two spectra are plotted at the same noise level to facilitate comparing signal intensities between the spectra.

Six- or five-membered ring lactols, 2-hydroxynaphthalic anhydrides, and 1,3-dihydroxyxanthones will, of course, also give signals in the carbonyl region. The signals observed in this work (Figure 2.2) and other work[16, 55, 289, 293] at 167-170 ppm are certainly consistent with an ester carbonyl. For reference, we note that the carbonyl carbon in the 7-membered-ring lactol generated by oxidation of pyrene gives a signal at 167.4 ppm [294]. Lactols could apparently cause only part of the signal intensity near 167 ppm, as this signal is clearly stronger than the signal near 100 ppm. The presence of numerous tertiary alcohols in GO allows for the possibility of some of them reacting with nearby carboxylic acids on the periphery (either on the same graphene sheet or an adjacent sheet) to generate an ester. Such ester carbonyl signals also appear near 167 ppm, as shown by the data for *t*-butyl benzoate in $CDCl_3$ (δ165.6)[295], 1-adamantyl benzoate in $CDCl_3$ (δ165.3) [296], and *t*-butyl 9-anthroate in $CDCl_3$ (δ169.0) [297]. The signals observed in this and other work[16]at 191 and 193 ppm can reasonably be attributed only to carbonyl groups, most likely ketones, but their precise nature is not yet clear. However, these signals do not appear to result from simple polycyclic aromatic ketones (e.g., benzanthrone, naphanthrone, and other 5-ring aromatic ketones), as the carbonyl carbon signals for solutions of these ketones in $CDCl_3$ range from 184-186 ppm [298, 299]. Hydroxyl and epoxy groups near the ketone carbonyl groups (in an as yet unknown functionalization pattern) most likely account for the downfield shift to about 192 ppm. In any event, the majority of the functional groups in GO are still epoxy and hydroxyl groups.

2.3.2. Two-step Reduction Process

Based on this chemical composition, we have developed a two-step reduction process, de-oxygenation with $NaBH_4$, followed by dehydration with concentrated sulfuric acid (H_2SO_4), which turns out to be really simple and effective in the restoration of graphene structure. Compared with other reported routes, including hydrazine reduction or direct GO thermal annealing, our strategy is far better as it produces graphene with a very low amount of remaining functional groups, high conductivity, larger crystallite size, and good solubility. In addition, our procedure does not involve the highly toxic reagent hydrazine or dimethylhydrazine, thus providing a more environmentally friendly protocol. A schematic illustration of the typical procedure proposed here is shown in Figure 2.4. The GO structure is the same as the one we have established above, which is a modified version of the Lerf-Klinowski model. The structure of the product obtained at every step is deduced from the solid state ^{13}C NMR spectra as well as from XPS analysis.

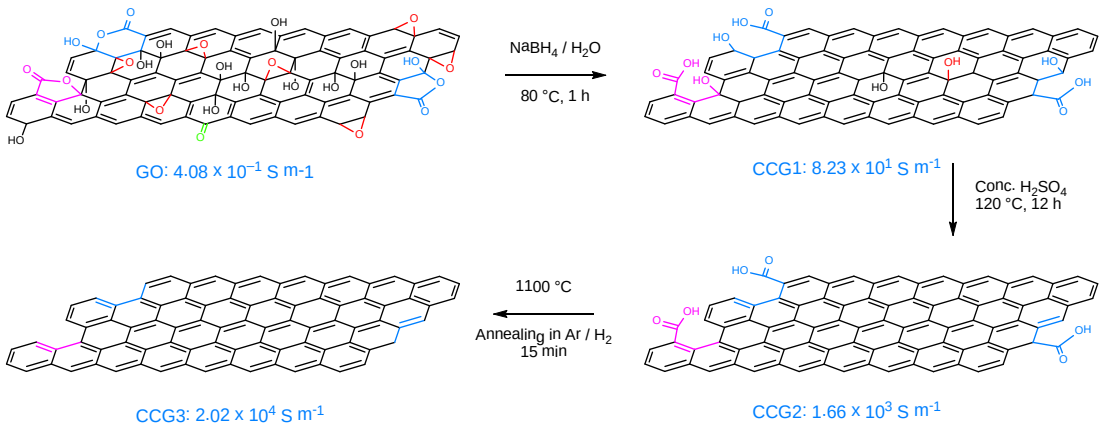

Figure 2.4 The two-step reduction process, followed by the annealing treatment, is an effective method to convert GO sheets into graphene-based materials (where CCG stands for chemically converted graphene).

2.3.3. Characterization of the Reduced Products

Treating GO with $NaBH_4$ causes enormous structural change (product CCG1). The signal for graphitic sp^2 carbon dominates both the CP and the direct ^{13}C pulse spectra (Figure 2.2b). This signal is also shifted upfield by 11 ppm. (Expanded plots of the spectra before and after $NaBH_4$ treatment are shown in Figure 2.5 to facilitate comparison).

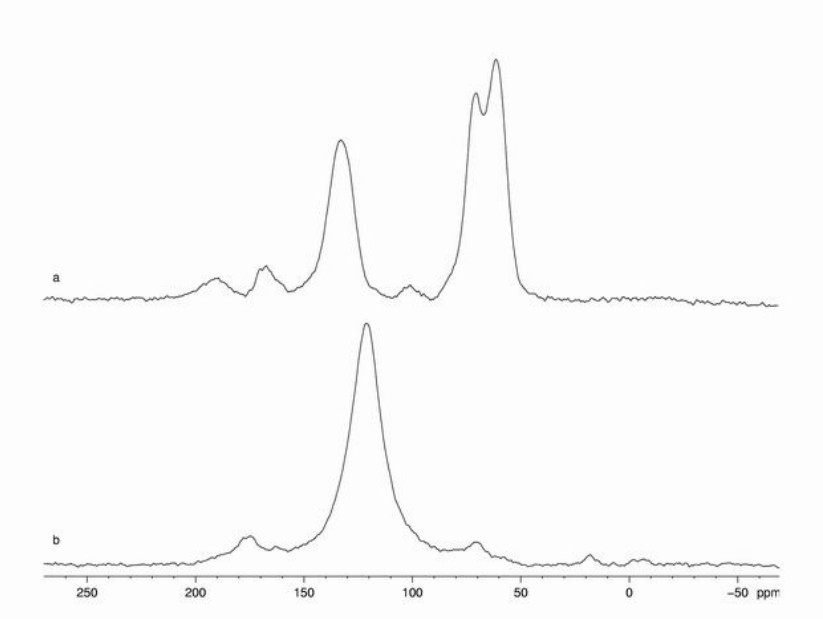

Figure 2.5 Effect of $NaBH_4$ treatment on GO. (a) Expanded plot of Figure 2.2a, direct ^{13}C pulse spectrum of GO. (b) Expanded plot of Figure 2.2b, direct ^{13}C pulse spectrum of CCG1.

The CP and direct ^{13}C pulse spectra of CCG1 show essentially complete elimination of all epoxides (60 ppm region), almost as large a decrease in the alcohol content (70 ppm region), complete elimination of all ketones (190 ppm region), the apparent elimination of all lactols (no shoulder recognizable in the 100 ppm region, much less intensity near 167 ppm), and the apparent elimination of any esters (again, much less intensity near 167 ppm). The intensity of a new signal at about 175 ppm in the direct ^{13}C pulse spectrum is clearly less than that of each of the carbonyl signals before $NaBH_4$ treatment. This new signal might result from aromatic carboxylic acids, which are known to give a signal in this region [benzoic acid in $CDCl_3$ at δ172.4 [300], *m*-toluic acid in $CDCl_3$ at δ172.8 [301], and biphenyl-2-carboxylic acid in $CDCl_3$ at δ174.1 (Spectral Database for Organic Compounds, SDBS http://riodb01.ibase.aist.go.jp/sdbs/cgi-bin/cre_index.cgi?lang=eng, compound #12557)] and to be resistant to reduction by $NaBH_4$ [302]. Any carboxyl signals in the precursor GO would be harder to recognize in the presence of other carbonyl groups and because the numerous hydroxyl and epoxy groups present in GO would presumably shift the carboxyl carbon signal from the region near 173-174 ppm typical of simple aromatic carboxylic acids. Treatment with $NaBH_4$ also generates some very shielded aliphatic signals whose origin is not clear.

In any event, the $NaBH_4$ reduction product CCG1 is considerably more like graphite, with a conductivity 200 times higher than the precursor GO. A spectrum similar to that given by sample CCG1 has been reported for a sample of GO reduced with $NaBH_4$ and then sulfonated[55]. The basic direct ^{13}C pulse MAS experiment can

detect all the carbons, while the basic ^{1}H-^{13}C CPMAS experiment detects only the carbons that experience a ^{1}H-^{13}C dipole-dipole interaction, i.e., carbons relatively near protons. In proton-rich solids, a ^{1}H-^{13}C CPMAS experiment with a contact time t_{cp} of about 1-2 ms can usually detect all the carbons with accurate relative signal intensities.[303] The CP experiment is normally the preferred experiment because less time is usually needed to obtain a CP spectrum with adequate S/N than to obtain a comparable spectrum by a direct ^{13}C pulse experiment.

However, in an ill-defined solid such as GO, the direct ^{13}C pulse experiment is clearly necessary as well. This is evident from a comparison of Figure 2.3a, Figure 2.3b, and Figure 2.3d; not only is a spectrum with higher S/N obtained in less time in the direct ^{13}C pulse experiment, but the relative signal intensities are clearly different than in the CP experiments, with some signals in the direct ^{13}C pulse experiment not even detected in the CP experiments. In the CP spectra, lengthening t_{cp} from 1 ms to 3 ms in an effort to allow carbons relatively far from protons more time to cross polarize clearly did not result in this happening. Indeed, the aliphatic signal is weaker with the longer contact time, indicating that ^{1}H spin-lattice relaxation in the rotating frame is relatively fast. Clearly, many carbons are too far from protons, including protons in relatively immobile water molecules intercalated between layers[31, 50] to be cross polarized efficiently or even at all. Cai *et al.* similarly noted that the direct ^{13}C pulse experiment on their sample of highly ^{13}C-enriched graphite oxide provided higher S/N than the CP experiment did.[16]

Therefore, the direct ^{13}C pulse spectrum of CCG1 is much more meaningful than the CP spectrum.

Subsequent treatment of CCG1 with H_2SO_4 increases the conductivity by another factor of 20 by eliminating the small amount of aliphatic functionality and leaving only graphitic sp^2 carbon and some carbonyl carbon in product CCG2 (Figure 2.2b). The carbonyl carbon is more evident in the CP spectrum. Acid treatment apparently caused the remaining tertiary alcohols to dehydrate to form alkenes that are part of a graphitic sp^2 carbon network with protons and carboxylic acid groups on the periphery. The treatment with H_2SO_4 results in a small additional upfield shift of the graphitic carbon signal (to 119 ppm), which also broadens noticeably, thereby reducing the S/N, even with many more pulses than in the corresponding spectrum of the $NaBH_4$ reduction product. Spectra similar to that given by sample CCG2 have been reported for a sample of GO reduced with $NaBH_4$, sulfonated, and then reduced with hydrazine[55] and for a sample of GO reduced with hydrazine hydrate[12].

Subsequent annealing of CCG2 in Ar/H_2 at 1100 °C for 15 minutes increases the conductivity by another factor of 12 and causes the sample (product CCG3) to behave very differently in the NMR magnet. More pressure than normal was required to spin the rotor, and tuning and matching the ^{13}C and ^{1}H channels in the probe proved much more difficult; indeed, the ^{1}H channel could not be adequately adjusted, as the tuning and matching adjustments needed exceeded the probe's range. Not surprisingly, the resulting CP spectrum was only noise (Figure 2.2b), and

the direct ^{13}C pulse spectrum exhibited only a broad, relatively weak signal shifted even further upfield, with a maximum at about 105 ppm (Figure 2.2b). Clearly, annealing generated a sample even more like pure graphite, for which sample spinning and probe tuning are even more problematic and for which a ^{13}C NMR signal cannot be obtained even in a direct ^{13}C pulse experiment.

Electrical conductivity of the reduced products is another important criterion to evaluate how the π conjugated system has been restored in this structure. Original GO is basically an insulator, with the conductivity around 0.5 S m^{-1}. The four orders of magnitude increase in conductivity after reduction here clearly indicates an efficient restoration of the π conjugated system in our product, induced by the de-oxygenation and dehydration. $NaBH_4$ de-oxygenation is necessary in our procedure, since in the control experiment when only concentrated H_2SO_4 was used, the conductivity obtained was only 46.4 S m^{-1}. Annealing of CCG2 at 1100 °C led to further increase of conductivity up to 2.02×10^4 S m^{-1}, which is on the same order of magnitude as graphite powder. The conductivity here was measured by a standardized "four-point probe" setup (Figure 2.6) in order to eliminate contact resistance, and each sample pellet was cut into rectangular shape and measured three times to get the average value.

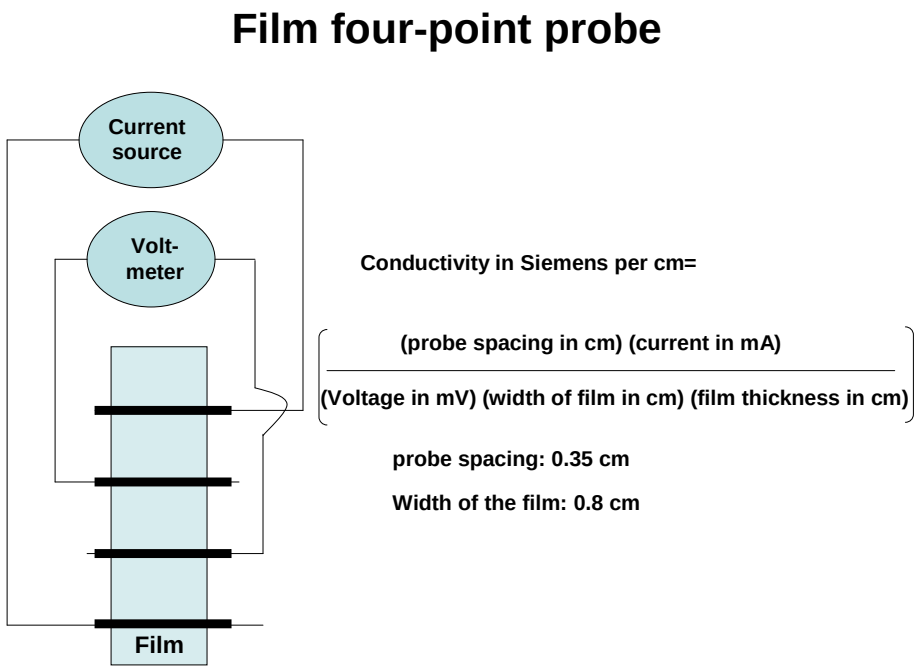

Figure 2.6 Film four-point probe setup for conductivity measurement.

Consistent with the ^{13}C NMR spectra, high resolution C1s peaks in XPS (Figure 2.7) also indicated good restoration of C=C bonds, as well as the existence of carbonyl groups in the final product. The original GO signal shows two separated peaks as expected, due to the high percentage of oxygen functionalities. After reduction, C=C bonds dominate, as shown as one single peak with small tails at the higher binding energy region. The small bump around 288.5 eV in the CCG2 curve is within the ketone and carboxyl carbon region. The π to π^* satellite peak around 291 eV was observed both in CCG3 and graphite powder curves, an indication that the delocalized π conjugation is restored in our sample.

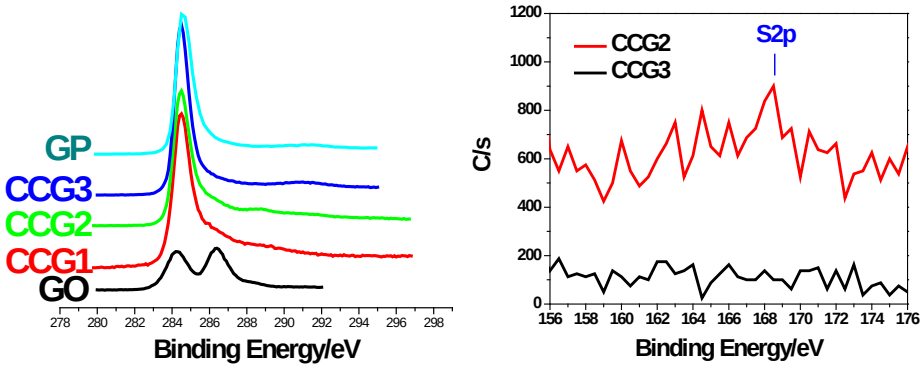

Figure 2.7 XPS characterizations indicate good restoration of the graphene structure, as well as little sulfur remaining in the final product. Left: XPS analysis of C1s in different samples. Each curve was obtained by 25 scans at high 3 sensitivity; right: XPS signal of Sulfur 2p from 156 to 176 eV (45° takeoff angle, 200 μm beam size).

Furthermore, the atomic composition (wt %) of all the samples was analyzed by both XPS and elemental analysis. Both Figure 2.7b and Table 2.1 show that there is little sulfur (< 0.518 wt%) or nitrogen (< 0.5 wt%) left in the final product CCG3, making our product distinct from the other CCGs, such as a hydrazine reduction product (N wt%~ 3.25%)[135] and sulfonation products (S mole% ~ 2.8%, N mole% ~3.2%)[55]. The oxygen percentage (12.68 wt%) in CCG2 is close to the value reported by others[55, 135]. Oxygen might be coming from two possible structures in CCG2: the chemically adsorbed water and the carboxyl functionalities remaining in this structure. After annealing, the oxygen content in CCG3 becomes less than 0.5 wt%, which is close to the value in graphite powder. In comparison, literature

reports show that when GO is directly annealed up to 1050 °C in Ar atmosphere, the oxygen content remains as high as ~ 9.3%.[304]

Table 2.1 Elemental analysis of GO and its reduction products. Performed by *Galbraith Laboratories, Inc*. C, H and N content was determined by combustion analysis, Na and B content was measured by ICP-OES/ FLAA/ GFAA/ ICP-MS, O content by pyrolysis, and S content by ASTM D4239 Method B/ D1552 (see www.galbraith.com for details). The atomic ratio of C/O and C/S was also calculated for each sample.

Sample	C/wt%	O/wt%	C/O	H/wt%	S/wt%	C/S	N/wt%	Na/wt%	B/wt%
GO	47.16	40.57	2.44[a]	2.68	1.20	105	<0.5	0.0152	<0.04
CCG1	69.66	19.43	4.78	1.63	<0.6	>310	<0.5	1.66	0.297
CCG2	81.54	12.68	8.57	0.94	0.715	304	<0.5	<0.0366	<0.1
CCG3	92.42	<0.5	>246	<0.5	<0.518	>476	<0.5	<0.0351	<0.09
GP	95.85	<0.5	>256	<0.5	<0.05	>5112	<0.5	<0.0191	<0.05

[a] Corrected for water content.

A TEM image of CCG2 was also obtained (Figure 2.8). Unfortunately but reasonably, most of the sheets aggregated into thicker flakes with a wide range of size distribution, ranging from 200 nm to 2 μm. Unlike the flakes that peel off from HOPG (highly ordered pyrolytic graphite), these sheets aggregated in a disordered manner; thus, on the periphery of these flakes, monolayer graphene sheets were frequently observed. The selected area electron diffraction pattern (Figure 2.8) here clearly indicated the graphitic crystalline structure. Furthermore, the relative intensity of the inner and outer circle spots turns out to be ~1, corresponding to a "single layer" graphene structure.

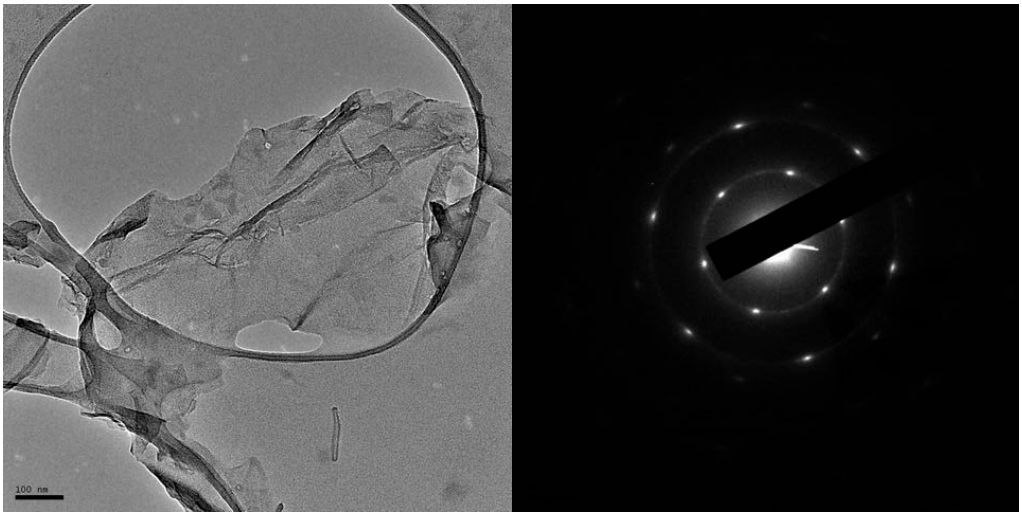

Figure 2.8 Left: TEM image of CCG2, in which scale bar is 100 nm; right: corresponding selected area electron diffraction pattern (SAED) taken at the relatively flat edge of the graphene sheet.

FT-IR spectra gave clear evidence for reduction. Spectra of GO, CCG1, CCG2, CCG3, and graphite powder are shown, after background subtraction for each spectrum, in Figure 2.9. The spectrum of GO shows significant bands around 1060 cm^{-1} ($\nu_{C\text{-}O}$), 1220 cm^{-1} ($\nu_{phenolic}$), 1370 cm^{-1} ($\nu_{O\text{-}H\ bending\ in\ tertiary\ alcohol}$), 1620 cm^{-1} ($\nu_{HOH\ bending\ in\ water}$) and 1720 cm^{-1} ($\nu_{C=O}$). After reduction, these signals decrease dramatically and are barely detectable. The inset shows expanded plots of the CCG2 and graphite powder spectra from 1400 to 1900 cm^{-1}. With a highly expanded vertical scale, the 1720 cm^{-1} peak is obvious in CCG2 when compared with the graphite powder signal. Virtually no signals for functional groups remain after annealing. Even though the material consists almost entirely of C=C bonds, the $\nu_{C=C}$ signal is extremely weak because most of these bonds are in essentially symmetrical environments, and thus the change in dipole moment is very small.

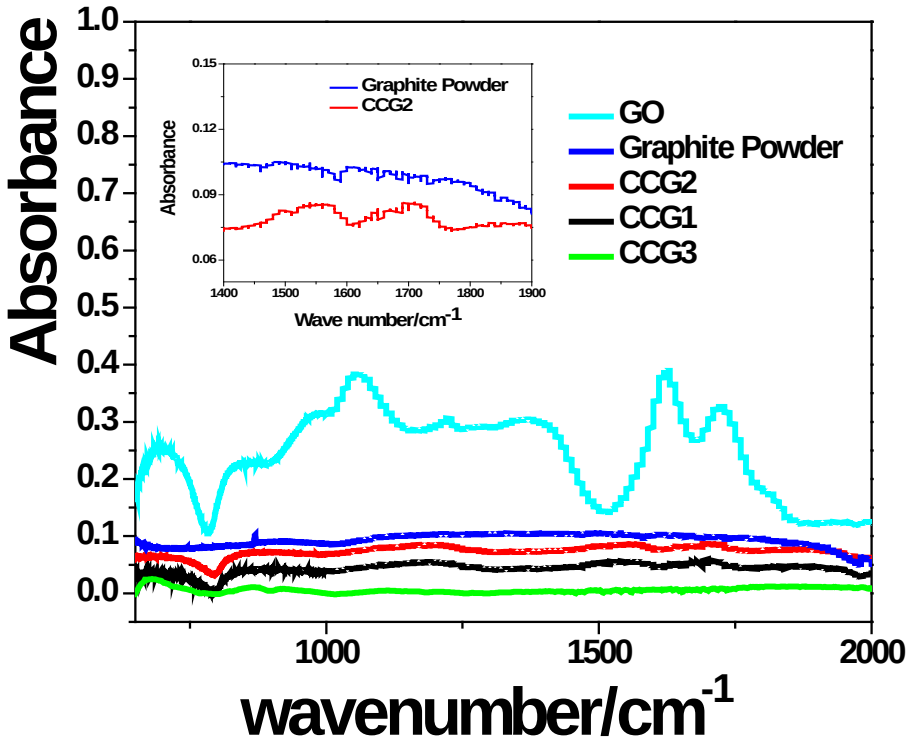

Figure 2.9 FTIR spectra of GO and reduction products. Attenuated Total Reflectance (ATR) mode is used, and all samples are in the solid state. The inset shows expanded plots of the CCG2 and graphite powder spectra from 1400 to 1900 cm^{-1}.

The interlayer spacing of GO changes from 8.8 Å in GO to 3.64 Å in CCG2, which is still a little larger than the *d*-spacing in graphite (3.36 Å) (Figure 2.10). The small amount of functional groups remaining might be the main reason for this difference. Meanwhile, annealing of CCG2 leads to a further decrease in *d*-spacing, and the product is almost the same as graphite at this point. The broadening of the

CCG3 peak indicates the smaller sheet size of the reduction products as compared to the original graphite powder and GO.

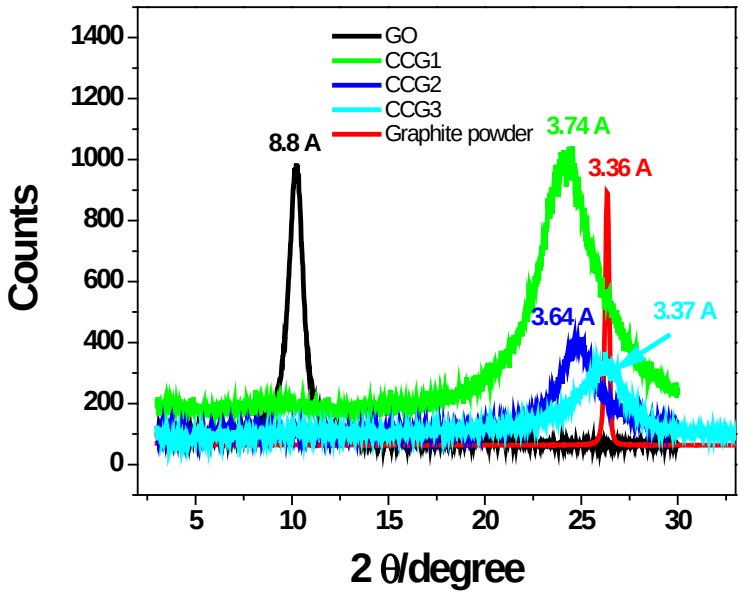

Figure 2.10 XRD data of GO and reduction products. Fixed Time mode, step size 0.02 degree, dwell time 1 second. Wavelength to compute *d*-spacing 1.54059 A, Cu/K-alpha 1.

Raman spectra show a decrease in the D/G ratio as well as a red shift of the G peak position from CCG1 to CCG3 (Figure 2.11 and Table 2.2). We noted a blue shift of D overtone peak position after reduction. The same phenomenon was observed by Ruoff et al[305]. However, when compared with the parent graphite powder, an obvious D peak, which corresponds to defects or edge areas, still exists in our final

product. These defects might be due to the smaller size of graphene sheets as well as the remaining functionalities.

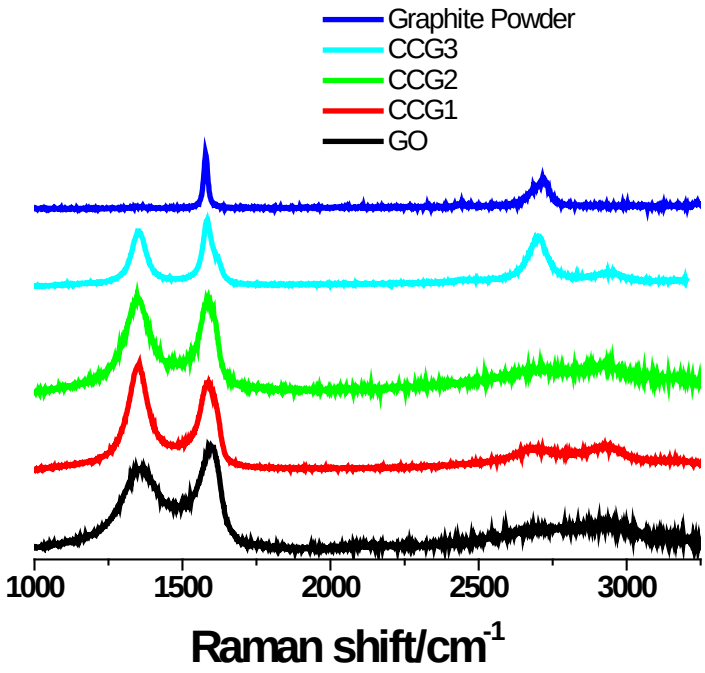

Figure 2.11 Raman spectra of GO and reduction products. (514.5 nm Laser beam, room temperature, solid samples on glass).

Table 2.2 Raman spectra analysis of GO and reduction products.

Sample	D position (cm^{-1})	G position (cm^{-1})	2D position (cm^{-1})	D/G	2D/G
GP	1353	1584	2715	0.20	0.70
GO	1350	1594	2681	0.95	0.27
CCG1	1349	1590	2702	1.91	0.31
CCG2	1347	1589	2709	1.00	0.34
CCG3	1346	1582	2706	0.82	0.76

TGA data of all the samples are available in Figure 2.12.

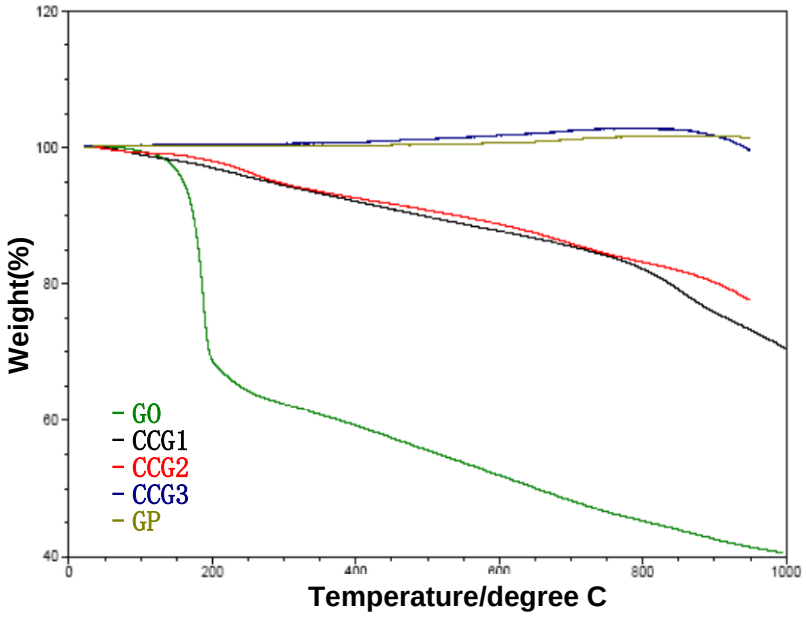

Figure 2.12 Decomposition behavior of GO, CCG1-3, and graphite powder (GP). The data were acquired with the following procedure: in Ar gas, equilibrium at 105 °C for 60 min to remove physically absorbed water, then cool down under N_2 gas, and heat at 5 °C/min to 950 °C under Ar again. Flow rate: 60

ml/min (For GO sample, the ramping rate is set to be 1 °C/min to avoid rapid volume expansion).

We were able to get stable suspensions of sample CCG3 in DMF. After 50 minutes' sonication, the suspension remained stable for at least several weeks. Figure 2.13 shows a comparison of solubility for GO and CCG3 in DI water and DMF separately. GO shows higher solubility in water, due to the hydroxyl, epoxy and carboxyl functionalities on its surface. After reduction, the product shows higher solubility in DMF than in water, which is reasonable, given its hydrophobic nature. This is quite different from CCGs reported in the literature[55, 135], as most of them maintain high solubility in water rather than in DMF. Tyndall scattering was shown by a red laser beam going through each suspension, as an indication of the colloidal nature of these mixtures.

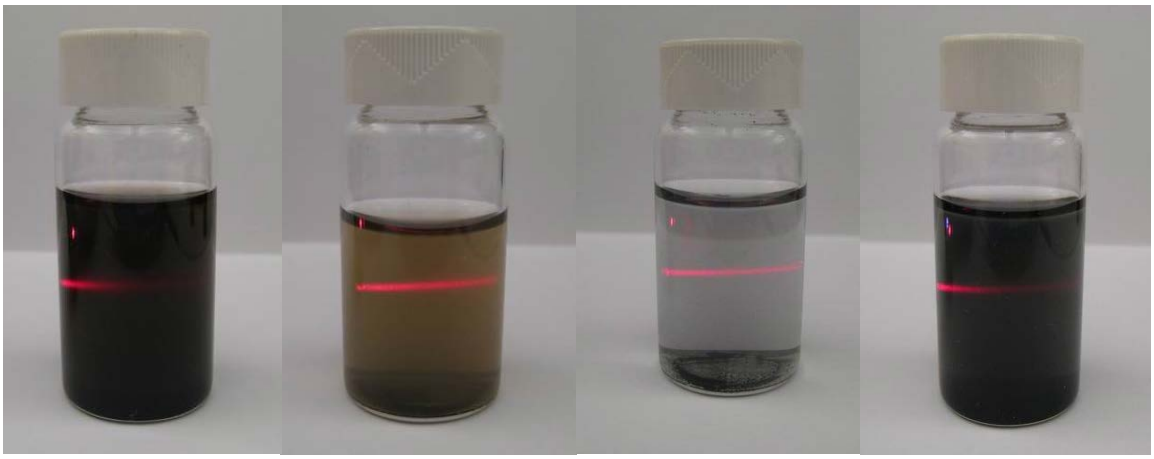

Figure 2.13 Solubility tests. From left to right: GO in DI water; GO in DMF; CCG3 in DI water; CCG3 in DMF after 50 minutes water bath sonication. A red laser

beam was put through dispersion to show the Tyndall effect of these colloidal solutions. Although GO is more soluble in water than in DMF, after reduction the product CCG3 is more soluble in DMF than in water. This is consistent with its hydrophobic nature.

2.4. Conclusion

In conclusion, interpreting solid state ^{13}C NMR spectra in the context of the major functional groups believed to be present in GO results in 6- and 5-membered-ring lactols along the periphery of the layers being proposed as the most likely functional groups responsible for the minor, but significant, signal near 100 ppm. 2-Hydroxynaphthalic anhydrides and 1,3-dihydroxyxanthones appear to contribute to only a very limited extent (if at all) to this signal. The functionalized anhydride could easily be accommodated along the periphery of a sheet, but a functionalized xanthone would require an interior defect site in the graphene structure in order to accommodate the 6-membered-ring ether functionality.

In principle, 1, 3-dihydroxyxanthones and 2-hydroxynaphthalic anhydrides could be differentiated from lactols through a 2D solid state ^{13}C NMR experiment detecting scalar-coupled pairs of ^{13}C nuclei[306-310]. 1,3-Dihydroxyxanthones and 2-hydroxynaphthalic anhydrides would exhibit a distinctive coupling between the carbonyl carbon and the adjacent enolic carbon (at about 100 ppm), while lactols would exhibit a coupling between the O-C-O carbon (at about 100 ppm) and the two adjacent non-carbonyl carbons. Such an experiment would require preparing GO

with ^{13}C-enriched graphite[16] and appears to be the most secure method[306] for definitively assigning the signal near 100 ppm.

In this context, it is worth noting that a ^{13}C-^{13}C dipolar recoupling experiment (i.e., exploiting through-space rather than through-bond coupling) applied to ^{13}C-enriched GO[16] demonstrated the spatial proximity of the ^{13}C nuclei giving signals at about 101 ppm to the ^{13}C nuclei giving signals at 60-70 ppm. [An epoxide group adjacent to a lactol would apparently have essentially no effect on the lactol O-C-O chemical shift.] However, the dipolar recoupling experiment did not detect any signals that could provide information on the spatial environment of the signals with comparable intensities at 169 and 193 ppm, which led the authors to conclude that these ^{13}C nuclei "are spatially separated from a majority of the sp^2, C-OH, and epoxide carbons."[16] It is hard to envision just what the environment of these nuclei would then be. Indeed, Cai *et al.* concluded that "Further studies would be needed to define all of the structural details of the system."[16]

The 2D solid state ^{13}C NMR experiment detecting scalar-coupled pairs of ^{13}C nuclei might also provide information on the functional groups near the ketone carbonyl carbon believed to be responsible for the signal at 191 ppm and on the functional groups near the carbonyl groups responsible for the signal at 167 ppm. In general, this experiment could potentially better define the structure of GO by providing much information on the specific types of functional groups on the periphery of the GO sheets, which is clearly important since about 11% of the carbon is in the signals near 100, 167, and 191 ppm. Still, even with this uncertainty

as to some of the structural details, our two-step reduction strategy yields nearly pure graphite that is highly conductive, has very few functional groups and no polymer coating, and is DMF soluble. This procedure offers an alternative way for large scale graphene production for applications that require such material.

Chapter 3 **Graphite Oxide Derivatives as Adsorbents for Water Purification**

Retaining the inherent hydrophilic character of GO nanosheets, sp^2 domains on GO are covalently modified with thiol groups by diazonium chemistry. The surface modified GO adsorbs six fold higher concentration of aqueous mercuric ions than the unmodified GO. 'Core-shell' adsorbent granules, readily usable in filtration columns, are synthesized by assembling aqueous GO over sand granules. The nanostructured GO-coated sand retains at least five fold higher concentration of heavy metal and organic dye than pure sand. The research results could open avenues for developing low-cost water purification materials for the developing economies.

3.1. Introduction

Graphene - a flat, sp^2 hybridized, two-dimensional (2D), honeycomb arrangement of carbon atoms with single carbon atom thickness - is expected to have far reaching consequences in not only understanding the fundamental aspects of these materials but also realizing real time applications[311]. Production of graphene through wet chemical oxidation of graphite to GO has become a popular method and a primary factor for an overwhelming interest in this new material. The oxygenated functional groups such as carboxylates, and lactols primarily lie at the edge of the nanographene sheets while the basal planes contains sp^2 hybridized graphene-domains along with some epoxy and hydroxyl groups. While the oxygen functional groups impart hydrophilicity[135], the graphene domains render hydrophobic character to these amphiphilic GO particles[56]. Consequently, GO is soluble in several polar and non-polar solvents including water but suffer from breakdown of electrical conductivity. The conductivity can be restored to a certain extent by thermal or chemical reduction of the oxygen functionalities, although such treatments also increase the hydrophobicity[17]. Nevertheless, the intrinsically large surface area of GO have found niche in electrochemical energy storage devices [312], hydrogen storage [313] and catalysis[314].

Historically, water purification technologies have utilized high surface area carbon materials in the form of activated carbon for decolorization[315] and heavy metal ion[316] retention. Compared to these materials, GO is produced by room temperature wet-chemical procedures and is likely to be cost-efficient. Only recently

has a report on magnetite-graphene hybrid materials for magnetically controlled speciation of arsenic[317] from water been published. The possibility of harnessing this readily available and inexpensive material has been relatively unexplored. In this article, we report key surface modification approaches and post-synthesis assembly steps which will enable exploitation of GO as a novel material for low-cost water purification processes.

Several protocols, including the versatile diazonium grafting chemistry [318], are reported for chemical derivatization of graphene nanosheets; however, these approaches target the electrically conductive and relatively hydrophobic end-product. The low accessibility of water molecules in these hydrophobic materials will reduce the ability of GO to sequester water soluble contaminants such as heavy metals. We therefore, covalently modify GO nanosheets with complexing groups without compromising its inherent hydrophilicity. This is achieved by covalent grafting of aromatic thiol groups on the remaining electron rich sp^2 carbon domains of GO, without using the chemically reduced intermediate.

Sand - an abundant natural resource of earth - is widely used for processes of the magnitude of municipal water supplies to small domestic water filters, particularly as packed bed filters. In History, affordability and the granular nature of sand that forms filter beds have popularized sand-filtration (SF). Indeed, early Indian and Greek writings dating back 6000 years refer to sand- and gravel-filtration as means to securing clean water [319] and currently is a water purification process endorsed by the World Health Organization [320]. Of the two

broad classifications of SF, fine-SF has higher retention of pathogens, organic matter, and heavy metal ions but has low throughput. Although the production rates are higher for the more popular coarse-SF, the absence of functionality and nanostructures limit pathogen, organics and heavy metal ions retention [320]. We demonstrate a simple technique for conversion of regular filtration sand into 'core-shell' GO coated sand (GO_{sand}) granules by assembling water dispersible GO on sand grains. Two model contaminants namely mercuric ions and a bulky dye molecule (Rhodamine B) are utilized to quantify the effects of the nanostructured GO coating for improvements to the well-established coarse sand-filtration process.

3.2. Experiments

3.2.1. Preparation of GO Dispersion

The GO is prepared according to the modified Hummers method that has been reported previously[11] and utilizes graphite powder purchased from Bay Carbon, Inc (SP-1 grade 325 mesh). In detail, concentrated H_2SO_4 (50 ml), $K_2S_2O_8$ (10 g) and P_2O_5 (10 g) are mixed in a 2 L Erlenmeyer flask and heated to 80 °C with a hotplate. 12 g of graphite powder (purchased from Bay Carbon, Inc. SP-1 grade 325 mesh) is added to the mixture under strong magnetic stirring for 4.5 hours. After that, 2 L of deionized (DI) water is added to the suspension (initially, water is added very slowly to avoid large amount of heat from the dilution of H_2SO_4). After dilution, the mixture is left overnight and then filtered through a 0.1 micron Teflon Millipore membrane; the filter cake is allowed to dry in air overnight. On the second

day, the filter cake is slowly dispersed into 0.46 L concentrated H_2SO_4 in a 4 L Erlenmeyer flask in an ice bath (keep temperature as low as 0 °C) with stirring. 60 grams of $KMnO_4$ was slowly added to the flask with stirring, during which the temperature of the mixture is carefully controlled not exceeding 10 °C. The dispersion is kept at 35 °C for 2 hours and then diluted with 900 ml of DI water. (Water should initially be added slowly to avoid rapid heating. During the whole process, the temperature is controlled below 50 °C.) Subsequently 2.8 L of DI water is added over 2 hours with continuous stirring, giving a brownish dispersion. Immediately after finishing dilution, 50 ml of 30 % H_2O_2 is slowly added to the dispersion, leading to tremendous bubbling as well as an obvious color change from brown to bright yellow. The mixture is left untouched for at least two days and then filtered through a 0.1 micron Millipore Teflon membrane, and washed with 10 % HCl and 5 L DI water sequentially. The final filter cake is left to dry in air and then kept in desiccators with P_2O_5. The GO product can be easily dispersed in water by mild sonication.

3.2.2. Preparation and Characterization of GO_{SAND}

Filpro-sand was a gift from US Silica Company. It was washed with 10 % HCl before use. 10 grams of clean sand was put in a Petri dish, with 10 ml 0.35wt% of GO/DI water dispersion, and heated up to 150 °C in a vacuum oven for two hours. The process could be repeated to increase the GO-coating thickness on sand. SEM and EDAX data were obtained on Hitachi SEM S-5500, with 4,000-fold magnification and 7100 nA emission current. TGA experiments were executed on the Q-600

Simultaneous TGA/DSC from TA Instruments under 100 ml/min Ar. Raman spectra were characterized with the Renishaw Raman instrument (514.5 nm Laser beam, 50 % power, room temperature, solid samples on glass).

3.2.3. Batch Adsorption Tests on GO and Column Tests on GO_{SAND}

For the batch tests, about 20 mg GO is added to 20 mL of 200 ppm Hg^{2+} solution while the pH of the solution was adjusted to 2.0. To facilitate thorough mixing the solution was mildly sonicated for 20 mins, then allowed to cool to room temperature and finally equilibrated for 24 hours at room temperature. The solution is separated from the solid by syringe filtration. The adsorption isotherm was obtained by changing the concentration of Hg^{2+} solution in the range of 4 ppb-4000 ppm and repeating the experiment under similar conditions.

For the column tests, a filtration column (6.6mm dia. x 400mm long) was filled with GO_{SAND}, and the feed solution was flowed through the column at controlled flow rate, the eluted solution was collected at specific time intervals, and concentrations of all the eluates were determined by ICP-MS analysis for mercury ion or by UV-Vis spectrometer for Rhodamine B. For mercury, the feed solution was 400 ppb mercury(II) nitrate solution in 1% nitric acid, and flow rate was 1.000 ml/min. For Rhodamine B, the feed solution was 10 ppm Rhodamine B in DI water, and flow rate was 1.000 ml/min.

3.2.4. Functionalization of GO by Diazonium Chemistry

The involved diazonium precursor here is 4-aminothiophenol. In detail, 12 mmol 4-aminothiophenol was added to 15 ml 1N HCl, gently heated to 53 °C while stirring (solution 1). 12 mmol $NaNO_2$ was dissolved in 20 ml DI water, cooled down in an ice bath, and then added dropwise to the solution under constant stirring. The resulting solution was separated equally into two batches, and to each batch, a certain amount of GO (500 mg in 100 ml DI water) and reduced GO (RGO) (240 mg in 1 wt% aqueous sodium dodecylsulfate (SDS)) was added, and the reaction was kept in an ice bath with gentle stirring overnight. The product was separated by filtration, washed with acetone, ethanol and copious amount of DI water. The resulting filter cake was re-dispersed in DI water and dialyzed in Cellu Sep membrane (H1 high grade regenerated Cellulose Tubular Membrane, Pore size 5,000) against DI water for over a week.

3.3. Results and Discussion

3.3.1. Adsorption on GO and f-GO: NMR Characterization and Batch Tests

GO is synthesized by exfoliation and chemical oxidization of graphite [14]. Recent solid state ^{13}C NMR [17]has shown that about 60% of the carbon atoms in GO are sp^3 hybridized and oxidized, mostly in the form of alcohols and epoxides but also as lactols, while the remaining 40% of the carbon atoms remain sp^2 hybridized,

mostly as unfunctionalized alkene or aromatic carbons but also as carbonyl groups in lactols, esters, acids, and ketones. The oxygen containing functional groups while imparting hydrophilicity can also exhibit limited complexing capacity with mercuric ions[321]. Figure 3.1a shows magic angle spinning (MAS) ^{13}C NMR spectra of GO before and after Hg^{2+} adsorption. Small spectral changes occur upon complexation of Hg^{2+}, presumably because Hg^{2+} is not directly bound to carbon in carboxylates and alkoxides and thus has only a modest influence on the ^{13}C chemical shifts, as shown by the similarity of the carbonyl carbon chemical shifts in phenylmercuric benzoate [322]and phenyl benzoate [323] and by the similarity of the carbonyl and methyl carbon chemical shifts in mercuric acetate [324], cyclohexylmercuric acetate [325]phenylmercuric acetate[322], and acetic acid[326]. Limited experiments performed so far indicate that the adsorption behavior of Hg^{2+} ions on the native GO nanosheets can be represented by Langmuir type adsorption models (Figure 3.1b and c).

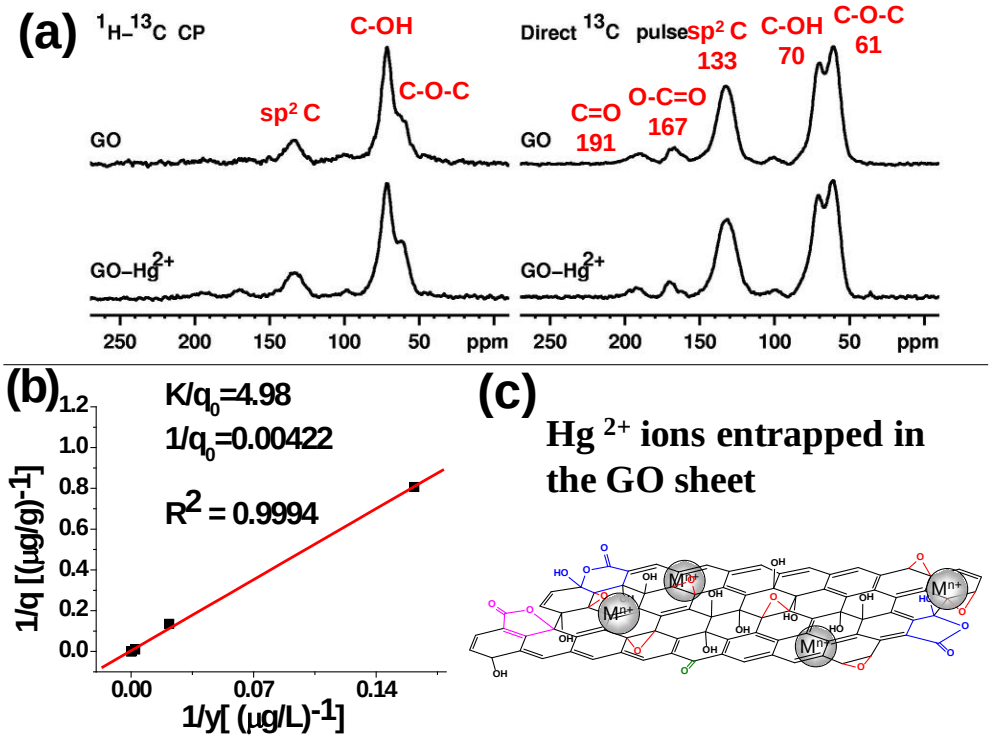

Figure 3.1 Adsorption of Hg^{2+} on GO. (a) Left: MAS ^{1}H-^{13}C cross polarization spectra before (top) and after (bottom) adsorption. Right: MAS direct ^{13}C pulse spectra before (top) and after (bottom) adsorption. b) Adsorption isotherm of GO toward mercuric ion. *q* and *y* refer to mercuric concentration in adsorbent and feed solution, respectively. c) Schematic of interaction between GO and mercuric ions.

Covalent modification of porous materials with complexing groups such as thiol (SH) [327] can significantly increase the adsorption efficiency. The Tour group has investigated the grafting of aromatic diazonium compounds for covalent modification of RGOs [133, 328]. But RGO is hydrophobic and has limited access to water molecules. The diazonium grafting chemistry, nevertheless, provides a means to modify electron rich graphene domains by carbon attachment to the nanosheets.

We performed a direct diazonium grafting without the intermediate reduction step in order to retain the available hydrophilic groups (see Figure 3.2(a)) and to modify the remaining sp^2 carbon domains. The strong increase in the intensity of the aromatic/alkene carbon region (~110-150 ppm) in the ^{1}H-^{13}C CP and direct ^{13}C pulse spectra of the product (GO-SH) in Figure 3.2(a) shows that covalent modification of GO occurred.

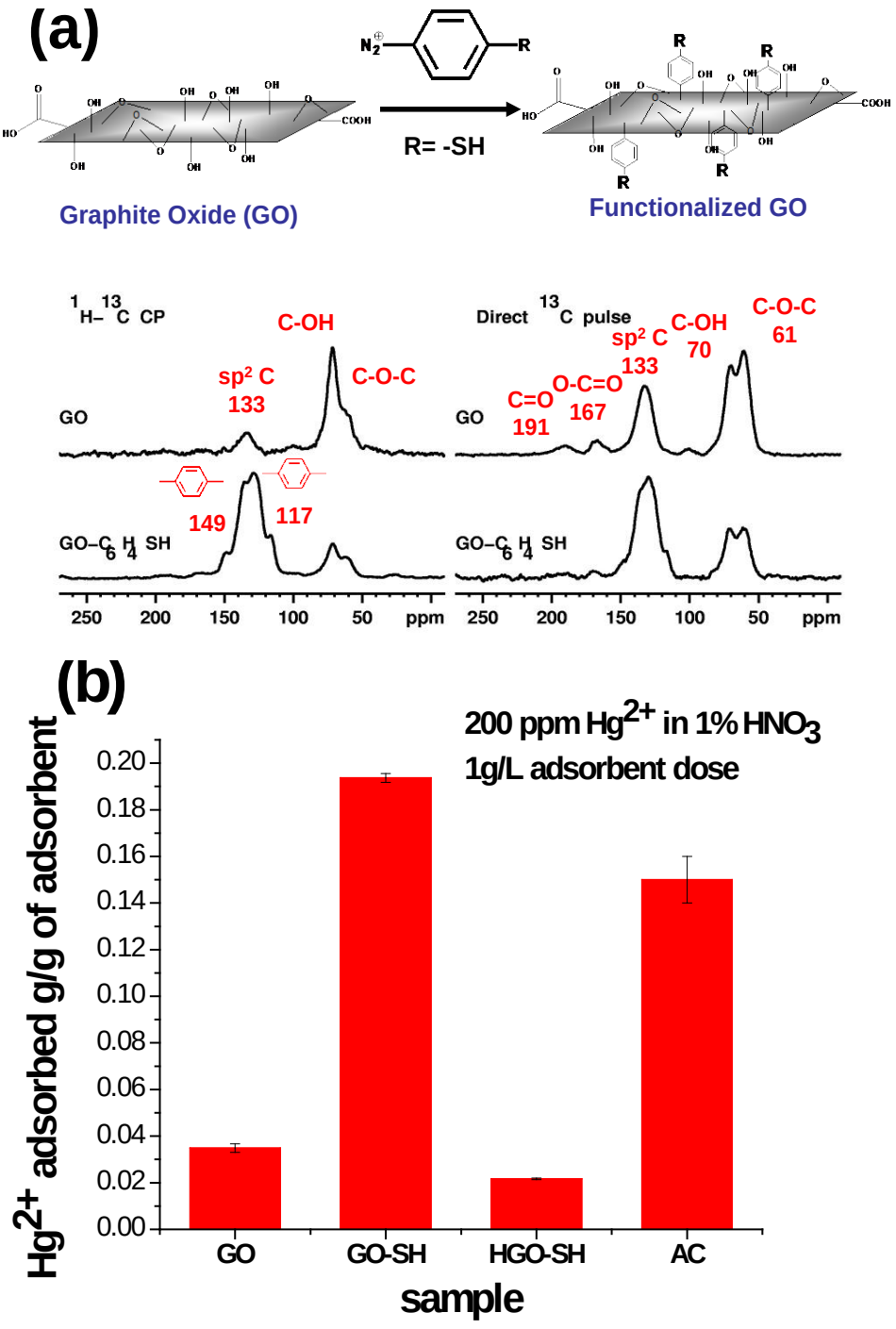

Figure 3.2 (a) Schematic of functionalization chemistry on GO, and corresponding NMR analysis of the functionalized product. (b) Batch tests of functionalized material for mercuric ion adsorption. The NMR spectra support

the functionalization chemistry by the increased intensity in the aromatic region (around 130 ppm).

Additional support for this conclusion is provided by dipolar dephasing experiments (Figure 3.3), which show a significant decrease in signal intensity in the aromatic/alkene region attributed to the elimination of the aromatic C-H signals. In contrast, the signal intensity from the quaternary aliphatic carbon atoms in the alcohol/epoxy region is, as expected, essentially unchanged.

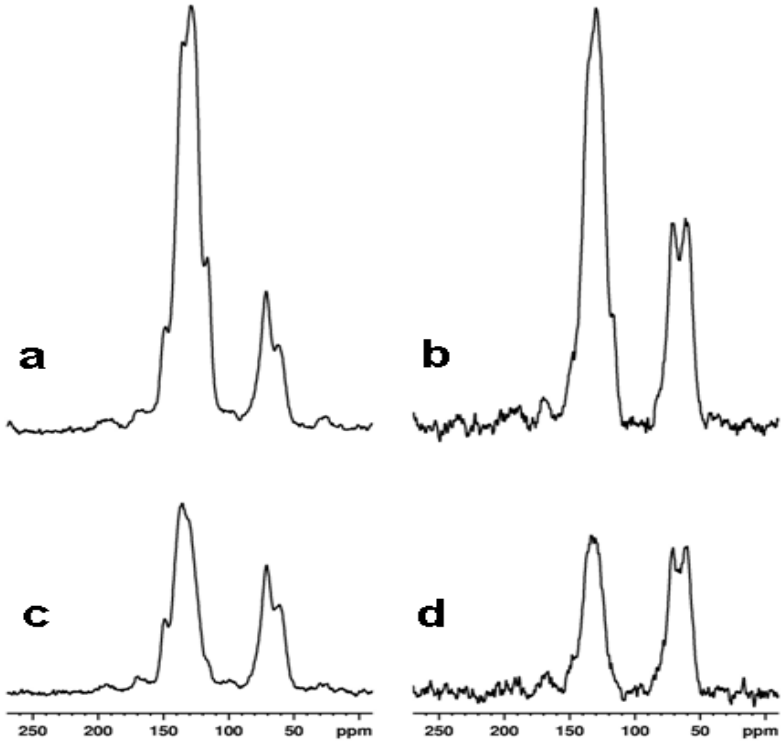

Figure 3.3 MAS ^{13}C NMR spectra of GO- SH: (a) ^{1}H-^{13}C CP spectrum. (b) as in (a) but with a 50-μs dephasing interval preceding FID acquisition. (c) Direct ^{13}C pulse spectrum. (d) as in (c) but with a 50-μs dephasing interval preceding FID acquisition.

A comparison of the abilities of various GO and the functionalized GO systems to adsorb Hg^{2+} is shown in Figure 3.2(b). Adsorption experiments were undertaken with ~ 200 ppm Hg^{2+} solution, acidic pH, and 1 gm/l of adsorbent dosage. While RGO-SH (thiol groups attached to GO with the intermediate reduction step) did not improve over the non-functionalized GO, a significant increase (~ 6 fold) was observed for the GO-SH material. More specifically, the Hg^{2+} uptake capacity of GO is ~0.03 gm/gm of adsorbent, which can be increased to ~ 0.2 gm/gm for GO-SH. These results conclusively show that this route of derivatization of GO creates a novel hydrophilic material with enhanced heavy metal removal efficiency. Under similar conditions, Mohan et al. reports in figure 1 of his article, an uptake of 0.15 gm of mercury/gm (AC in Figure 3.2(b)) of activated carbon formed by high temperature pyrolysis[316]. Compared to the above cited report, these tailored GO-SH material have better performance, but their capacities are lower than the self-assembled monolayer functionalized mesoporous silica (~ 0.05-0.3-gm/gm) discovered in the late 1990s [329] and currently being commercialized. We believe that more efficient adsorbent systems can be created using similar derivatization approaches to modify the sp^2 graphene domains of the GO nanosheets.

3.3.2. A Novel 'Core-shell' Adsorbent System and Implications to Sand Filtration

Packed bed columns are the preferred mode of operation in most water-purification systems owing to their simplicity and rapid kinetics [330]. We show a

simple assembly process (see Figure 3.4) for conversion of conventional sand granules to a 'core-shell' adsorbent granules in which the GO coating imparts nanostructural features on the surface of sand granules. The assembly process essentially consists of physical mixing of the water dispersible GO colloids with sand, followed by a mild heat treatment that causes the nanosheets to adhere to each other over the sand surface, likely through van der Waals interaction.

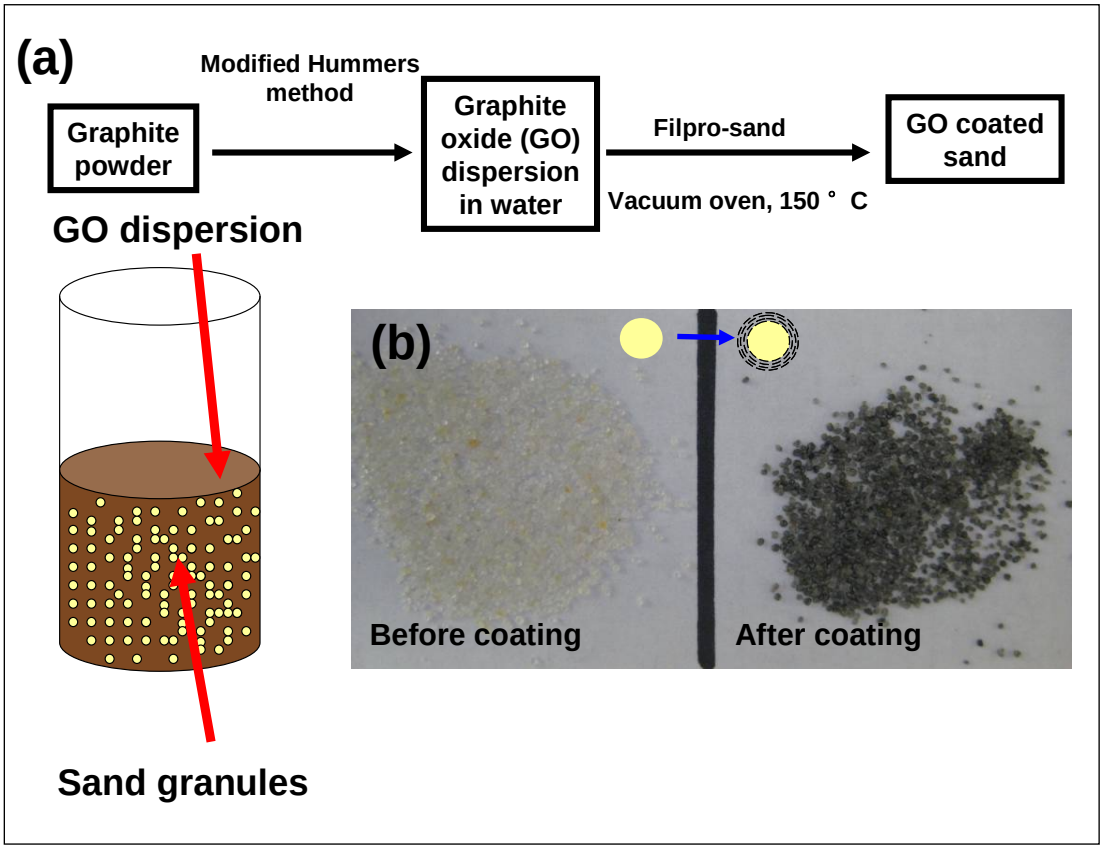

Figure 3.4 (a) Flow chart and schematic illustration of preparation of GO_{SAND}™; and (b) photographic images of sand and GO_{SAND}™ product. Inset: Idealized schematic of conversion of regular sand to GO_{SAND}™.

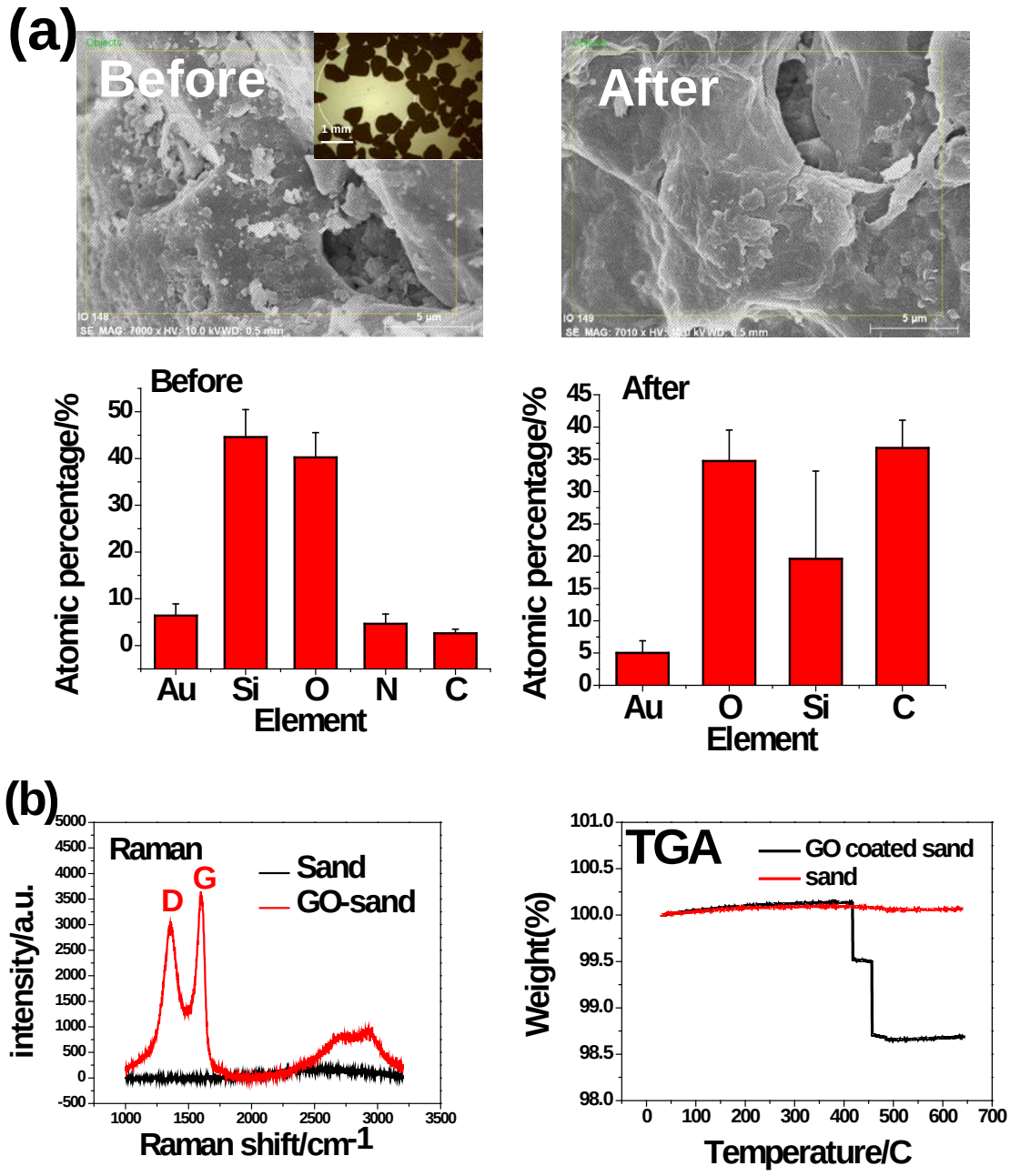

Figure 3.5 (a) Photographic images and EDAX analysis of sand and GO_{SAND}. EDAX analysis from the surface of the grains clearly showed a significant increase in carbon content. (b) Clearer evidence for coating from Raman spectra, and estimation of the coating thickness from TGA data.

Easily apparent in the photographs of Figure 3.4(b) is the change in color from yellowish white to blackish grey after the coating process. In the inset of Figure 3.4 (b) is shown the idealized schematic of the many-layer GO coating and the resultant GO_{SAND} filtration granules. Because the small field-of-view of the SEM does not allow us to discern the coating on the mm-scale granules, and because there is lack of contrast between the sand and the heavily oxidized carbon particles, we resorted to EDAX analysis (see Figure 3.5(a)) at different locations on the surface of the sand granules. A typical elemental composition of the sand granules is compared to GO_{SAND} granules which demonstrates a large (~ 30 %) increase in carbon abundance and hence the presence of a carbon coating. We note that these results do not confirm that the coating is conformal as idealized in inset of Figure 3.4(a), but is likely to coat majority of the surface of individual sand granule. This many-layer GO coating can additionally be confirmed with Raman spectra as well as its thickness estimated by TGA (Figure 3.5(b)). Prominent D (1359 cm-1) and G (1598 cm^{-1}) peaks, consistent with the GO Raman data reported previously[17], are observed from GO_{SAND} sample, while barely any features are obtained from pristine sand spectrum. Shown in Figure 3.5(b) right is typical TGA data for GO_{SAND} showing a weight loss of ~1.5% contrasted with that of sand. The thickness can be estimated from this weight loss data, the size of the sand granules (measured) ~ 597 μm (Figure 3.6), density of sand (~ 2 g/cm^3) [331], and the density of GO (~ 1.68 g/cm^3) [332]. This thickness can be adjusted by changing the concentration of GO solution

or repeating of the vacuum heating process and in our typical experiments vary from ~0.15 to 1.5 μm.

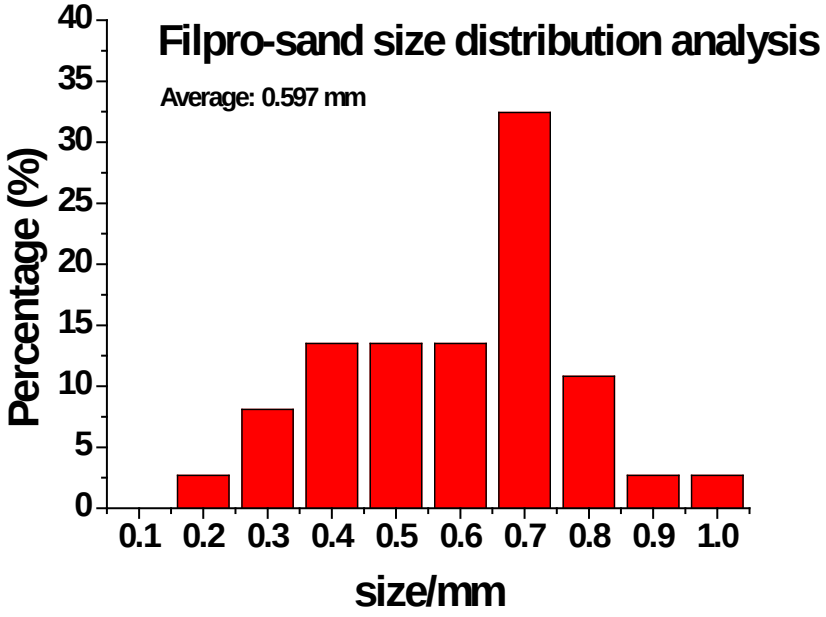

Figure 3.6 Filpro-sand size distribution analysis. Mean size: 0.597 mm.

This novel GO-coated sand material easily fills the filtration column (see Figure 3.7(a)) and can be used in typical packed-bed experiments. We have utilized two model contaminants: Hg^{2+} (400 ppb in 1% HNO_3) and Rhodamine B dye (10 ppm) to experimentally measure the adsorption breakthrough of GO_{SAND} and to compare it with sand. While the adsorption capacity of sand granules towards Hg^{2+} (Figure 3.7(b)) was saturated within ten minutes of filtration, the GO_{SAND} maintained the adsorption capacity for more than fifty minutes of fluid flow. The treated water had less than 1 ppb of Hg^{2+}. Similar results were also obtained for the dye molecule,

where the dye molecule evolves through the GO_{SAND} column after 100 minutes, whereas it is after 20 minutes that the dye evolves in the sand column. We have checked the possibility of solubilization of GO by attaching a piece of filter paper on top of the column. After a series of column filtration experiments running 2-3 hours, we did not observe any precipitation on the paper evidencing the stability of the GO sand composites.

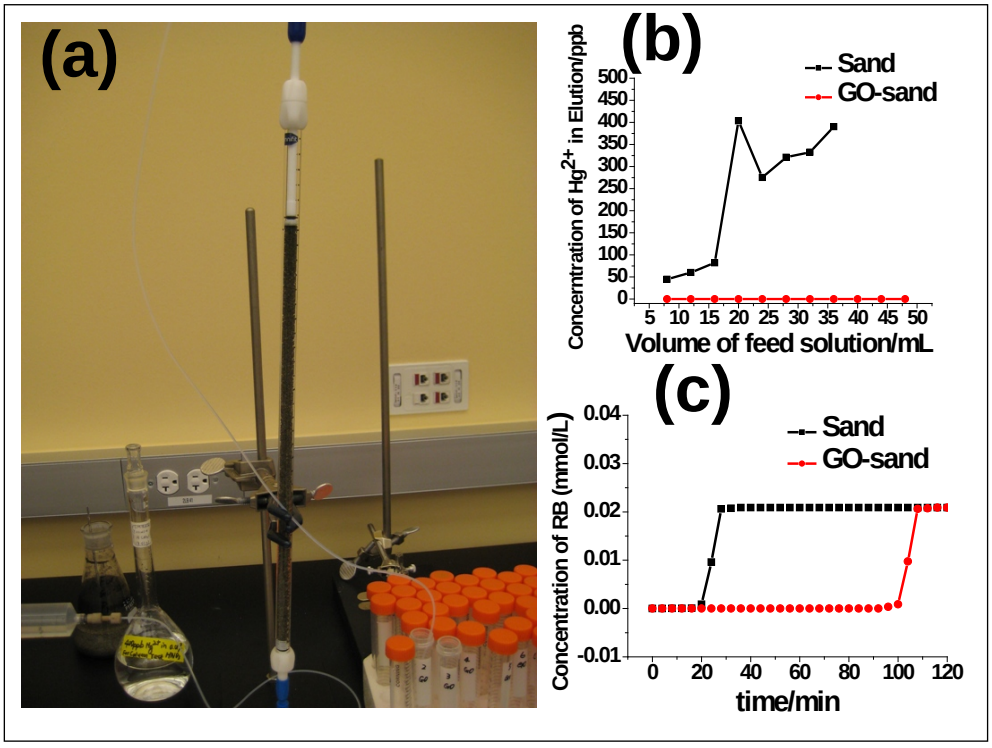

Figure 3.7 Photographic images of adsorption column using GO_{sand} granules (a) and column test results for removal of Hg^{2+} (b) and Rhodamine dye B (c). Feed solution: 400 ppb Hg^{2+} in 1 % HNO_3 for (b) and 10 ppm (~ 0.02 mmol/L) Rhodamine B in DI water for (c). Flow rate: 1 ml/min. Column height: 400 mm; Column diameter: 6.6 mm.

We were also interested in comparing the performance of GO_{SAND} with activated carbon granules (Darco, 400-800 micron). We note that a large dye molecule will have high diffusion resistance inside the granules and consequently observe that the 'core-shell' GO_{SAND} granules with micron thick coating on ~ 600 micron sand granules perform comparably to the commercially available ~ 600 micron activated carbon granules.(Figure 3.8). We are investigating the diffusion mechanisms in these 'core-shell' filtration granules that is likely to overcome the intra-granular diffusion limitations in more conventional adsorbents[321]. Nevertheless, the experimental evidences imply that this novel 'core-shell' adsorbent system can sequester heavy metal or organic contaminants at five fold higher capacity than regular sand and its performance is comparable to some commercially available activated carbon. We are currently investigating strategies that will enable us to assemble functionalized GO particles on the sand grains to further enhance contaminant removal efficiencies.

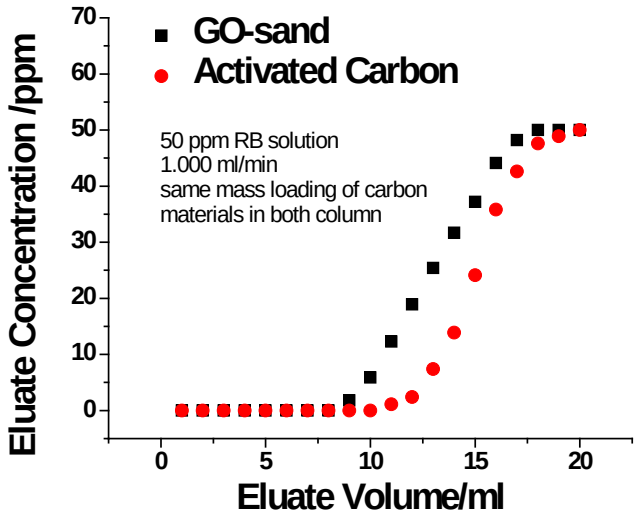

Figure 3.8 Column test results for Rhodamine B removal with GO $_{SAND}$ and activated carbon. Flow rate: 1 ml/min. Column height: 400 mm; Column diameter: 6.6 mm.

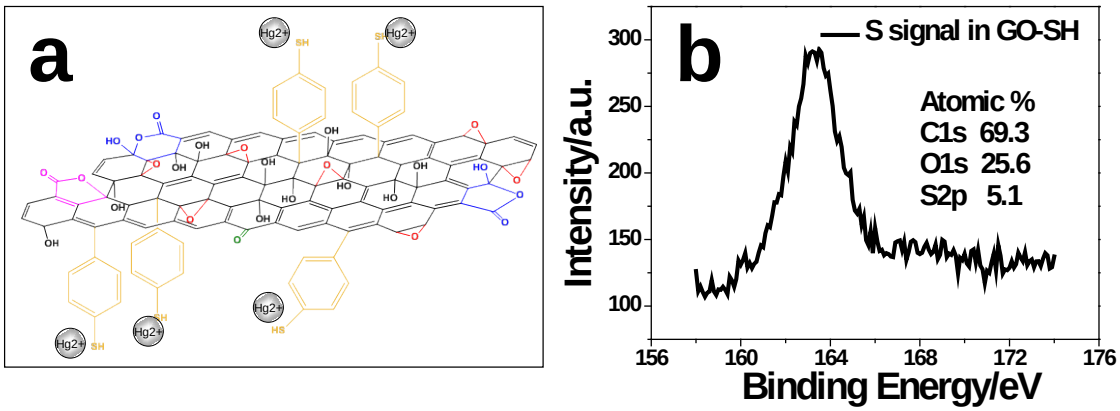

Figure 3.9 a) Schematics of interaction between f-GO and mercuric ions. b) X-ray Photoelectron Spectroscopy (XPS) analysis of GO-SH sample. The carbon the sulfur atomic ratio is 13.5:1, indicating high degree of functionalization. It has been reported earlier that sulfur content is around 1.20 at% in GO[17].

3.4. Conclusion

We have employed a surface modification technique, originally utilized for functionalization of chemically reduced and hydrophobic graphene nanosheets, to synthesize hydrophilic GO nanosheets containing covalently attached thiol groups. The modification is affected through carbon-carbon attachment of benzene-thiol groups to the sp^2 lattice within the nanosheets, as confirmed by NMR spectroscopy. We therefore demonstrate that the intermediate chemical reduction step isn't necessary for the diazonium chemistry and that the GO nanosheets retain significant electron-rich sp^2 domains that can be utilized for grafting additional complexing groups. This modification results in around six fold increase in adsorption capacity of mercuric ions.

Water soluble GO, prior to chemical modification, can be assembled on sand to create novel 'core-shell' granules that find use in filtration columns readily. We conclude that the nanostructured GO coating can significantly increase the retention of heavy metals and organic dye over the parent sand granules.

Thus suitably engineered GO, particularly derived from natural graphite, can improve existing processes and spawn low-cost water purification technologies suited for the developing economies.

Chapter 4 **Direct Writing of Supercapacitors on Graphite Oxide Films**

Microscale supercapacitors provide an important complement to batteries in several applications of power delivery including electronics. While they can be manufactured with a variety of printing and lithography techniques[333-335], continued improvements in cost, scalability and form factor are required to realize their full potential. Here we demonstrate the scalable fabrication of a new type of all-carbon, monolithic supercapacitor by laser reduction and patterning of GO films. We pattern both in-plane and conventional electrodes consisting of RGO with micron resolution, between which GO serves as a new type of solid electrolyte[11, 14, 17, 336-338]. Substantial amounts of trapped water in GO makes it a simultaneous good ionic conductor and an electrical insulator, allowing it to serve as both an electrolyte and an electrode separator with ion transport characteristics similar to that observed for Nafion membranes [339, 340]. The resulting micro-supercapacitor devices show good cyclic stability, and energy storage capacities comparable to existing thin-film supercapacitors[333].

4.1. Introduction

In recent times GO has attracted attention since it offers a low-cost, scalable and wet-chemical approach to graphene [16, 86, 341-343]. The conductivity of GO, dominated by ionic conductivity, depends on the environment and varies from 5E-6 S/cm to 4E-3 S/cm[17, 84] suggesting that GO is close to electrical insulating. We demonstrate here that with water entrapped during processing or absorbed on exposure to environment or moisture, hydrated GO offers very interesting applications in energy storage devices. The substantial amount of entrapped water in the layered GO structure[336] makes it a strongly anisotropic ionic conductor but an electrical insulator, allowing its use as a viable electrolyte and electrode separator. The ability to laser-reduce GO into conducting RGO allows the facile and nontoxic writing of RGO-GO-RGO patterns in various configurations to build electrical double layer capacitors (EDLC) or supercapacitors. Recent reports[344, 345] describe the laser reduction process of GO into RGO with various levels of reduction and electrical conductivity improvements. It is possible to pattern any GO surface into RGO-GO-RGO structures with micron resolution in various geometries.

4.2. Methods

4.2.1. Preparation of Hydrated GO Film

GO was prepared according to the modified Hummers method.[11, 14] The as-prepared hydrated GO was stored in a vacuum chamber together with P_2O_5.

To make free-standing films, GO was dispersed in DI water at a concentration of 6 mg/ml. The colloidal solution was sonicated in water bath for 1 hour to achieve homogeneous dispersion. For a typical film preparation, 50 ml of the dispersion was poured into a vacuum filtration setup, filtered under low vacuum for 3 days with a nitrocellulose membrane (0.025 μm, Millipore). The resulting film was around 22 μm in thickness (Figure 4.1), approximately 240 mg in mass, 8.7 cm in diameter, free-standing and flexible. It was directly used for X-ray photoelectron spectroscopy (XPS, PHI Quantera) and X-ray diffraction (XRD, Rigaku/D, Cu Ka radiation) characterizations.

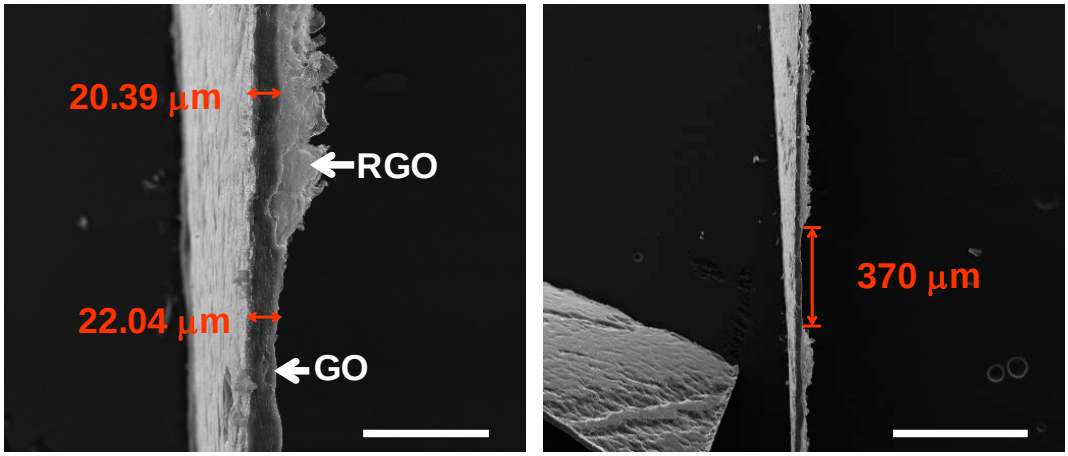

Figure 4.1 SEM characterization of the laser-patterned hydrated GO film (parallel column sample). a) Cross-sectional image of the interface between hydrated GO and RGO, from the thickness measurement, around 7.5 % of hydrated GO thickness is reduced. Scale bar: 100 μm; b) Zoom-out image of a), scale bar: 500 μm. The spacing between two parallel RGO parts is measured to be 0.37 mm.

Laser reduction was conducted with the CO_2 laser printer (Universal X-660 Laser Cutter Platform, power of 2.4 W, 30 % scanning speed). Sheet resistivity was measured by a four-point probe resistivity meter (*Jandel RM3*) with a fixed current of 1 μA in a clean room. SEM images of the as-prepared device were obtained on a high resolution field emission scanning electron microscope (FEI Quanta 400).

4.2.2. Supercapacitor Fabrication and Characterizations

The patterned hydrated GO film was covered with the corresponding current collectors (from Exopack Advanced Coatings, polyvinyl tape patterned for in-plane and carbon coated Al foil for sandwich) and placed between two pieces of glass slides for easier handling. Copper tape was pasted to the current collector for external electrical contact. Electrolytes were injected into the devices by syringes. Cyclic Voltammogram (CV), Galvanostatic charge-discharge (GAL) and Electrochemical Impedance Spectroscopy (EIS) measurements were used to characterize the supercapacitor performance, with an Autolab workstation (PGSTAT302N). The aqueous electrolyte used was 1.0 M Na_2SO_4 (ACS grade) and the organic electrolyte was 1.0 M tetraethylammonium tetrafluoroborate ($TEABF_4$, electrochemical grade, >99 %, Sigma Aldrich) in anhydrous acetonitrile (99.8 %,

Sigma Aldrich). Devices in organic electrolyte were assembled in Ar atmosphere in a dry glove box.

CV curves were obtained at the scan rates of 20 mV/s and 40 mV/s. GAL curves were measured at a constant current of 5 μA or 10 μA. EIS was done using a sinusoidal signal with the mean voltage of 0 V and amplitude of 10 mV over a frequency range of 1 MHz to 10 mHz. The capacitance value was calculated from the CV and GAL data according to the following formula:

$$C(device) = I/(dV/dt)$$

Where *I* refers to the mean current in CV curves and set current in GAL, respectively; *dV/dt* refers to the scan rate in CV curves and slope of the discharge curves in GAL.

Capacitance density was calculated by the formula:

$$C_A = \frac{C(device)}{A} \text{ or } C_V = \frac{C(device)}{V}$$

Where *A* and *V* refer to the total surface area and volume of the positive and negative electrodes in cm^2 and cm^3, respectively. In the concentric circular device, *A* is 0.1413 cm^2, and *V* is calculated to be 2.33 E-5 cm^3 according to the following formula:

$$V = 2 \times \pi \times r_1^2 \times d_r$$

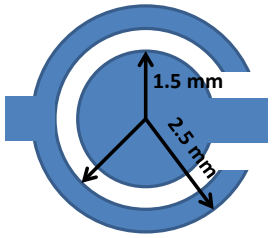

Figure 4.2 Schematic of the circentric circular geometry. The area of the outer ring is designed to be the same as that of the inner circle. The total area of both electrodes is calculated to be $2\times\pi\times(0.15\ cm)^2=0.1413\ cm^2$.

Where r_1 refers to the radius of the inner RGO circle that is used as one electrode, and d_r refers to the depth of reduction applied to the original film (Figure 4.1); for sandwich structure, the electrode area A becomes 1.28 cm^2, corresponding to the total area of both 8 mm × 8 mm squares, and V is calculated to be 2.11 E-4 cm^3 accordingly.

Maximum Power density was obtained from $P=\frac{U^2}{4\times ESR\times V}$, where P is the power density in W/cm^3, U is the potential window used in Volt and ESR is the equivalent series resistance value in Ω, measured with impedance spectroscopy.

Energy density was calculated according to $E=\frac{C_V\times U^2}{2}\times\frac{1}{3600}$, where E is the energy density in Wh/cm^3, C_V is the volume-based specific capacitance in F/cm^3, and U is the potential window used in Volt.

4.2.3. Ionic Conductivity Measurement of Pristine GO films

The ionic conductivity of the pristine GO is determined from complex impedance spectra measured using the Autolab (PGSTST302N) with a frequency range from 1MHz to 100 Hz. A conductivity cell containing two stainless steel blocking electrodes with an intact GO film was used for this measurement.[346] Silver (Ag) was sputter coated onto both surfaces of the GO film to improve the contact. Silver was chosen as the contact metal according to its reported preference over gold and platinum at temperatures below 600 °C.[347] For the ionic conductivity measurement, the impedance spectra obtained turned out to be a depressed semicircle with a slanted line at lower frequencies. In solid electrolyte system, the corresponding equivalent circuit for this type of spectra is typically represented by electrode resistance in series with a parallel combination of electrolyte resistance and capacitance.[346] Therefore, our impedance data at high frequencies were fitted by Zview according to this equivalent circuit, where the depressed semicircles were simulated by the electrolyte resistance in parallel with a Constant Phase Element (CPE) that is generally a result of electrode roughness. The corresponding ionic conductivity was calculated from the resistance value according to the following formula:

$$\rho = \frac{R \times l}{S},$$

Where ρ is the ionic conductivity, R is the resistance value in Ω, obtained by Zview fitting, l is the thickness of the pristine hydrated GO film in cm, and S is the

cross-sectional area of the electrodes in cm^2. The calculated ionic conductivity is in S/cm.

4.2.4. Four-probe Electrical Measurement of a Pristine GO film

In order to verify that GO is ionically conducting and electronically insulating, a four-probe measurement with a Keithley SourceMeter (2410 C) was done on a single piece of GO film with 10 μm thickness. The spacing between each probe is 0.42 cm, and the lengths of those probes are 1.65 cm. The measured resistance in ambient condition was ~2.5 MΩ (estimated conductivity was 1.0E-4 S/cm), and after the same film was kept in vacuum overnight (1E-5 Torr), the resistance increased to 9 GΩ (estimated conductivity was 2.8E-8 S/cm). At least three orders of magnitude change in resistance was observed under vacuum, suggesting that the major contribution to conductivity is ionic, facilitated by the presence of water in GO.

4.3. Result and Discussion

We constructed both in-plane as well as conventional sandwich supercapacitor designs, in various patterns and shapes as described in Figure 4.3. All the proposed configurations of supercapacitor, conventional sandwich-like configuration and novel in-plane configurations can be directly built on single piece of GO paper.

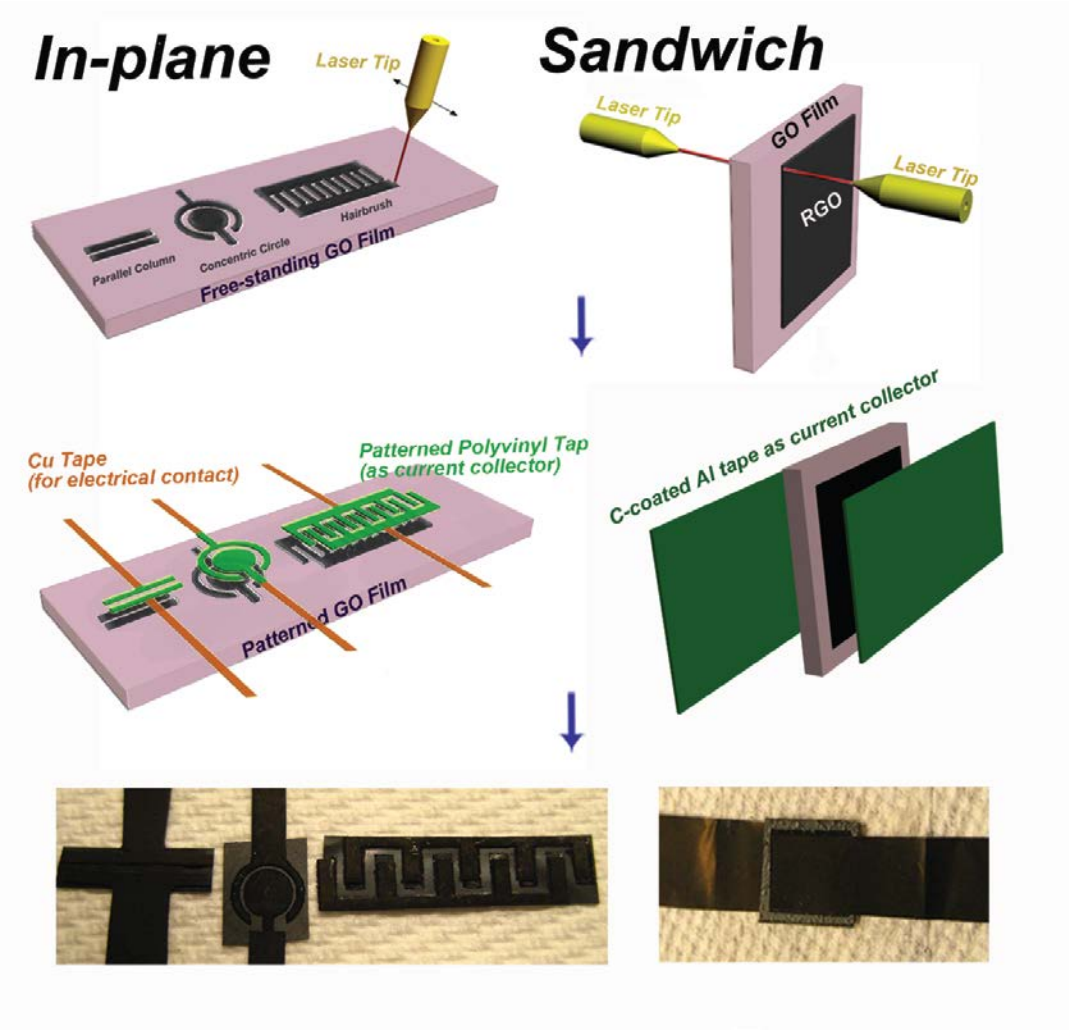

Figure 4.3 Schematic showing the detailed fabrication process for RGO-GO-RGO supercapacitor devices with in-plane and sandwich geometries. The black contrast in the top schematic corresponds to RGO and the light contrast to unmodified hydrated GO. After laser patterning, the patterns were cut out from current collector tapes (polyvinyl tape for in-plane, and carbon-coated aluminum tape for sandwich devices). The bottom row shows corresponding photographic images of the final devices. Typical dimensions of the devices we have fabricated are as follows: Parallel column:1 cm by 1 mm with 0.3 mm spacing; concentric circular pattern: 3 mm diameter inner circle, 4 mm diameter separating circle, and 5 mm diameter outer circle; hairbrush: 2 cm by 5 mm rectangle with five 3.5 mm by 1.5 mm branches equally distributed on each brush; sandwich: 8 mm × 8 mm square of RGO on both sides of a 1 cm × 1 cm square of hydrated GO film, the edge of the film is patterned to define

the outer square on the original film, helping locate the center square on the other side.

4.3.1. Characterizations of As-prepared Devices (Without External Electrolyte)

4.3.1.1. Electrochemical Characterizations

Quite surprisingly, the as-prepared laser patterned devices (RGO-GO-RGO) show good electrochemical performance without the use of any external electrolyte (Figure 4.4). Due to the uncertainty in the measurement of the exact mass of the laser reduced active electrode material, we will mostly report the capacitance values in area and volume density units.

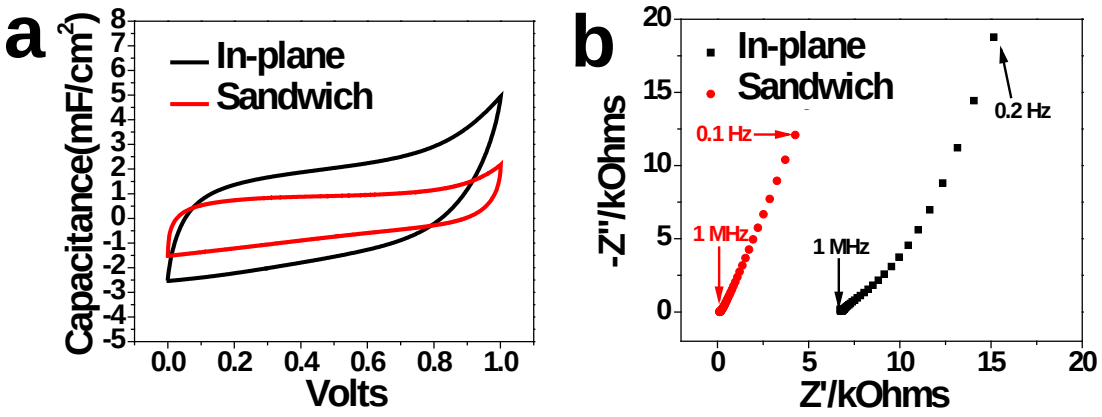

Figure 4.4 Comparisons of CV and impedance behavior of the in-plane and sandwich devices. a) CV curves of in-plane circular and sandwich devices at a scan rate of 40 mV/s. The in-plane circular structure is giving specific capacitance twice as high as that of sandwich structure. b) Impedance spectra from 1MHz to 10 mHz at 10 mV sinusoidal signal, zoomed in at the high frequency region, demonstrating much higher ESR value (the intercept of

slanted straight line with the Z' axis) for the in-plane device than that of a sandwich, leading to lower power density of the in-plane device. Z': the real part of impedance, Z": the imaginary part of impedance.

The capacitance measured seems to depend on the geometry of the design, as the ionic mobilities and transport distances (thickness of the separator section) are anisotropic and different for different geometries. The in-plane supercapacitor structure in a circular geometry is seen to give the highest capacitance (0.51 mF/cm^2), nearly twice as that of a sandwich structure (Figure 4.4a). The control experiment was done with pristine hydrated GO films and current collectors (having no RGO part), and no capacitance was detectable. The equivalent series resistance (ESR) values obtained from the impedance spectra offers information about how fast the cells are charged/discharged. The in-plane structure has higher ESR value than the sandwich structure (6.5 kΩ versus 126 Ω) as seen in Figure 4.4b, indicating lower charge/discharge rate also shown in Figure 4.5a and b.

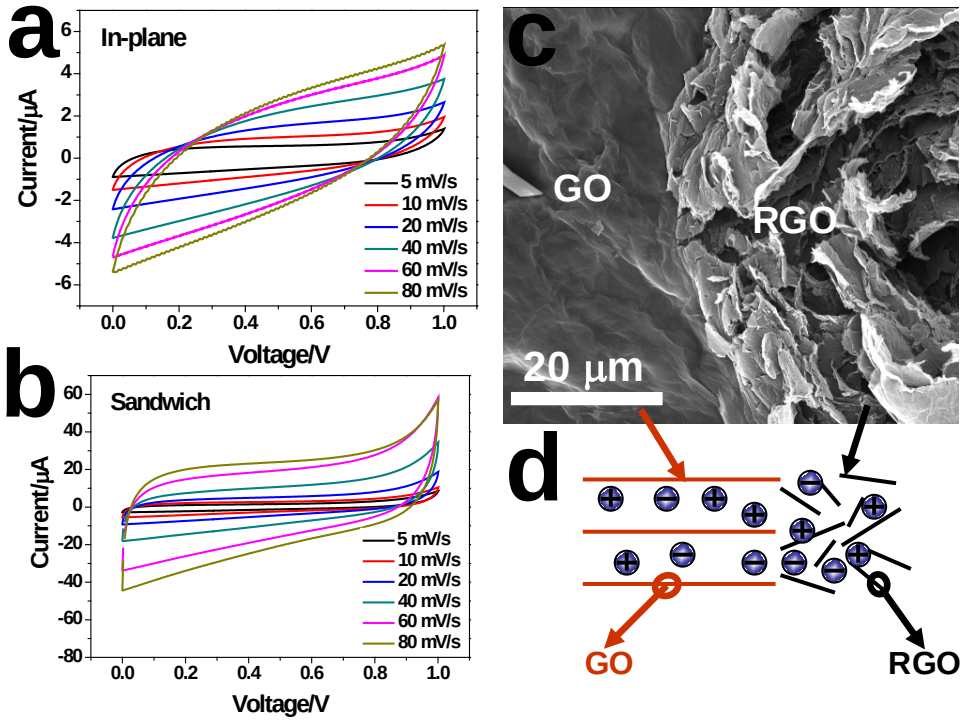

Figure 4.5 Characterization of the device performance and microstructure. a, b) Scan rate dependence in cyclic voltammetry measurement for in-plane structure (a) and sandwich structure (b); c) SEM image showing the interface between GO and RGO in the films; scale bar shown is 20 μm. d) Schematic of the proposed microstructure and chemical structure of the interface. Blue circles represent freely diffusing charge carriers between the graphitic planes.

In comparison, a well designed recently reported, inkjet-printed carbon supercapacitor, with inter-digitated electrode structure and similar electrode thickness, has a mean capacitance density of 0.4 mF/cm^2 with an organic electrolyte[335], showing that the performance of our device without external electrolyte is in the same range as reported for other systems. For electrochemical double-layer microcapacitors, typical capacitance values reported in literature fall between 0.4~2 mF/cm^2.[334]

4.3.1.2. Morphology Characterizations

The ionic conductivity of hydrated GO is calculated from the impedance spectra obtained for the devices (see 4.2.3 for details) [346]and the value is 1.1E-5 S/cm for the sandwich geometry and 2.8E-3 S/cm for the in-plane one. This anisotropy can be easily explained by the microscopic GO-sheet arrangement shown in Figure 4.5 c and d. The hydrated GO film has an anisotropic structure with z-lattice distance of 0.86 nm shown by XRD characterization (Figure 4.6), and thus ions can move more easily along the intralayer direction rather than in direction normal to the layers. This is similar to the anisotropic electrical conductivity reported for graphite and GO platelets.[348]

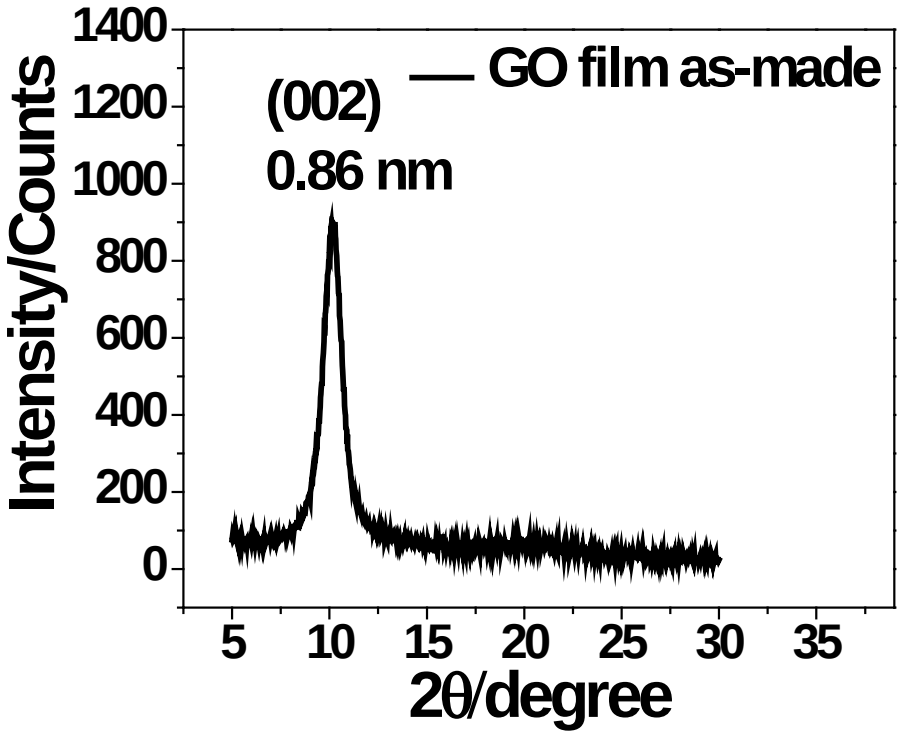

Figure 4.6 The XRD pattern of as-prepared Hydrated GO film. The interlayer spacing is defined by the (002) peak, corresponding to a spacing of 8.6 Å.

4.3.1.3. GO as an Anisotropic Proton Conductor

In EDLC, electrical energy storage is achieved by nanoscopic charge (ion) separation at the interface between electrode and electrolyte. In our system, the only source of ions is hydrated GO. The morphology and structure of a GO film is shown in Figure 4.5 c and d. The higher value of the interlayer spacing (0.86 nm, Figure 4.6) in hydrated GO as compared to completely dehydrated GO (reported to be 0.567 nm)[336] is an indication of the high water content within our films. We have also characterized the water content in hydrated GO to be ~16 wt% with Karl-Fischer Titration[17]. The interaction between the trapped water and GO layers is key to the ionic conductivity observed here. At low concentration, H_2O molecules bind to GO sheets via strong intermolecular interaction (hydrogen bonding); as the water content increases, the active sites on GO sheets get saturated, and the excess water molecules become free to rotate and diffuse. The reported transition point of water content between the bonded-water state and free-water state is ~15 wt%.[336] We speculate that the protons, which are the species here taking part in ionic conduction, come from the hydrolysis of the functional groups (carboxyl, sulfonic[349] and/or hydroxyl) present on GO, and the resulting protons can move via Grotthuss Mechanism[350], which is hopping via hydrogen bonding network, or even freely migrate in the hydronium form (H_3O^+) within the intralayer spaces (Figure 4.5). The proton transport here seems to be similar to that seen in Nafion, a

well-investigated polymer system which shows water induced proton transport following a hopping mechanism.[351]

To study the dehydration-rehydration influence on pristine hydrated GO films, impedance spectroscopy measurements were conducted on the films (4.2.3) with control over environment (under vacuum and at various humidity levels). A stepwise decrease in the ionic conductivity (Figure 4.7a) is observed with increase in exposure time to vacuum, and a full recovery is seen after re-exposure to air for three hours. The ionic conductivity calculated from the impedance spectra versus exposure time is shown in Figure 4.7b. After six hours under vacuum, there is two orders of magnitude decrease in the ionic conductivity of the device, which is also fully recovered after exposure to air, indicating the reversibility of this process at room temperature.

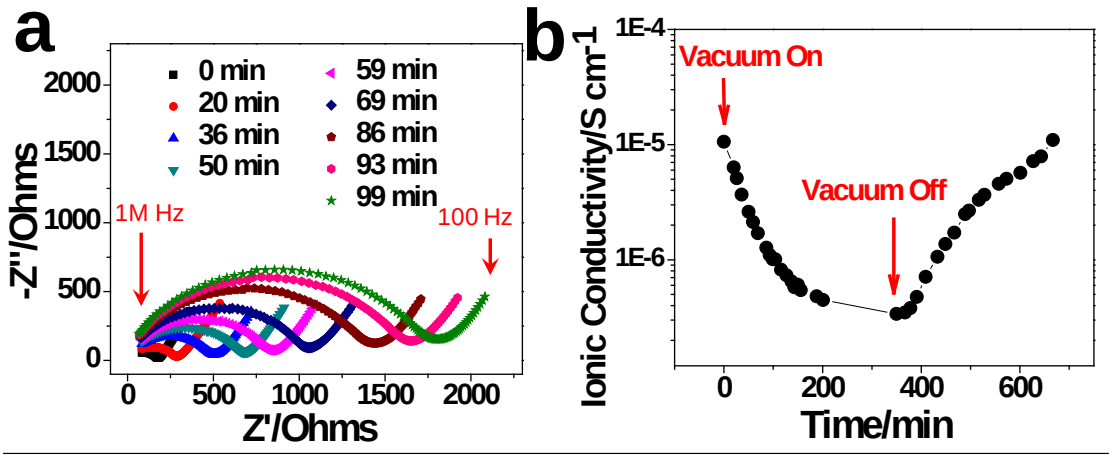

Chemical composition	density	Water content	Color	Ionic conductivity (from impedance spectroscopy)
$C_{3.9}O_{2.5}H_{0.9}$	1.1 g/cm³	16 wt%	Yellowish-brown	1.1E-5 S/cm~ 2.8E-3 S/cm

Figure 4.7 Characterization of water effect in GO ionic conductivity. a) A stepwise change in impedance spectra versus exposure time to vacuum (0.08 MPa) at 25 °C. Cell structure: a pristine GO film coated with Ag on both sides, and sandwiched between two pieces of stainless steel foil (1 cm by 1.2 cm square), frequency range: 1 MHz to 100 Hz at 10 mV sinusoidal signal. Water is slowly evaporated out of the film under vacuum, leading to the increase in the arc diameter in the high frequency range which indicates the decrease in the ionic conductivity. b) Dependence of ionic conductivity on exposure time to vacuum and air. Conductivity data were obtained from Zview fitting of the impedance spectra. Hydrated GO film became less conductive under vacuum, but recovered its full conductivity after three hours of re-exposure to air. Four-probe electrical measurement on a single piece of pristine GO film also showed at least three orders of magnitude decrease in conductance under vacuum, indicating the major contribution to the measured conductivity is ionic in GO. c) Schematic of GO chemical structure reported earlier and table showing the measured physical properties of GO in ambient environment (*sandwich geometry with well-defined cross-sectional area offered accurate

conductivity value of 1.1E-5 S/cm, whereas in-plane structure with estimated cross-sectional area showed a higher ionic conductivity of 2.8E-3 S/cm. We believe due to the lamella structure of GO, its ionic conductivity is anisotropic. Upon hydration, the ionic conductivity further increases (Figure 4.8 a & b), and becomes comparable to Nafion[340].)

In order to study the effect of moisture on the ionic conductivity of GO, impedance spectra measurements were conducted at various humidity levels of GO film (Figure 4.8 a & b). Almost three orders of change in magnitude of ionic conductivity has been observed upon hydration of GO film (Figure 4.8 b). The dramatic changes in ionic conductivity resemble the proton-conducting behavior of Nafion[351]. The chemical structure and properties of GO and Nafion are shown in Figure 4.7c and Figure 4.8d, respectively. The active group in Nafion is sulfonic acid group[352], while in GO, it could be carboxylic acid group, sulfonic acid group[349], or even tertiary alcohol group; furthermore, large amount of existing epoxy groups in GO could also help proton migration. The application of Nafion as an electrolyte and a separator in supercapacitor devices has been reported[339]. Our observations in relevance to the Nafion-like conduction strongly suggest that hydrated GO is acting like an ionic conductor, with its ionic/proton conductivity influenced by the water content.

To further support the water assisted ion-conduction mechanism working in the real device, the dehydration-rehydration process on the sandwich-like supercapacitor structure was studied. The device was put in a vacuum oven and

heated up to 105°C for two days. After it was taken out and exposed to air, impedance spectroscopy measurements were immediately conducted. A stepwise increase in the ionic conductivity of the electrolyte (Figure 4.8c) was observed with increase in exposure time in air. The ionic conductivity calculated from the impedance spectra versus exposure time is presented in Figure 4.8c (insert). After around two hours, there is at least 3 orders of magnitude increase in the ionic conductivity. This dramatic change resembles the proton-conducting behavior of the well-known cationic conducting polymer –Nafion[351].

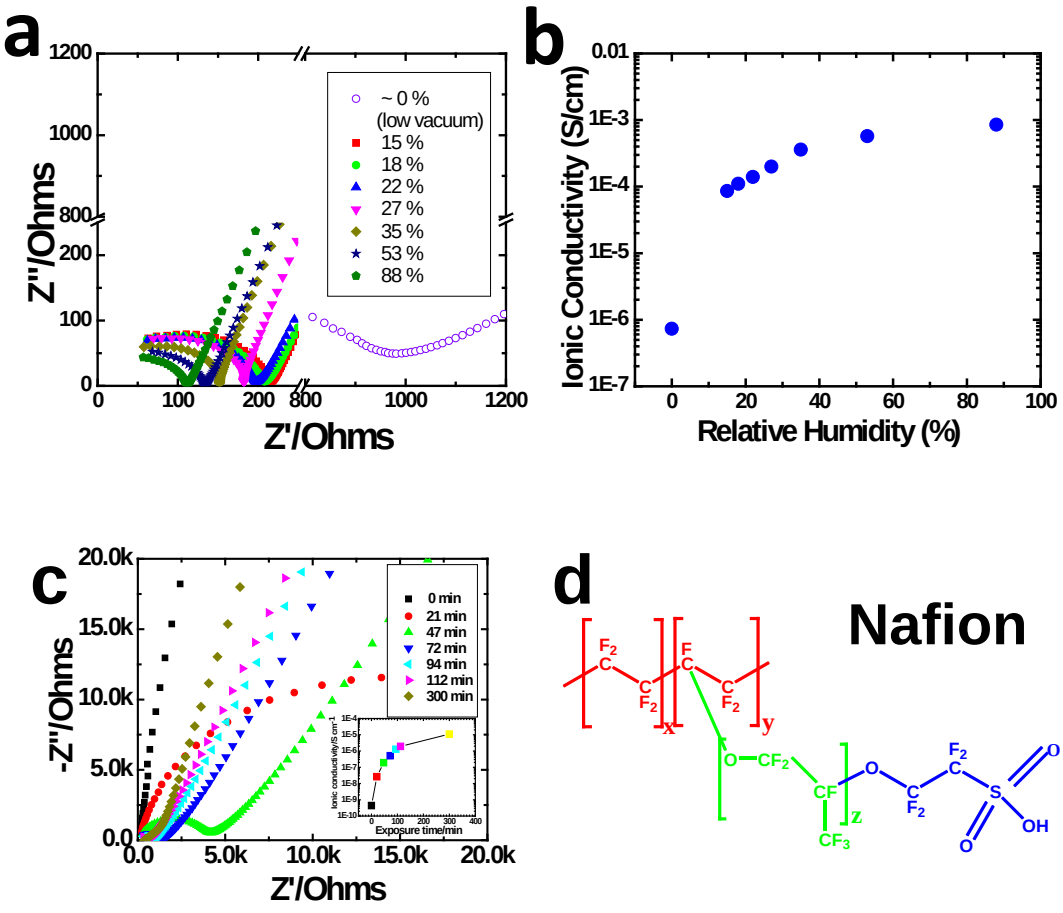

Figure 4.8 a) The evolution of the impedance spectra of GO film at various humidity conditions, 1 MHz to 10 mHz at 10 mV sinusoidal signal, zoomed in at the high frequency region. b) Calculated ionic conductivity dependence upon relative humidity, obtained from the arc diameters in the impedance spectra at high frequencies. c) The evolution of the impedance spectra of a pre-dried sandwich device upon exposure time in air, 1 MHz to 10 mHz at 10 mV sinusoidal signal, zoomed in at the high frequency region; (Insert: Calculated ionic conductivity dependence upon exposure time in air, obtained from the arc diameters in the impedance spectra at high frequencies). d) Chemical structure of Nafion.

4.3.1.4. Characterization of the Laser-patterning Process

The fact that GO can easily be converted to RGO via laser radiation, enables us to scalably produce any number of in-plane or sandwiched RGO-GO-RGO supercapacitor devices via laser patterning of hydrated GO in a simple way. The active electrode material, RGO, formed from hydrated GO using laser heating is porous due to the evolved gases from the decomposition of functional groups[17] and water during localized laser heating (Figure 4.9b, and Figure 4.5c).

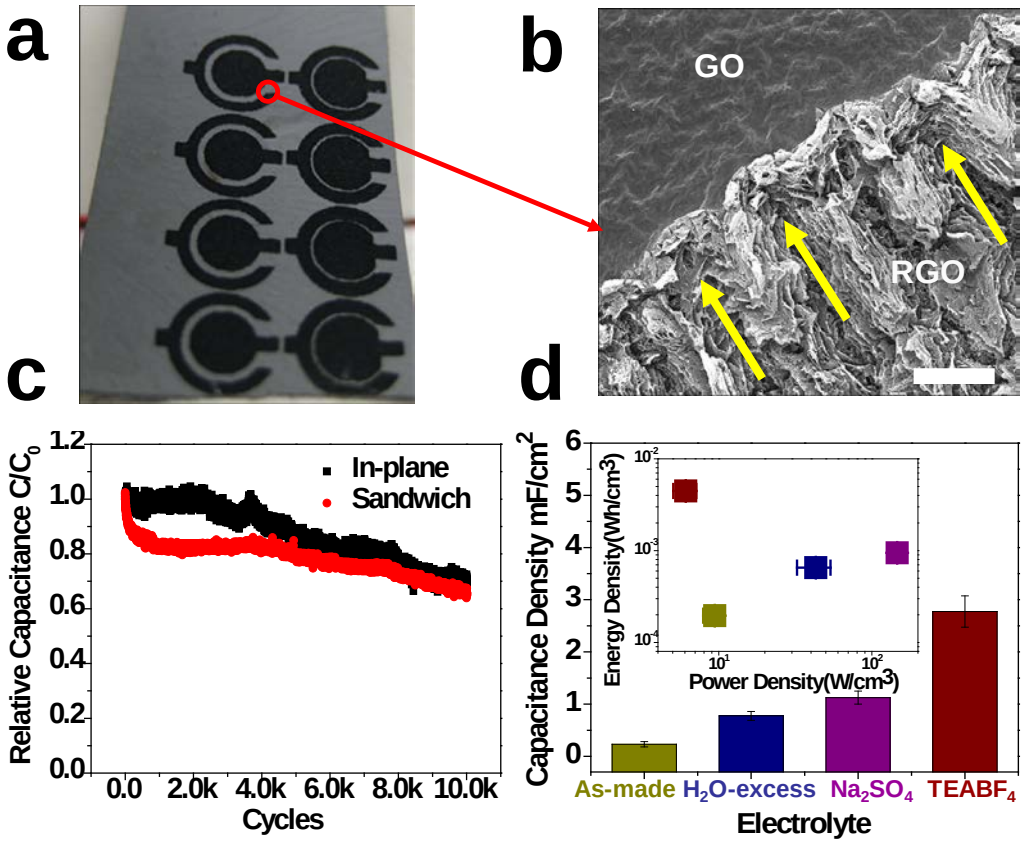

Figure 4.9 A photograph of an array of concentric circular patterns fabricated on a free-standing hydrated GO film; b) SEM image of the interface between GO and RGO (scale bar 100 μm), with yellow arrows indicating long range pseudo-ordered structure generated by the laser-beam scanning; c) Long cyclability tests of the as-prepared sandwich and concentric circular devices, with less than 35 % drop in capacitance after 10,000 cycles; d) Histogram comparison of area-based capacitance density of a sandwich device as-prepared (dark yellow), with excess DI water (navy), aqueous electrolyte (1.0 M Na_2SO_4, purple), and organic electrolyte (1.0 M $TEABF_4$, wine red), inset: volumetric energy density versus power density data of the corresponding devices shown in the same colors. Error bars represent the standard error of the mean of five independent experiments.

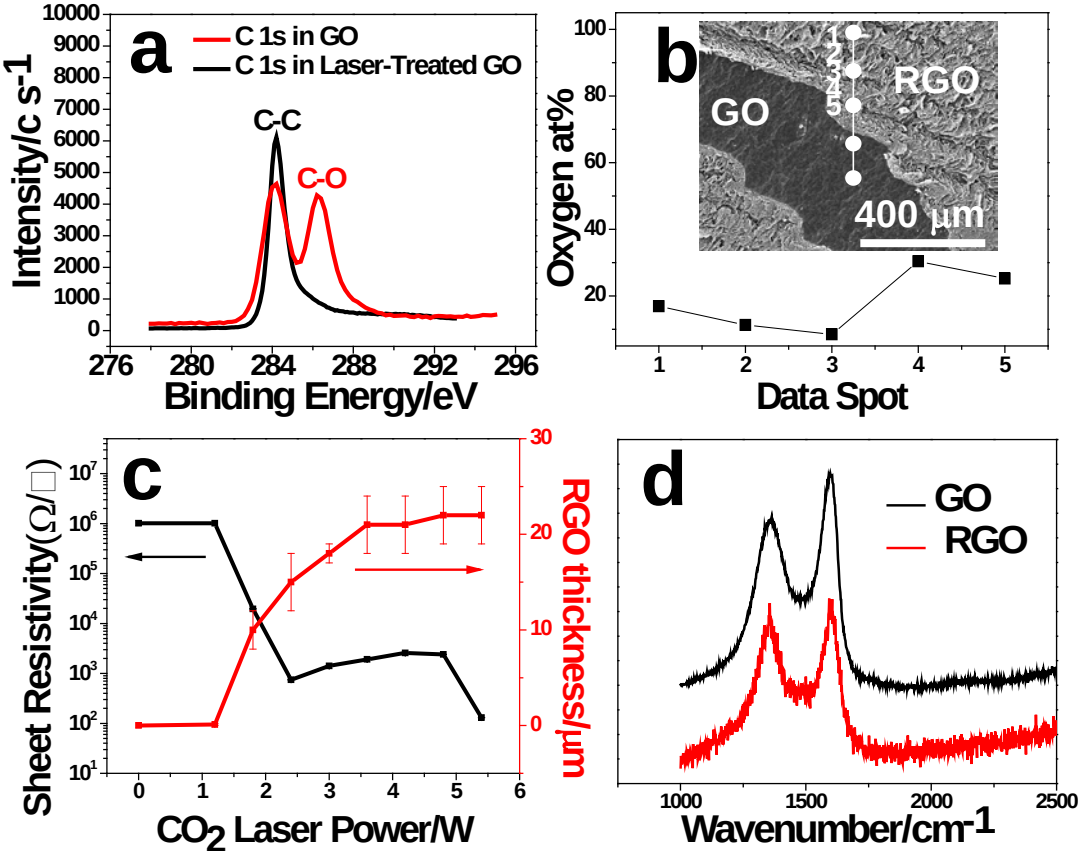

Figure 4.10 a) XPS (X-ray Photoelectron Spectroscopy) high resolution C1s signal of original GO film and laser treated GO film (RGO); b) Local oxygen atomic percentage (O at%) by XPS scan through the interface between RGO and GO. Insert: SEM image of the RGO/GO interface, and the corresponding data spot locations, X-ray beam size: 9 μm. The RGO/GO interface lies between spot No. 3 and 4, obvious oxygen content change was observed across the interface, whereas the O at% variation within each part were probably due to thermal diffusion or adsorption of small organic molecules on the surfaces; c) Dependence of sheet resistivity and RGO thickness on laser power in the laser treatment process, thickness data were obtained by SEM analysis; d) Raman spectra characterization of GO and laser treated GO (RGO). Acquisition parameters: 514.5 nm laser with 1.65 mW power, 10 s exposure time, 5

accumulation, and 1800 l/m gridding, where signals are adjusted in intensity to facilitate comparison.

The dependence of RGO resistivity and reduction depth upon laser power is shown in Figure 4.10b and up to four orders of magnitude decrease in resistivity can be achieved by this laser treatment, in consistent with previously reported work[344]. The long-range ordered structure[353] in RGO (Figure 4.9b) facilitates the ion-diffusion within the electrode. However, the short-range random arrangement of RGO flakes could lead to resistance for ion migration[354], as indicated in the impedance spectra (Figure 4.4b).

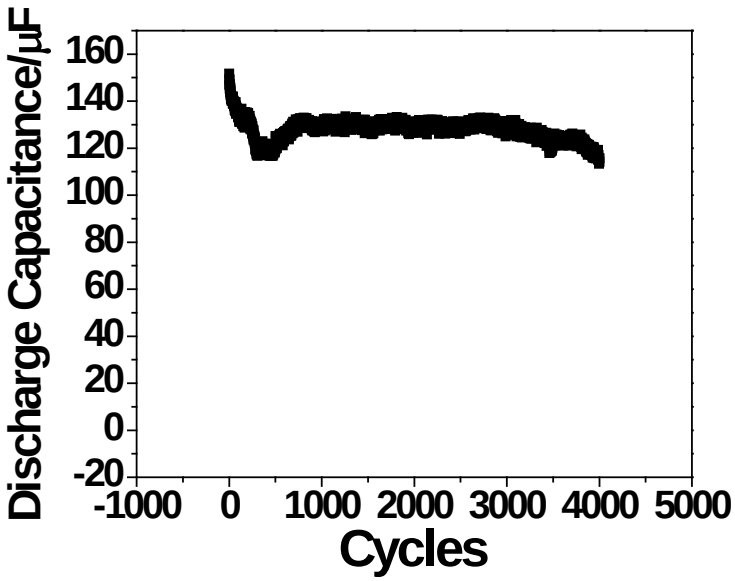

Figure 4.11 Cyclability test of the device with concentric circular geometry for a week in ambient after its first 10,000 cycling test. The capacitance almost doubled and remained stable for ~4,000 cycles of testing.

4.3.1.5. Technical Performance of Our As-made Devices

The cyclic stability tests performed on the supercapacitor devices are shown in Figure 4.9c. After 10,000 cycles, there is ~30% drop in the capacitance of the in-plane circular device, whereas a ~35% drop is noticed for the sandwich devices. The drop seen in capacitance upon cycling is typical of many supercapacitor devices reported in literature.[355, 356] The decline in capacitance could be due to water loss in the device; interestingly, the capacitance doubled after the device was kept in ambient after long cycling for a week (see Figure 4.11).

The in-plane circular design shows the highest specific capacitance of ~0.51 mF/cm^2. Considering only the active thickness of the electrodes, the volumetric capacitance corresponds to ~3.1 F/cm^3, where the electrode volume is estimated from the thickness of the reduced region (Figure 4.1). The energy density for this device is calculated to be approximately 4.3E-4 Wh/cm^3, with a power density of 1.7 W/cm^3. Due to the lower ESR value, the sandwich device geometry gives higher power density of ~9.4 W/cm^3, although the energy density for this device is lower (1.9E-4 Wh/cm^3). A good match between the 20 mV/s and 40 mV/s CV scan rates (Figure 4.12a) indicates similar ion diffusion paths within this scan rate range[357]. However, we did see the decrease of capacitance when the scan rate was increased to 100 mV/s. This could be due to the inhomogeneous pore structure within the

electrodes or the pseudo-capacitance caused by the impurities and hetero-atoms remaining in RGO.

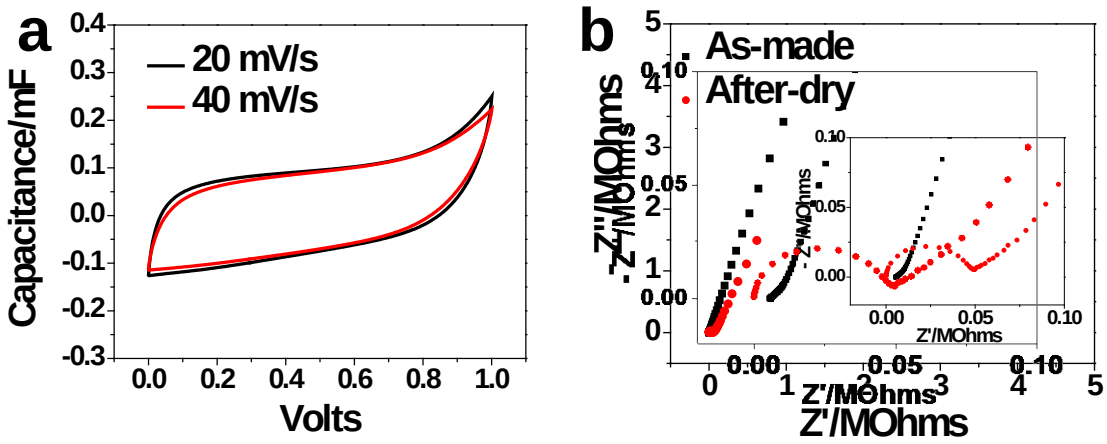

Figure 4.12 a) CV curves of a concentric circular in-plane device at 20 and 40 mV/s scan rate. b) The impedance spectra of the device before and after drying in vacuum oven; 1 MHz to 10 mHz at 10 mV sinusoidal signal. Insert: zoom-in diagram at high frequencies, obvious increase in the arc diameter is observed after drying, corresponding to lower ionic conductivity.

Self-discharge data of a concentric circular device is also presented in Figure 4.13; the data shows about 80% voltage retention within the first half hour and about 50% retention over a period of eight hours. Some of the discharge is caused by the non-zero input current of the measurement apparatus, meaning the actual charge retaining time could be longer. The voltage retention in our devices is more than 80% after half hour discharge, a good indication of limited current leakage in these devices. Further optimization of the device geometry and thicknesses should lead to better self-discharge profiles for our devices

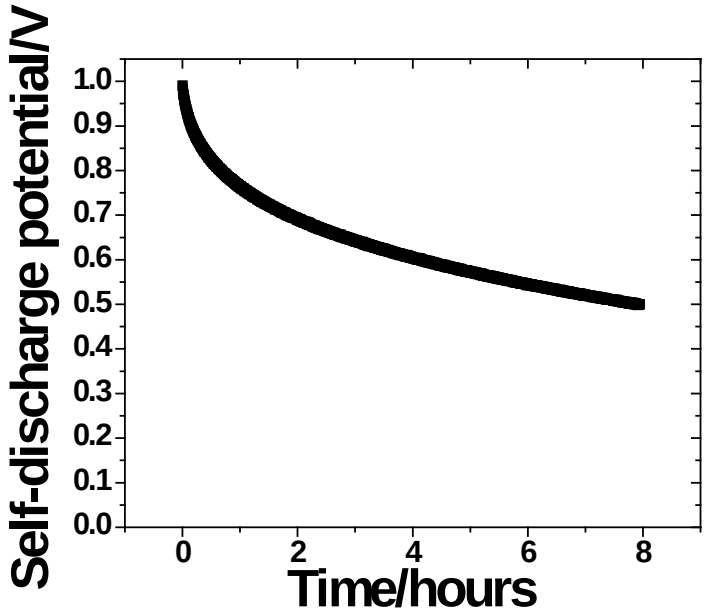

Figure 4.13 Experimental data for the self-discharge of a concentric circular device. Using standard self-discharge measurement technique we obtained 50% voltage loss in approximately eight hours.

4.3.2. Characterizations of Devices with External Electrolyte

When an extra drop of deionized (DI) water was added into the as-prepared device, the ion transport was enhanced, showing a three-fold increase in capacitance (Figure 4.9d). In the presence of external electrolytes, the performance of the devices is further improved. The capacitive behavior with external aqueous (1.0 M Na_2SO_4) and organic (1.0 M $TEABF_4$ in acetonitrile) electrolyte was characterized and results for the sandwich device is shown in Figure 4.9d and Figure 4.14. For devices with added external electrolytes, nearly five-fold increase in capacitance and 95% decrease in ESR were observed right after addition of a few

drops of Na_2SO_4 solution, due to the presence of additional inorganic ions within the device. As for organic electrolyte the as-prepared device was put in a vacuum oven and heated up to 105°C for 2 days to remove all the absorbed water, and after drying, the device was immediately transferred to a dry glove box where the organic electrolyte was added. In the end the device was laminated between two sheets of moisture-resistant plastic. The CV response showed twelve-fold enhancement in capacitance and five-fold increase in ESR immediately after organic electrolyte addition (Figure 4.14). Larger capacitance obtained with organic over aqueous electrolyte is simply due to the larger amount of organic electrolyte added into the device, since solubility of GO limited the total amount of water present in the device. Furthermore, the capacitance in organic electrolyte was strongly influenced by the scan rate in CV, indicating less uniform ion-migration path within structures than those of as-prepared and aqueous-electrolyte cases. However, it is worth mentioning that, the capacitance and ESR value with external electrolyte degrades faster with increasing number of cycles, probably due to the chemical activity of GO.

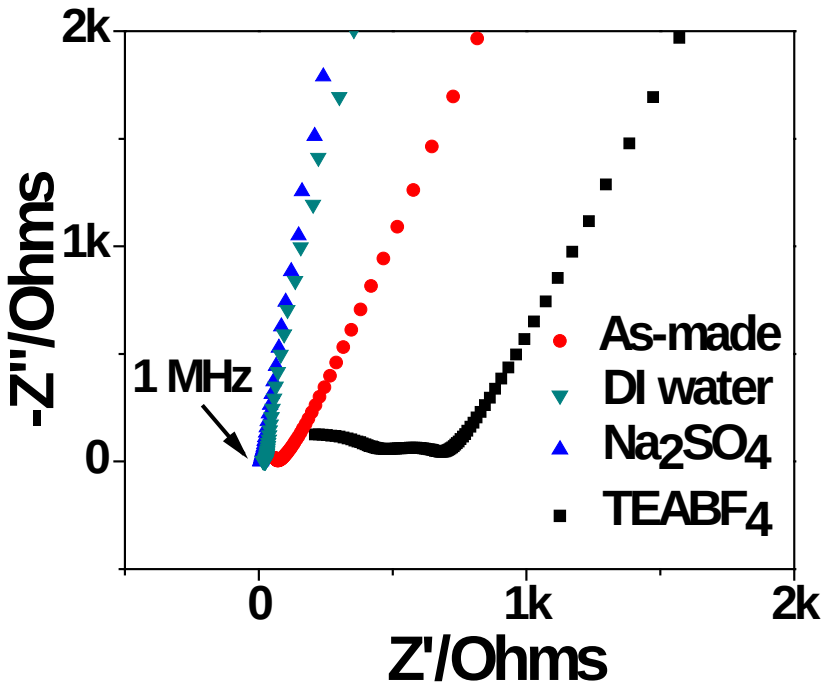

Figure 4.14 Impedance spectra of a sandwich device as prepared, with water and external electrolytes added. 1 MHz to 10 mHz at 10 mV sinusoidal signal, zoomed in at the high frequency region.

4.4. Conclusion

Here, we have successfully demonstrated the ionic conductivity and the use of as-prepared hydrated GO films as a new type of separator/electrolyte membrane system. The ability to reduce and pattern hydrated GO films by laser irradiation enables the development of a scalable process to write micro-supercapacitors on these films, which work with or without the use of external electrolytes. The process we have offers a unique method compared to typical printing processes used for building micro-supercapacitors and could serve complimentary to the latter which

is widely used technique. Also, the GO films offer an entirely different type of porous solid electrolyte and could find applications as lightweight membranes in several energy storage applications.

Notes

Media reports for work in Chapter 2
http://www.rsc.org/chemistryworld/News/2009/July/05070901.asp
Media reports for work in Chapter 3
http://www.bbc.co.uk/news/business-13895077
http://www.youtube.com/watch?v=1nfddpRfEq0
Media reports for work in Chapter 4
http://www.futurity.org/science-technology/lasers-create-slice-of-energy-storage/
http://www.youtube.com/watch?v=3O4YV0mrkfQ.

References

1. J.N. Coleman, M. Lotya, A. O'Neill, S.D. Bergin, P.J. King, U. Khan, K. Young, A. Gaucher, S. De, R.J. Smith, I.V. Shvets, S.K. Arora, G. Stanton, H.-Y. Kim, K. Lee, G.T. Kim, G.S. Duesberg, T. Hallam, J.J. Boland, J.J. Wang, J.F. Donegan, J.C. Grunlan, G. Moriarty, A. Shmeliov, R.J. Nicholls, J.M. Perkins, E.M. Grieveson, K. Theuwissen, D.W. McComb, P.D. Nellist, and V. Nicolosi, *Two-Dimensional Nanosheets Produced by Liquid Exfoliation of Layered Materials.* Science, 2011. **331**(6017): p. 568-571.
2. K.S. Novoselov, A.K. Geim, S.V. Morozov, D. Jiang, M.I. Katsnelson, I.V. Grigorieva, S.V. Dubonos, and A.A. Firsov, *Two-dimensional gas of massless Dirac fermions in graphene.* Nature, 2005. **438**(7065): p. 197-200.
3. K.S. Novoselov, A.K. Geim, S.V. Morozov, D. Jiang, Y. Zhang, S.V. Dubonos, I.V. Grigorieva, and A.A. Firsov, *Electric Field Effect in Atomically Thin Carbon Films.* Science, 2004. **306**(5696): p. 666-669.
4. L.M. Viculis, J.J. Mack, and R.B. Kaner, *A Chemical Route to Carbon Nanoscrolls.* Science, 2003. **299**(5611): p. 1361.
5. Y. Hernandez, V. Nicolosi, M. Lotya, F.M. Blighe, Z. Sun, S. De, I.T. McGovern, B. Holland, M. Byrne, Y.K. Gun'Ko, J.J. Boland, P. Niraj, G. Duesberg, S. Krishnamurthy, R. Goodhue, J. Hutchison, V. Scardaci, A.C. Ferrari, and J.N. Coleman, *High-yield production of graphene by liquid-phase exfoliation of graphite.* Nature Nanotechnology, 2008. **3**(9): p. 563-568.
6. X. Li, W. Cai, J. An, S. Kim, J. Nah, D. Yang, R. Piner, A. Velamakanni, I. Jung, E. Tutuc, S.K. Banerjee, L. Colombo, and R.S. Ruoff, *Large-Area Synthesis of High-Quality and Uniform Graphene Films on Copper Foils.* Science, 2009. **324**(5932): p. 1312-1314.
7. C. Berger, Z. Song, X. Li, X. Wu, N. Brown, C. Naud, D. Mayou, T. Li, J. Hass, A.N. Marchenkov, E.H. Conrad, P.N. First, and W.A. de Heer, *Electronic Confinement and Coherence in Patterned Epitaxial Graphene.* Science, 2006. **312**(5777): p. 1191-1196.
8. J. Cai, P. Ruffieux, R. Jaafar, M. Bieri, T. Braun, S. Blankenburg, M. Muoth, A.P. Seitsonen, M. Saleh, X. Feng, K. Mullen, and R. Fasel, *Atomically precise bottom-up fabrication of graphene nanoribbons.* Nature, 2010. **466**(7305): p. 470-473.
9. Ž. Tomović, M.D. Watson, and K. Müllen, *Superphenalene-Based Columnar Liquid Crystals.* Angewandte Chemie International Edition, 2004. **43**(6): p. 755-758.
10. M. Treier, C.A. Pignedoli, T. Laino, R. Rieger, K. Mullen, D. Passerone, and R. Fasel, *Surface-assisted cyclodehydrogenation provides a synthetic route towards easily processable and chemically tailored nanographenes.* Nature Chemistry, 2011. **3**(1): p. 61-67.
11. S. Gilje, S. Han, M. Wang, K.L. Wang, and R.B. Kaner, *A Chemical Route to Graphene for Device Applications.* Nano Letters, 2007. **7**(11): p. 3394-3398.

12. S. Stankovich, D.A. Dikin, R.D. Piner, K.A. Kohlhaas, A. Kleinhammes, Y. Jia, Y. Wu, S.T. Nguyen, and R.S. Ruoff, *Synthesis of graphene-based nanosheets via chemical reduction of exfoliated graphite oxide.* Carbon, 2007. **45**(7): p. 1558-1565.
13. B.C. Brodie, *On the Atomic Weight of Graphite.* Philosophical Transactions of the Royal Society of London, 1859. **149**: p. 249-259.
14. W.S. Hummers and R.E. Offeman, *Preparation of Graphitic Oxide.* Journal of the American Chemical Society, 1958. **80**(6): p. 1339-1339.
15. D.C. Marcano, D.V. Kosynkin, J.M. Berlin, A. Sinitskii, Z. Sun, A. Slesarev, L.B. Alemany, W. Lu, and J.M. Tour, *Improved Synthesis of Graphene Oxide.* ACS Nano, 2010. **4**(8): p. 4806-4814.
16. W. Cai, R.D. Piner, F.J. Stadermann, S. Park, M.A. Shaibat, Y. Ishii, D. Yang, A. Velamakanni, S.J. An, M. Stoller, J. An, D. Chen, and R.S. Ruoff, *Synthesis and Solid-State NMR Structural Characterization of 13C-Labeled Graphite Oxide.* Science, 2008. **321**(5897): p. 1815-1817.
17. W. Gao, L.B. Alemany, L. Ci, and P.M. Ajayan, *New insights into the structure and reduction of graphite oxide.* Nature Chemistry, 2009. **1**(5): p. 403-408.
18. C. Mattevi, G. Eda, S. Agnoli, S. Miller, K.A. Mkhoyan, O. Celik, D. Mostrogiovanni, G. Granozzi, E. Garfunkel, and M. Chhowalla, *Evolution of Electrical, Chemical, and Structural Properties of Transparent and Conducting Chemically Derived Graphene Thin Films.* Advanced Functional Materials, 2009. **19**(16): p. 2577-2583.
19. K. Erickson, R. Erni, Z. Lee, N. Alem, W. Gannett, and A. Zettl, *Determination of the Local Chemical Structure of Graphene Oxide and Reduced Graphene Oxide.* Advanced Materials, 2010. **22**(40): p. 4467-4472.
20. L. Staudenmaier, *Verfahren zur Darstellung der Graphitsäure.* Berichte der deutschen chemischen Gesellschaft, 1898. **31**(2): p. 1481-1487.
21. L. Staudenmaier, *Verfahren zur Darstellung der Graphitsäure.* Berichte der deutschen chemischen Gesellschaft, 1899. **32**(2): p. 1394-1399.
22. N.I. Kovtyukhova, P.J. Ollivier, B.R. Martin, T.E. Mallouk, S.A. Chizhik, E.V. Buzaneva, and A.D. Gorchinskiy, *Layer-by-Layer Assembly of Ultrathin Composite Films from Micron-Sized Graphite Oxide Sheets and Polycations.* Chemistry of Materials, 1999. **11**(3): p. 771-778.
23. J. Luo, L.J. Cote, V.C. Tung, A.T.L. Tan, P.E. Goins, J. Wu, and J. Huang, *Graphene Oxide Nanocolloids.* Journal of the American Chemical Society, 2010. **132**(50): p. 17667-17669.
24. I.D. Rosca, F. Watari, M. Uo, and T. Akasaka, *Oxidation of multiwalled carbon nanotubes by nitric acid.* Carbon, 2005. **43**(15): p. 3124-3131.
25. L. Becker, R.J. Poreda, and T.E. Bunch, *Fullerenes: An extraterrestrial carbon carrier phase for noble gases.* Proceedings of the National Academy of Sciences of the United States of America, 2000. **97**(7): p. 2979-2983.
26. J.A. McCleverty, *ADVANCED INORGANIC-CHEMISTRY, 5TH EDITION - COTTON,FA, WILKINSON,G.* Nature, 1989. **338**(6211): p. 182-182.

27. K.R. Koch, *Oxidation by Mn207: An impressive demonstration of the powerful oxidizing property of dimanganeseheptoxide.* Journal of Chemical Education, 1982. **59**(11): p. 973.
28. A. Simon, R. Dronskowski, B. Krebs, and B. Hettich, *The Crystal Structure of Mn2O7.* Angewandte Chemie International Edition in English, 1987. **26**(2): p. 139-140.
29. A.L. Higginbotham, D.V. Kosynkin, A. Sinitskii, Z. Sun, and J.M. Tour, *Lower-Defect Graphene Oxide Nanoribbons from Multiwalled Carbon Nanotubes.* ACS Nano, 2010. **4**(4): p. 2059-2069.
30. F. Kim, J. Luo, R. Cruz-Silva, L.J. Cote, K. Sohn, and J. Huang, *Self-Propagating Domino-like Reactions in Oxidized Graphite.* Advanced Functional Materials, 2010. **20**(17): p. 2867-2873.
31. A. Lerf, H.Y. He, M. Forster, and J. Klinowski, *Structure of graphite oxide revisited.* Journal of Physical Chemistry B, 1998. **102**(23): p. 4477-4482.
32. L.B. Casabianca, M.A. Shaibat, W.W. Cai, S. Park, R. Piner, R.S. Ruoff, and Y. Ishii, *NMR-Based Structural Modeling of Graphite Oxide Using Multidimensional 13C Solid-State NMR and ab Initio Chemical Shift Calculations.* Journal of the American Chemical Society, 2010. **132**(16): p. 5672-5676.
33. T. Szabo, O. Berkesi, and I. Dekany, *DRIFT study of deuterium-exchanged graphite oxide.* Carbon, 2005. **43**(15): p. 3186-3189.
34. K.N. Kudin, B. Ozbas, H.C. Schniepp, R.K. Prud'homme, I.A. Aksay, and R. Car, *Raman spectra of graphite oxide and functionalized graphene sheets.* Nano Letters, 2008. **8**(1): p. 36-41.
35. M. Ishigami, J.H. Chen, W.G. Cullen, M.S. Fuhrer, and E.D. Williams, *Atomic structure of graphene on SiO2.* Nano Letters, 2007. **7**(6): p. 1643-1648.
36. J.I. Paredes, S. Villar-Rodil, P. Solis-Fernandez, A. Martinez-Alonso, and J.M.D. Tascon, *Atomic Force and Scanning Tunneling Microscopy Imaging of Graphene Nanosheets Derived from Graphite Oxide.* Langmuir, 2009. **25**(10): p. 5957-5968.
37. C. Gomez-Navarro, J.C. Meyer, R.S. Sundaram, A. Chuvilin, S. Kurasch, M. Burghard, K. Kern, and U. Kaiser, *Atomic Structure of Reduced Graphene Oxide.* Nano Letters, 2010. **10**(4): p. 1144-1148.
38. N.R. Wilson, P.A. Pandey, R. Beanland, R.J. Young, I.A. Kinloch, L. Gong, Z. Liu, K. Suenaga, J.P. Rourke, S.J. York, and J. Sloan, *Graphene Oxide: Structural Analysis and Application as a Highly Transparent Support for Electron Microscopy.* ACS Nano, 2009. **3**(9): p. 2547-2556.
39. G. Eda, C. Mattevi, H. Yamaguchi, H. Kim, and M. Chhowalla, *Insulator to Semimetal Transition in Graphene Oxide.* Journal of Physical Chemistry C, 2009. **113**(35): p. 15768-15771.
40. A.B. Kaiser, C. Gomez-Navarro, R.S. Sundaram, M. Burghard, and K. Kern, *Electrical Conduction Mechanism in Chemically Derived Graphene Monolayers.* Nano Letters, 2009. **9**(5): p. 1787-1792.

41. Z.T. Luo, Y. Lu, L.A. Somers, and A.T.C. Johnson, *High Yield Preparation of Macroscopic Graphene Oxide Membranes.* Journal of the American Chemical Society, 2009. **131**(3): p. 898-+.
42. H.A. Becerril, J. Mao, Z. Liu, R.M. Stoltenberg, Z. Bao, and Y. Chen, *Evaluation of solution-processed reduced graphene oxide films as transparent conductors.* ACS Nano, 2008. **2**(3): p. 463-470.
43. T. Szabo, O. Berkesi, P. Forgo, K. Josepovits, Y. Sanakis, D. Petridis, and I. Dekany, *Evolution of Surface Functional Groups in a Series of Progressively Oxidized Graphite Oxides.* Chemistry of Materials, 2006. **18**(11): p. 2740-2749.
44. U. Hofmann and R. Holst, *The acidic nature and the methylation of graphitoxide.* Berichte der deutschen chemischen Gesellschaft, 1939. **72**: p. 754-771.
45. G. Ruess, *Über das Graphitoxyhydroxyd (Graphitoxyd).* Monatshefte für Chemie / Chemical Monthly, 1947. **76**(3): p. 381-417.
46. M. Mermoux, Y. Chabre, and A. Rousseau, *FTIR AND C-13 NMR-STUDY OF GRAPHITE OXIDE.* Carbon, 1991. **29**(3): p. 469-474.
47. H.P. Boehm, A. Clauss, U. Hofmann, and G.O. Fischer, *DUNNSTE KOHLENSTOFF-FOLIEN.* Zeitschrift Fur Naturforschung Part B-Chemie Biochemie Biophysik Biologie Und Verwandten Gebiete, 1962. **B 17**(3): p. 150-&.
48. W. Scholz and H.P. Boehm, *GRAPHITE OXIDE .6. STRUCTURE OF GRAPHITE OXIDE.* Zeitschrift Fur Anorganische Und Allgemeine Chemie, 1969. **369**(3-6): p. 327-&.
49. T. Nakajima, A. Mabuchi, and R. Hagiwara, *A NEW STRUCTURE MODEL OF GRAPHITE OXIDE.* Carbon, 1988. **26**(3): p. 357-361.
50. H.Y. He, T. Riedl, A. Lerf, and J. Klinowski, *Solid-state NMR studies of the structure of graphite oxide.* Journal of Physical Chemistry, 1996. **100**(51): p. 19954-19958.
51. A. Lerf, H.Y. He, T. Riedl, M. Forster, and J. Klinowski, *C-13 and H-1 MAS NMR studies of graphite oxide and its chemically modified derivatives.* Solid State Ionics, 1997. **101**: p. 857-862.
52. H. He, J. Klinowski, M. Forster, and A. Lerf, *A new structural model for graphite oxide.* Chemical Physics Letters, 1998. **287**(1-2): p. 53-56.
53. C. Gomez-Navarro, R.T. Weitz, A.M. Bittner, M. Scolari, A. Mews, M. Burghard, and K. Kern, *Electronic transport properties of individual chemically reduced graphene oxide sheets.* Nano Letters, 2007. **7**(11): p. 3499-3503.
54. S. Stankovich, R.D. Piner, X.Q. Chen, N.Q. Wu, S.T. Nguyen, and R.S. Ruoff, *Stable aqueous dispersions of graphitic nanoplatelets via the reduction of exfoliated graphite oxide in the presence of poly(sodium 4-styrenesulfonate).* Journal of Materials Chemistry, 2006. **16**(2): p. 155-158.
55. Y. Si and E.T. Samulski, *Synthesis of water soluble graphene.* Nano Letters, 2008. **8**(6): p. 1679-1682.

56. J. Kim, L.J. Cote, F. Kim, W. Yuan, K.R. Shull, and J. Huang, *Graphene Oxide Sheets at Interfaces.* Journal of the American Chemical Society, 2010. **132**(23): p. 8180-8186.
57. J.I. Paredes, S. Villar-Rodil, A. Martinez-Alonso, and J.M.D. Tascon, *Graphene oxide dispersions in organic solvents.* Langmuir, 2008. **24**(19): p. 10560-10564.
58. L.J. Cote, J. Kim, V.C. Tung, J.Y. Luo, F. Kim, and J.X. Huang, *Graphene oxide as surfactant sheets.* Pure and Applied Chemistry, 2011. **83**(1): p. 95-110.
59. L.J. Cote, F. Kim, and J. Huang, *Langmuir-blodgett Assembly of Graphite Oxide Single Layers.* Journal of the American Chemical Society, 2008. **131**(3): p. 1043-1049.
60. L.J. Cote, J. Kim, Z. Zhang, C. Sun, and J. Huang, *Tunable assembly of graphene oxide surfactant sheets: wrinkles, overlaps and impacts on thin film properties.* Soft Matter, 2010. **6**(24).
61. F. Kim, L.J. Cote, and J. Huang, *Graphene Oxide: Surface Activity and Two-Dimensional Assembly.* Advanced Materials, 2009. **22**(17): p. 1954-1958.
62. O. Akhavan and E. Ghaderi, *Toxicity of Graphene and Graphene Oxide Nanowalls Against Bacteria.* ACS Nano, 2010. **4**(10): p. 5731-5736.
63. W. Hu, C. Peng, M. Lv, X. Li, Y. Zhang, N. Chen, C. Fan, and Q. Huang, *Protein Corona-Mediated Mitigation of Cytotoxicity of Graphene Oxide.* ACS Nano, 2011. **5**(5): p. 3693-3700.
64. K. Wang, J. Ruan, H. Song, J.L. Zhang, Y. Wo, S.W. Guo, and D.X. Cui, *Biocompatibility of Graphene Oxide.* Nanoscale Research Letters, 2011. **6**: p. 8.
65. S.K. Behera, *Enhanced rate performance and cyclic stability of Fe(3)O(4)-graphene nanocomposites for Li ion battery anodes.* Chemical Communications, 2011. **47**(37): p. 10371-10373.
66. K.H. Liao, Y.S. Lin, C.W. Macosko, and C.L. Haynes, *Cytotoxicity of Graphene Oxide and Graphene in Human Erythrocytes and Skin Fibroblasts.* Acs Applied Materials & Interfaces, 2011. **3**(7): p. 2607-2615.
67. M. Wojtoniszak, X. Chen, R.J. Kalenczuk, A. Wajda, J. Lapczuk, M. Kurzewski, M. Drozdzik, P.K. Chu, and E. Borowiak-Palen, *Synthesis, dispersion, and cytocompatibility of graphene oxide and reduced graphene oxide.* Colloids and surfaces. B, Biointerfaces, 2012. **89**: p. 79-85.
68. Y. Zhang, S.F. Ali, E. Dervishi, Y. Xu, Z. Li, D. Casciano, and A.S. Biris, *Cytotoxicity Effects of Graphene and Single-Wall Carbon Nanotubes in Neural Phaeochromocytoma-Derived PC12 Cells.* ACS Nano, 2010. **4**(6): p. 3181-3186.
69. X.M. Sun, Z. Liu, K. Welsher, J.T. Robinson, A. Goodwin, S. Zaric, and H.J. Dai, *Nano-Graphene Oxide for Cellular Imaging and Drug Delivery.* Nano Research, 2008. **1**(3): p. 203-212.
70. Y.L. Chang, S.T. Yang, J.H. Liu, E. Dong, Y.W. Wang, A.N. Cao, Y.F. Liu, and H.F. Wang, *In vitro toxicity evaluation of graphene oxide on A549 cells.* Toxicology Letters, 2011. **200**(3): p. 201-210.

71. S.R. Ryoo, Y.K. Kim, M.H. Kim, and D.H. Min, *Behaviors of NIH-3T3 Fibroblasts on Graphene/Carbon Nanotubes: Proliferation, Focal Adhesion, and Gene Transfection Studies.* ACS Nano, 2010. **4**(11): p. 6587-6598.
72. S. Agarwal, X.Z. Zhou, F. Ye, Q.Y. He, G.C.K. Chen, J. Soo, F. Boey, H. Zhang, and P. Chen, *Interfacing Live Cells with Nanocarbon Substrates.* Langmuir, 2010. **26**(4): p. 2244-2247.
73. H. Chen, M.B. Muller, K.J. Gilmore, G.G. Wallace, and D. Li, *Mechanically strong, electrically conductive, and biocompatible graphene paper.* Advanced Materials, 2008. **20**(18): p. 3557-+.
74. S. Park, N. Mohanty, J.W. Suk, A. Nagaraja, J.H. An, R.D. Piner, W.W. Cai, D.R. Dreyer, V. Berry, and R.S. Ruoff, *Biocompatible, Robust Free-Standing Paper Composed of a TWEEN/Graphene Composite.* Advanced Materials, 2010. **22**(15): p. 1736-+.
75. O.N. Ruiz, K.A.S. Fernando, B.J. Wang, N.A. Brown, P.G. Luo, N.D. McNamara, M. Vangsness, Y.P. Sun, and C.E. Bunker, *Graphene Oxide: A Nonspecific Enhancer of Cellular Growth.* ACS Nano, 2011. **5**(10): p. 8100-8107.
76. Q. Bao, D. Zhang, and P. Qi, *Synthesis and characterization of silver nanoparticle and graphene oxide nanosheet composites as a bactericidal agent for water disinfection.* Journal of Colloid and Interface Science, 2011. **360**(2): p. 463-470.
77. M.R. Das, R.K. Sarma, R. Saikia, V.S. Kale, M.V. Shelke, and P. Sengupta, *Synthesis of silver nanoparticles in an aqueous suspension of graphene oxide sheets and its antimicrobial activity.* Colloids and Surfaces B-Biointerfaces, 2011. **83**(1): p. 16-22.
78. D.A. Dikin, S. Stankovich, E.J. Zimney, R.D. Piner, G.H.B. Dommett, G. Evmenenko, S.T. Nguyen, and R.S. Ruoff, *Preparation and characterization of graphene oxide paper.* Nature, 2007. **448**(7152): p. 457-460.
79. A. Buchsteiner, A. Lerf, and J. Pieper, *Water Dynamics in Graphite Oxide Investigated with Neutron Scattering.* The Journal of Physical Chemistry B, 2006. **110**(45): p. 22328-22338.
80. I. Jung, D. Dikin, S. Park, W. Cai, S.L. Mielke, and R.S. Ruoff, *Effect of Water Vapor on Electrical Properties of Individual Reduced Graphene Oxide Sheets.* The Journal of Physical Chemistry C, 2008. **112**(51): p. 20264-20268.
81. A. Lerf, A. Buchsteiner, J. Pieper, S. Schottl, I. Dekany, T. Szabo, and H.P. Boehm, *Hydration behavior and dynamics of water molecules in graphite oxide.* Journal of Physics and Chemistry of Solids, 2006. **67**(5-6): p. 1106-1110.
82. N.V. Medhekar, A. Ramasubramaniam, R.S. Ruoff, and V.B. Shenoy, *Hydrogen Bond Networks in Graphene Oxide Composite Paper: Structure and Mechanical Properties.* ACS Nano, 2010. **4**(4): p. 2300-2306.
83. U. Hofmann and A. Frenzel, *The reduction of graphite oxide with hydrogen sulphide.* Kolloid-Zeitschrift, 1934. **68**(2): p. 149-151.
84. S. Park, J.H. An, R.D. Piner, I. Jung, D.X. Yang, A. Velamakanni, S.T. Nguyen, and R.S. Ruoff, *Aqueous Suspension and Characterization of Chemically Modified Graphene Sheets.* Chemistry of Materials, 2008. **20**(21): p. 6592-6594.

85. H.J. Shin, K.K. Kim, A. Benayad, S.M. Yoon, H.K. Park, I.S. Jung, M.H. Jin, H.K. Jeong, J.M. Kim, J.Y. Choi, and Y.H. Lee, *Efficient Reduction of Graphite Oxide by Sodium Borohydrilde and Its Effect on Electrical Conductance.* Advanced Functional Materials, 2009. **19**(12): p. 1987-1992.
86. V.C. Tung, M.J. Allen, Y. Yang, and R.B. Kaner, *High-throughput solution processing of large-scale graphene.* Nature Nanotechnology, 2009. **4**(1): p. 25-29.
87. S. Stankovich, D.A. Dikin, G.H.B. Dommett, K.M. Kohlhaas, E.J. Zimney, E.A. Stach, R.D. Piner, S.T. Nguyen, and R.S. Ruoff, *Graphene-based composite materials.* Nature, 2006. **442**(7100): p. 282-286.
88. J.M. Yun, J.S. Yeo, J. Kim, H.G. Jeong, D.Y. Kim, Y.J. Noh, S.S. Kim, B.C. Ku, and S.I. Na, *Solution-Processable Reduced Graphene Oxide as a Novel Alternative to PEDOT:PSS Hole Transport Layers for Highly Efficient and Stable Polymer Solar Cells.* Advanced Materials, 2011. **23**(42): p. 4923-4928.
89. J. Liu, H. Jeong, J. Liu, K. Lee, J.Y. Park, Y.H. Ahn, and S. Lee, *Reduction of functionalized graphite oxides by trioctylphosphine in non-polar organic solvents.* Carbon, 2010. **48**(8): p. 2282-2289.
90. I.K. Moon, J. Lee, R.S. Ruoff, and H. Lee, *Reduced graphene oxide by chemical graphitization.* Nature Communications, 2010. **1**: p. 1-6.
91. F. Cataldo, O. Ursini, and G. Angelini, *Graphite Oxide and Graphene Nanoribbons Reduction with Hydrogen Iodide.* Fullerenes Nanotubes and Carbon Nanostructures, 2011. **19**(5): p. 461-468.
92. A. Esfandiar, O. Akhavan, and A. Irajizad, *Melatonin as a powerful bio-antioxidant for reduction of graphene oxide.* Journal of Materials Chemistry, 2011. **21**(29): p. 10907-10914.
93. K.H. Liao, A. Mittal, S. Bose, C. Leighton, K.A. Mkhoyan, and C.W. Macosko, *Aqueous Only Route toward Graphene from Graphite Oxide.* ACS Nano, 2011. **5**(2): p. 1253-1258.
94. T.H. Han, Y.-K. Huang, A.T.L. Tan, V.P. Dravid, and J. Huang, *Steam Etched Porous Graphene Oxide Network for Chemical Sensing.* Journal of the American Chemical Society, 2011. **133**(39): p. 15264-15267.
95. Y. Long, C.C. Zhang, X.X. Wang, J.P. Gao, W. Wang, and Y. Liu, *Oxidation of SO(2) to SO(3) catalyzed by graphene oxide foams.* Journal of Materials Chemistry, 2011. **21**(36): p. 13934-13941.
96. I.K. Moon, J. Lee, and H. Lee, *Highly qualified reduced graphene oxides: the best chemical reduction.* Chemical Communications, 2011. **47**(34): p. 9681-9683.
97. W.F. Chen, L.F. Yan, and P.R. Bangal, *Preparation of graphene by the rapid and mild thermal reduction of graphene oxide induced by microwaves.* Carbon, 2010. **48**(4): p. 1146-1152.
98. A.V. Murugan, T. Muraliganth, and A. Manthiram, *Rapid, Facile Microwave-Solvothermal Synthesis of Graphene Nanosheets and Their Polyaniline Nanocomposites for Energy Strorage.* Chemistry of Materials, 2009. **21**(21): p. 5004-5006.

99. K. Wang, T. Feng, M. Qian, H.I. Ding, Y.W. Chen, and Z.O. Sun, *The field emission of vacuum filtered graphene films reduced by microwave.* Applied Surface Science, 2011. **257**(13): p. 5808-5812.
100. T.N. Zhou, F. Chen, K. Liu, H. Deng, Q. Zhang, J.W. Feng, and Q.A. Fu, *A simple and efficient method to prepare graphene by reduction of graphite oxide with sodium hydrosulfite.* Nanotechnology, 2011. **22**(4).
101. R.J. Liao, Z.H. Tang, Y.D. Lei, and B.C. Guo, *Polyphenol-Reduced Graphene Oxide: Mechanism and Derivatization.* Journal of Physical Chemistry C, 2011. **115**(42): p. 20740-20746.
102. C. Chen, T. Chen, H. Wang, G. Sun, and X. Yang, *A rapid, one-step, variable-valence metal ion assisted reduction method for graphene oxide.* Nanotechnology, 2011. **22**(40).
103. I. Jung, D.A. Dikin, R.D. Piner, and R.S. Ruoff, *Tunable Electrical Conductivity of Individual Graphene Oxide Sheets Reduced at "Low" Temperatures.* Nano Letters, 2008. **8**(12): p. 4283-4287.
104. S. Wang, P.K. Ang, Z. Wang, A.L.L. Tang, J.T.L. Thong, and K.P. Loh, *High Mobility, Printable, and Solution-Processed Graphene Electronics.* Nano Letters, 2009. **10**(1): p. 92-98.
105. W.F. Chen and L.F. Yan, *Preparation of graphene by a low-temperature thermal reduction at atmosphere pressure.* Nanoscale, 2010. **2**(4): p. 559-563.
106. C. Nethravathi and M. Rajamathi, *Chemically modified graphene sheets produced by the solvothermal reduction of colloidal dispersions of graphite oxide.* Carbon, 2008. **46**(14): p. 1994-1998.
107. Y.W. Zhu, M.D. Stoller, W.W. Cai, A. Velamakanni, R.D. Piner, D. Chen, and R.S. Ruoff, *Exfoliation of Graphite Oxide in Propylene Carbonate and Thermal Reduction of the Resulting Graphene Oxide Platelets.* ACS Nano, 2010. **4**(2): p. 1227-1233.
108. M. Zhou, Y.L. Wang, Y.M. Zhai, J.F. Zhai, W. Ren, F.A. Wang, and S.J. Dong, *Controlled Synthesis of Large-Area and Patterned Electrochemically Reduced Graphene Oxide Films.* Chemistry-a European Journal, 2009. **15**(25): p. 6116-6120.
109. W.F. Chen, L.F. Yan, and P.R. Bangal, *Chemical Reduction of Graphene Oxide to Graphene by Sulfur-Containing Compounds.* Journal of Physical Chemistry C, 2010. **114**(47): p. 19885-19890.
110. Y. Chen, Y. Shen, D. Sun, H. Zhang, D. Tian, J. Zhang, and J.-J. Zhu, *Fabrication of a dispersible graphene/gold nanoclusters hybrid and its potential application in electrogenerated chemiluminescence.* Chemical communications (Cambridge, England), 2011. **47**(42): p. 11733-5.
111. V. Dua, S.P. Surwade, S. Ammu, S.R. Agnihotra, S. Jain, K.E. Roberts, S. Park, R.S. Ruoff, and S.K. Manohar, *All-Organic Vapor Sensor Using Inkjet-Printed Reduced Graphene Oxide.* Angewandte Chemie-International Edition, 2010. **49**(12): p. 2154-2157.
112. M.J. Fernandez-Merino, L. Guardia, J.I. Paredes, S. Villar-Rodil, P. Solis-Fernandez, A. Martinez-Alonso, and J.M.D. Tascon, *Vitamin C Is an Ideal*

Substitute for Hydrazine in the Reduction of Graphene Oxide Suspensions. Journal of Physical Chemistry C, 2010. **114**(14): p. 6426-6432.
113. J. Gao, F. Liu, Y.L. Liu, N. Ma, Z.Q. Wang, and X. Zhang, *Environment-Friendly Method To Produce Graphene That Employs Vitamin C and Amino Acid.* Chemistry of Materials, 2010. **22**(7): p. 2213-2218.
114. Z. Sui, X. Zhang, Y. Lei, and Y. Luo, *Easy and green synthesis of reduced graphite oxide-based hydrogels.* Carbon, 2011. **49**(13): p. 4314-4321.
115. X.B. Fan, W.C. Peng, Y. Li, X.Y. Li, S.L. Wang, G.L. Zhang, and F.B. Zhang, *Deoxygenation of Exfoliated Graphite Oxide under Alkaline Conditions: A Green Route to Graphene Preparation.* Advanced Materials, 2008. **20**(23): p. 4490-4493.
116. C.Z. Zhu, S.J. Guo, Y.X. Fang, and S.J. Dong, *Reducing Sugar: New Functional Molecules for the Green Synthesis of Graphene Nanosheets.* ACS Nano, 2010. **4**(4): p. 2429-2437.
117. J.B. Liu, S.H. Fu, B. Yuan, Y.L. Li, and Z.X. Deng, *Toward a Universal "Adhesive Nanosheet" for the Assembly of Multiple Nanoparticles Based on a Protein-Induced Reduction/Decoration of Graphene Oxide.* Journal of the American Chemical Society, 2010. **132**(21): p. 7279-+.
118. J.L. Chen and X.P. Yan, *A dehydration and stabilizer-free approach to production of stable water dispersions of graphene nanosheets.* Journal of Materials Chemistry, 2010. **20**(21): p. 4328-4332.
119. S.J. An, Y.W. Zhu, S.H. Lee, M.D. Stoller, T. Emilsson, S. Park, A. Velamakanni, J.H. An, and R.S. Ruoff, *Thin Film Fabrication and Simultaneous Anodic Reduction of Deposited Graphene Oxide Platelets by Electrophoretic Deposition.* Journal of Physical Chemistry Letters, 2010. **1**(8): p. 1259-1263.
120. H.L. Guo, X.F. Wang, Q.Y. Qian, F.B. Wang, and X.H. Xia, *A Green Approach to the Synthesis of Graphene Nanosheets.* ACS Nano, 2009. **3**(9): p. 2653-2659.
121. Y. Guo, B. Wu, H. Liu, Y. Ma, Y. Yang, J. Zheng, G. Yu, and Y. Liu, *Electrical assembly and reduction of graphene oxide in a single solution step for use in flexible sensors.* Advanced materials (Deerfield Beach, Fla.), 2011. **23**(40): p. 4626-30.
122. J. Ping, Y. Wang, K. Fan, J. Wu, and Y. Ying, *Direct electrochemical reduction of graphene oxide on ionic liquid doped screen-printed electrode and its electrochemical biosensing application.* Biosensors & Bioelectronics, 2011. **28**(1): p. 204-209.
123. G.K. Ramesha and S. Sampath, *Electrochemical Reduction of Oriented Graphene Oxide Films: An in Situ Raman Spectroelectrochemical Study.* Journal of Physical Chemistry C, 2009. **113**(19): p. 7985-7989.
124. Y.Y. Shao, J. Wang, M. Engelhard, C.M. Wang, and Y.H. Lin, *Facile and controllable electrochemical reduction of graphene oxide and its applications.* Journal of Materials Chemistry, 2010. **20**(4): p. 743-748.
125. R.S. Sundaram, C. Gomez-Navarro, K. Balasubramanian, M. Burghard, and K. Kern, *Electrochemical modification of graphene.* Advanced Materials, 2008. **20**(16): p. 3050-3053.

126. Z. Fan, K. Wang, T. Wei, J. Yan, L. Song, and B. Shao, *An environmentally friendly and efficient route for the reduction of graphene oxide by aluminum powder.* Carbon, 2010. **48**(5): p. 1686-1689.
127. G. Wang, J. Yang, J. Park, X. Gou, B. Wang, H. Liu, and J. Yao, *Facile synthesis and characterization of graphene nanosheets.* Journal of Physical Chemistry C, 2008. **112**(22): p. 8192-8195.
128. Z.S. Wu, W.C. Ren, L.B. Gao, B.L. Liu, C.B. Jiang, and H.M. Cheng, *Synthesis of high-quality graphene with a pre-determined number of layers.* Carbon, 2009. **47**(2): p. 493-499.
129. Y. Matsumoto, M. Koinuma, S. Ida, S. Hayami, T. Taniguchi, K. Hatakeyama, H. Tateishi, Y. Watanabe, and S. Amano, *Photoreaction of Graphene Oxide Nanosheets in Water.* Journal of Physical Chemistry C, 2011. **115**(39): p. 19280-19286.
130. G. Williams, B. Seger, and P.V. Kamat, *TiO2-Graphene Nanocomposites. UV-Assisted Photocatalytic Reduction of Graphene Oxide.* ACS Nano, 2008. **2**(7): p. 1487-1491.
131. L.J. Cote, R. Cruz-Silva, and J.X. Huang, *Flash Reduction and Patterning of Graphite Oxide and Its Polymer Composite.* Journal of the American Chemical Society, 2009. **131**(31): p. 11027-11032.
132. S.J. Kang, C. Kocabas, T. Ozel, M. Shim, N. Pimparkar, M.A. Alam, S.V. Rotkin, and J.A. Rogers, *High-performance electronics using dense, perfectly aligned arrays of single-walled carbon nanotubes.* Nature Nanotechnology, 2007. **2**(4): p. 230-236.
133. J.R. Lomeda, C.D. Doyle, D.V. Kosynkin, W.F. Hwang, and J.M. Tour, *Diazonium Functionalization of Surfactant-Wrapped Chemically Converted Graphene Sheets.* Journal of the American Chemical Society, 2008. **130**(48): p. 16201-16206.
134. M.C. Kim, G.S. Hwang, and R.S. Ruoff, *Epoxide reduction with hydrazine on graphene: A first principles study.* Journal of Chemical Physics, 2009. **131**(6).
135. D. Li, M.B. Muller, S. Gilje, R.B. Kaner, and G.G. Wallace, *Processable aqueous dispersions of graphene nanosheets.* Nature Nanotechnology, 2008. **3**(2): p. 101-105.
136. J. Robertson and E.P. Oreilly, *ELECTRONIC AND ATOMIC-STRUCTURE OF AMORPHOUS-CARBON.* Physical Review B, 1987. **35**(6): p. 2946-2957.
137. C.W. Chen and J. Robertson, *Nature of disorder and localization in amorphous carbon.* Journal of Non-Crystalline Solids, 1998. **227**: p. 602-606.
138. M. Koos, M. Veres, M. Fule, and I. Pocsik, *Ultraviolet photoluminescence and its relation to atomic bonding properties of hydrogenated amorphous carbon.* Diamond and Related Materials, 2002. **11**(1): p. 53-58.
139. F. Demichelis, S. Schreiter, and A. Tagliaferro, *PHOTOLUMINESCENCE IN A-C-H FILMS.* Physical Review B, 1995. **51**(4): p. 2143-2147.
140. Rusli, J. Robertson, and G.A.J. Amaratunga, *Photoluminescence behavior of hydrogenated amorphous carbon.* Journal of Applied Physics, 1996. **80**(5): p. 2998-3003.

141. G. Eda, Y.-Y. Lin, C. Mattevi, H. Yamaguchi, H.-A. Chen, I.S. Chen, C.-W. Chen, and M. Chhowalla, *Blue Photoluminescence from Chemically Derived Graphene Oxide.* Advanced Materials, 2010. **22**(4): p. 505-+.
142. Y. He, Z.-G. Wang, H.-W. Tang, and D.-W. Pang, *Low background signal platform for the detection of ATP: When a molecular aptamer beacon meets graphene oxide.* Biosensors & bioelectronics, 2011. **29**(1): p. 76-81.
143. L.R. Radovic and B. Bockrath, *On the chemical nature of graphene edges: Origin of stability and potential for magnetism in carbon materials.* Journal of the American Chemical Society, 2005. **127**(16): p. 5917-5927.
144. S. Mrozowski, *SEMICONDUCTIVITY AND DIAMAGNETISM OF POLYCRYSTALLINE GRAPHITE AND CONDENSED RING SYSTEMS.* Physical Review, 1952. **85**(4): p. 609-620.
145. C. Galande, A.D. Mohite, A.V. Naumov, W. Gao, L.J. Ci, A. Ajayan, H. Gao, A. Srivastava, R.B. Weisman, and P.M. Ajayan, *Quasi-Molecular Fluorescence from Graphene Oxide.* Scientific Reports, 2011. **1**.
146. T.V. Cuong, V.H. Pham, Q.T. Tran, S.H. Hahn, J.S. Chung, E.W. Shin, and E.J. Kim, *Photoluminescence and Raman studies of graphene thin films prepared by reduction of graphene oxide.* Materials Letters, 2010. **64**(3): p. 399-401.
147. Z. Liu, J.T. Robinson, X.M. Sun, and H.J. Dai, *PEGylated nanographene oxide for delivery of water-insoluble cancer drugs.* Journal of the American Chemical Society, 2008. **130**(33): p. 10876-+.
148. Z.T. Luo, P.M. Vora, E.J. Mele, A.T.C. Johnson, and J.M. Kikkawa, *Photoluminescence and band gap modulation in graphene oxide.* Applied Physics Letters, 2009. **94**(11): p. 3.
149. K.S. Subrahmanyam, P. Kumar, A. Nag, and C.N.R. Rao, *Blue light emitting graphene-based materials and their use in generating white light.* Solid State Communications, 2010. **150**(37-38): p. 1774-1777.
150. H.F. Dong, W.C. Gao, F. Yan, H.X. Ji, and H.X. Ju, *Fluorescence Resonance Energy Transfer between Quantum Dots and Graphene Oxide for Sensing Biomolecules.* Analytical Chemistry, 2010. **82**(13): p. 5511-5517.
151. J. Kim, L.J. Cote, F. Kim, and J.X. Huang, *Visualizing Graphene Based Sheets by Fluorescence Quenching Microscopy.* Journal of the American Chemical Society, 2010. **132**(1): p. 260-267.
152. Q. Liu, Z.F. Liu, X.Y. Zhang, N. Zhang, L.Y. Yang, S.G. Yin, and Y.S. Chen, *Organic photovoltaic cells based on an acceptor of soluble graphene.* Applied Physics Letters, 2008. **92**(22): p. 3.
153. E. Treossi, M. Melucci, A. Liscio, M. Gazzano, P. Samori, and V. Palermo, *High-Contrast Visualization of Graphene Oxide on Dye-Sensitized Glass, Quartz, and Silicon by Fluorescence Quenching.* Journal of the American Chemical Society, 2009. **131**(43): p. 15576-+.
154. Y.B. Wang, D. Kurunthu, G.W. Scott, and C.J. Bardeen, *Fluorescence Quenching in Conjugated Polymers Blended with Reduced Graphitic Oxide.* Journal of Physical Chemistry C, 2010. **114**(9): p. 4153-4159.

155. L.M. Xie, X. Ling, Y. Fang, J. Zhang, and Z.F. Liu, *Graphene as a Substrate To Suppress Fluorescence in Resonance Raman Spectroscopy.* Journal of the American Chemical Society, 2009. **131**(29): p. 9890-+.
156. S.J. He, B. Song, D. Li, C.F. Zhu, W.P. Qi, Y.Q. Wen, L.H. Wang, S.P. Song, H.P. Fang, and C.H. Fan, *A Graphene Nanoprobe for Rapid, Sensitive, and Multicolor Fluorescent DNA Analysis.* Advanced Functional Materials, 2010. **20**(3): p. 453-459.
157. C.H. Lu, H.H. Yang, C.L. Zhu, X. Chen, and G.N. Chen, *A Graphene Platform for Sensing Biomolecules.* Angewandte Chemie-International Edition, 2009. **48**(26): p. 4785-4787.
158. S. Kumar, M. Anija, N. Kamaraju, K.S. Vasu, K.S. Subrahmanyam, A.K. Sood, and C.N.R. Rao, *Femtosecond carrier dynamics and saturable absorption in graphene suspensions.* Applied Physics Letters, 2009. **95**(19): p. 3.
159. Z.B. Liu, Y. Wang, X.L. Zhang, Y.F. Xu, Y.S. Chen, and J.G. Tian, *Nonlinear optical properties of graphene oxide in nanosecond and picosecond regimes.* Applied Physics Letters, 2009. **94**(2): p. 3.
160. J. Wang, Y. Hernandez, M. Lotya, J.N. Coleman, and W.J. Blau, *Broadband Nonlinear Optical Response of Graphene Dispersions.* Advanced Materials, 2009. **21**(23): p. 2430-+.
161. K.S. Choi, Y. Park, K.C. Kwon, J. Kim, C.K. Kim, S.Y. Kim, K. Hong, and J.L. Lee, *Reduced Graphite Oxide-Indium Tin Oxide Hybrid Materials for use as a Transparent Electrode.* Journal of the Electrochemical Society, 2011. **158**(8): p. J231-J235.
162. J.H. Kim, J.M. Jung, J.Y. Kwak, J.H. Jeong, B.C. Choi, and K.T. Lim, *Preparation of Properties of SWNT/Graphene Oxide Type Flexible Transparent Conductive Films.* Journal of Nanoscience and Nanotechnology, 2011. **11**(8): p. 7424-7427.
163. Y.Q. Liu, L. Gao, J. Sun, Y. Wang, and J. Zhang, *Stable Nafion-functionalized graphene dispersions for transparent conducting films.* Nanotechnology, 2009. **20**(46).
164. Y. Matsuo, K. Iwasa, Y. Sugie, H. Usami, and M. Kawaguchi, *Effect of the perfluoroalkyl groups on the preparation of carbon-based transparent and conductive thin films from silylated graphite oxides.* Journal of Fluorine Chemistry, 2011. **132**(10): p. 669-672.
165. S.K. Bhunia and N.R. Jana, *Peptide-Functionalized Colloidal Graphene via Interdigited Bilayer Coating and Fluorescence Turn-on Detection of Enzyme.* Acs Applied Materials & Interfaces, 2011. **3**(9): p. 3335-3341.
166. X. Dong, Q. Long, J. Wang, M.B. Chan-Park, Y. Huang, W. Huang, and P. Chen, *A graphene nanoribbon network and its biosensing application.* Nanoscale, 2011. **3**(12): p. 5156-5160.
167. T. Gan and S. Hu, *Electrochemical sensors based on graphene materials.* Microchimica Acta, 2011. **175**(1-2): p. 1-19.

168. Y.P. He, Q.L. Sheng, J.B. Zheng, M.Z. Wang, and B. Liu, *Magnetite-graphene for the direct electrochemistry of hemoglobin and its biosensing application.* Electrochimica Acta, 2011. **56**(5): p. 2471-2476.
169. K.-J. Huang, Q.-S. Jing, Z.-W. Wu, L. Wang, and C.-Y. Wei, *Enhanced sensing of dopamine in the present of ascorbic acid based on graphene/poly(p-aminobenzoic acid) composite film.* Colloids and Surfaces B-Biointerfaces, 2011. **88**(1): p. 310-314.
170. F.-Y. Kong, M.-T. Xu, J.-J. Xu, and H.-Y. Chen, *A novel lable-free electrochemical immunosensor for carcinoembryonic antigen based on gold nanoparticles-thionine-reduced graphene oxide nanocomposite film modified glassy carbon electrode.* Talanta, 2011. **85**(5): p. 2620-5.
171. N. Lei, P. Li, W. Xue, and J. Xu, *Simple graphene chemiresistors as pH sensors: fabrication and characterization.* Measurement Science & Technology, 2011. **22**(10).
172. W. Li, X. Geng, Y. Guo, J. Rong, Y. Gong, L. Wu, X. Zhang, P. Li, J. Xu, G. Cheng, M. Sun, and L. Liu, *Reduced Graphene Oxide Electrically Contacted Graphene Sensor for Highly Sensitive Nitric Oxide Detection.* ACS Nano, 2011. **5**(9): p. 6955-6961.
173. H. Liu, J. Gao, M.Q. Xue, N. Zhu, M.N. Zhang, and T.B. Cao, *Processing of Graphene for Electrochemical Application: Noncovalently Functionalize Graphene Sheets with Water-Soluble Electroactive Methylene Green.* Langmuir, 2009. **25**(20): p. 12006-12010.
174. S. Liu, L. Wang, J. Tian, Y. Luo, X. Zhang, and X. Sun, *Aniline as a dispersing and stabilizing agent for reduced graphene oxide and its subsequent decoration with Ag nanoparticles for enzymeless hydrogen peroxide detection.* Journal of Colloid and Interface Science, 2011. **363**(2): p. 615-619.
175. L.M. Lu, H.B. Li, F.L. Qu, X.B. Zhang, G.L. Shen, and R.Q. Yu, *In situ synthesis of palladium nanoparticle-graphene nanohybrids and their application in nonenzymatic glucose biosensors.* Biosensors & Bioelectronics, 2011. **26**(8): p. 3500-3504.
176. X.J. Lu, H. Dou, B. Gao, C.Z. Yuan, S.D. Yang, L. Hao, L.F. Shen, and X.G. Zhang, *A flexible graphene/multiwalled carbon nanotube film as a high performance electrode material for supercapacitors.* Electrochimica Acta, 2011. **56**(14): p. 5115-5121.
177. Y. Mao, Y. Bao, S. Gan, F. Li, and L. Niu, *Electrochemical sensor for dopamine based on a novel graphene-molecular imprinted polymers composite recognition element.* Biosensors & Bioelectronics, 2011. **28**(1): p. 291-297.
178. Y. Pu, Z. Zhu, D. Han, H. Liu, J. Liu, J. Liao, K. Zhang, and W. Tan, *Insulin-binding aptamer-conjugated graphene oxide for insulin detection.* Analyst, 2011. **136**(20): p. 4138-4140.
179. J.T. Robinson, F.K. Perkins, E.S. Snow, Z.Q. Wei, and P.E. Sheehan, *Reduced Graphene Oxide Molecular Sensors.* Nano Letters, 2008. **8**(10): p. 3137-3140.

180. T. Sun, L. Wang, N. Li, and X. Gan, *Label-free electrochemical aptasensor for thrombin detection based on the nafion@graphene as platform.* Bioprocess and biosystems engineering, 2011. **34**(9): p. 1081-5.
181. H. Vedala, D.C. Sorescu, G.P. Kotchey, and A. Star, *Chemical Sensitivity of Graphene Edges Decorated with Metal Nanoparticles.* Nano Letters, 2011. **11**(6): p. 2342-2347.
182. L. Wang, K.-Y. Pu, J. Li, X. Qi, H. Li, H. Zhang, C. Fan, and B. Liu, *A graphene-conjugated oligomer hybrid probe for light-up sensing of lectin and Escherichia coli.* Advanced materials (Deerfield Beach, Fla.), 2011. **23**(38): p. 4386-91.
183. F. Xu, Y. Sun, Y. Zhang, Y. Shi, Z. Wen, and Z. Li, *Graphene-Pt nanocomposite for nonenzymatic detection of hydrogen peroxide with enhanced sensitivity.* Electrochemistry Communications, 2011. **13**(10): p. 1131-1134.
184. D. Ye, L. Luo, Y. Ding, Q. Chen, and X. Liu, *A novel nitrite sensor based on graphene/polypyrrole/chitosan nanocomposite modified glassy carbon electrode.* Analyst, 2011. **136**(21): p. 4563-4569.
185. J.W. Yi, J. Park, K.S. Kim, and B.H. Kim, *pH-Responsive self-duplex of (Py)A-substituted oligodeoxyadenylate in graphene oxide solution as a molecular switch.* Organic & Biomolecular Chemistry, 2011. **9**(21): p. 7434-7438.
186. B. Zhang, D. Tang, B. Liu, H. Chen, Y. Cui, and G. Chen, *GoldMag nanocomposite-functionalized graphene sensing platform for one-step electrochemical immunoassay of alpha-fetoprotein.* Biosensors & bioelectronics, 2011. **28**(1): p. 174-180.
187. W. Zhang, Z. Guo, D. Huang, Z. Liu, X. Guo, and H. Zhong, *Synergistic effect of chemo-photothermal therapy using PEGylated graphene oxide.* Biomaterials, 2011. **32**(33): p. 8555-61.
188. H.R. Byon, J. Suntivich, and Y. Shao-Horn, *Graphene-Based Non-Noble-Metal Catalysts for Oxygen Reduction Reaction in Acid.* Chemistry of Materials, 2011. **23**(15): p. 3421-3428.
189. W.Q. Fan, Q.H. Lai, Q.H. Zhang, and Y. Wang, *Nanocomposites of TiO(2) and Reduced Graphene Oxide as Efficient Photocatalysts for Hydrogen Evolution.* Journal of Physical Chemistry C, 2011. **115**(21): p. 10694-10701.
190. L.L. Feng, G. Gao, P. Huang, X.S. Wang, C.L. Zhang, J.L. Zhang, S.W. Guo, and D.X. Cui, *Preparation of Pt Ag alloy nanoisland/graphene hybrid composites and its high stability and catalytic activity in methanol electro-oxidation.* Nanoscale Research Letters, 2011. **6**.
191. Y.J. Gao, D. Ma, C.L. Wang, J. Guan, and X.H. Bao, *Reduced graphene oxide as a catalyst for hydrogenation of nitrobenzene at room temperature.* Chemical Communications, 2011. **47**(8): p. 2432-2434.
192. J.-S. Lee, T. Lee, H.-K. Song, J. Cho, and B.-S. Kim, *Ionic liquid modified graphene nanosheets anchoring manganese oxide nanoparticles as efficient electrocatalysts for Zn-air batteries.* Energy & Environmental Science, 2011. **4**(10): p. 4148-4154.

193. S.H. Lee, N. Kakati, S.H. Jee, J. Maiti, and Y.-S. Yoon, *Hydrothermal synthesis of PtRu nanoparticles supported on graphene sheets for methanol oxidation in direct methanol fuel cell.* Materials Letters, 2011. **65**(21-22): p. 3281-3284.
194. Y.J. Li, W. Gao, L.J. Ci, C.M. Wang, and P.M. Ajayan, *Catalytic performance of Pt nanoparticles on reduced graphene oxide for methanol electro-oxidation.* Carbon, 2010. **48**(4): p. 1124-1130.
195. Y. Liang, Y. Li, H. Wang, J. Zhou, J. Wang, T. Regier, and H. Dai, *Co(3)O(4) nanocrystals on graphene as a synergistic catalyst for oxygen reduction reaction.* Nature Materials, 2011. **10**(10): p. 780-786.
196. C.-S. Liao, C.-T. Liao, C.-Y. Tso, and H.-J. Shy, *Microwave-polyol synthesis and electrocatalytic performance of Pt/graphene nanocomposites.* Materials Chemistry and Physics, 2011. **130**(1-2): p. 270-274.
197. B. Neppolian, A. Bruno, C.L. Bianchi, and M. Ashokkumar, *Graphene oxide based Pt-TiO(2) photocatalyst: Ultrasound assisted synthesis, characterization and catalytic efficiency.* Ultrasonics Sonochemistry, 2012. **19**(1): p. 9-15.
198. R.F. Nie, J.H. Wang, L.N. Wang, Y. Qin, P. Chen, and Z.Y. Hou, *Platinum supported on reduced graphene oxide as a catalyst for hydrogenation of nitroarenes.* Carbon, 2012. **50**(2): p. 586-596.
199. C. Peng, B.W. Jiang, Q. Liu, Z. Guo, Z.J. Xu, Q. Huang, H.J. Xu, R.Z. Tai, and C.H. Fan, *Graphene-templated formation of two-dimensional lepidocrocite nanostructures for high-efficiency catalytic degradation of phenols.* Energy & Environmental Science, 2011. **4**(6): p. 2035-2040.
200. B. Seger and P.V. Kamat, *Electrocatalytically Active Graphene-Platinum Nanocomposites. Role of 2-D Carbon Support in PEM Fuel Cells.* Journal of Physical Chemistry C, 2009. **113**(19): p. 7990-7995.
201. D.V. Stergiou, E.K. Diamanti, D. Gournis, and M.I. Prodromidis, *Comparative study of different types of graphenes as electrocatalysts for ascorbic acid.* Electrochemistry Communications, 2010. **12**(10): p. 1307-1309.
202. Y. Wen, H. Ding, and Y. Shan, *Preparation and visible light photocatalytic activity of Ag/TiO(2)/graphene nanocomposite.* Nanoscale, 2011. **3**(10): p. 4411-4417.
203. Q.J. Xiang, J.G. Yu, and M. Jaroniec, *Preparation and Enhanced Visible-Light Photocatalytic H(2)-Production Activity of Graphene/C(3)N(4) Composites.* Journal of Physical Chemistry C, 2011. **115**(15): p. 7355-7363.
204. P. Zeng, Q.G. Zhang, T.Y. Peng, and X.H. Zhang, *One-pot synthesis of reduced graphene oxide-cadmium sulfide nanocomposite and its photocatalytic hydrogen production.* Physical Chemistry Chemical Physics, 2011. **13**(48): p. 21496-21502.
205. Y. Zhang, Y.-e. Gu, S. Lin, J. Wei, Z. Wang, C. Wang, Y. Du, and W. Ye, *One-step synthesis of PtPdAu ternary alloy nanoparticles on graphene with superior methanol electrooxidation activity.* Electrochimica Acta, 2011. **56**(24): p. 8746-8751.
206. Y. Zhang, Z.-R. Tang, X. Fu, and Y.-J. Xu, *Engineering the Unique 2D Mat of Graphene to Achieve Graphene-TiO(2) Nanocomposite for Photocatalytic*

Selective Transformation: What Advantage does Graphene Have over Its Forebear Carbon Nanotube? Acs Nano, 2011. **5**(9): p. 7426-7435.
207. C. Zhu, P. Wang, L. Wang, L. Han, and S. Dong, *Facile synthesis of two-dimensional graphene/SnO(2)/Pt ternary hybrid nanomaterials and their catalytic properties.* Nanoscale, 2011. **3**(10): p. 4376-4382.
208. Y. Zu, J. Tang, W. Zhu, M. Zhang, G. Liu, Y. Liu, W. Zhang, and M. Jia, *Graphite oxide-supported CaO catalysts for transesterification of soybean oil with methanol.* Bioresource Technology, 2011. **102**(19): p. 8939-8944.
209. K. Min, J.Y. Jung, T.H. Han, Y. Park, C. Jung, S.M. Hong, and C.M. Koo, *Graphene Electrodes for Artificial Muscles.* Molecular Crystals and Liquid Crystals, 2011. **539**: p. 260-265.
210. S. Chen, P. Chen, and Y. Wang, *Carbon nanotubes grown in situ on graphene nanosheets as superior anodes for Li-ion batteries.* Nanoscale, 2011. **3**(10): p. 4323-4329.
211. P.A. Denis, *Improving the Chemical Reactivity of Single-Wall Carbon Nanotubes with Lithium Doping.* Journal of Physical Chemistry C, 2011. **115**(41): p. 20282-20288.
212. S. Dong, X. Chen, K. Zhang, L. Gu, L. Zhang, X. Zhou, L. Li, Z. Liu, P. Han, H. Xu, J. Yao, C. Zhang, X. Zhang, C. Shang, G. Cui, and L. Chen, *Molybdenum nitride based hybrid cathode for rechargeable lithium-O(2) batteries.* Chemical Communications, 2011. **47**(40): p. 11291-11293.
213. C.X. Guo, M. Wang, T. Chen, X.W. Lou, and C.M. Li, *A Hierarchically Nanostructured Composite of MnO(2)/Conjugated Polymer/Graphene for High-Performance Lithium Ion Batteries.* Advanced Energy Materials, 2011. **1**(5): p. 736-741.
214. C.-T. Hsieh, C.-Y. Lin, and J.-Y. Lin, *High reversibility of Li intercalation and de-intercalation in MnO-attached graphene anodes for Li-ion batteries.* Electrochimica Acta, 2011. **56**(24): p. 8861-8867.
215. H. Liu and W. Yang, *Ultralong single crystalline V(2)O(5) nanowire/graphene composite fabricated by a facile green approach and its lithium storage behavior.* Energy & Environmental Science, 2011. **4**(10): p. 4000-4008.
216. Y.J. Mai, X.L. Wang, J.Y. Xiang, Y.Q. Qiao, D. Zhang, C.D. Gu, and J.P. Tu, *CuO/graphene composite as anode materials for lithium-ion batteries.* Electrochimica Acta, 2011. **56**(5): p. 2306-2311.
217. D.Y. Pan, S. Wang, B. Zhao, M.H. Wu, H.J. Zhang, Y. Wang, and Z. Jiao, *Li Storage Properties of Disordered Graphene Nanosheets.* Chemistry of Materials, 2009. **21**(14): p. 3136-3142.
218. Y. Shi, L. Wen, F. Li, and H.-M. Cheng, *Nanosized Li(4)Ti(5)O(12)/graphene hybrid materials with low polarization for high rate lithium ion batteries.* Journal of Power Sources, 2011. **196**(20): p. 8610-8617.
219. L. Su, Y. Jing, and Z. Zhou, *Li ion battery materials with core-shell nanostructures.* Nanoscale, 2011. **3**(10): p. 3967-3983.
220. Y. Sun, X. Hu, W. Luo, and Y. Huang, *Self-Assembled Hierarchical MoO(2)/Graphene Nanoarchitectures and Their Application as a High-*

Performance Anode Material for Lithium-Ion Batteries. ACS Nano, 2011. **5**(9): p. 7100-7107.
221. L. Tian, Q. Zhuang, J. Li, Y. Shi, J. Chen, F. Lu, and S. Sun, *Mechanism of intercalation and deintercalation of lithium ions in graphene nanosheets.* Chinese Science Bulletin, 2011. **56**(30): p. 3204-3212.
222. J. Zhu, K. Sun, D. Sim, C. Xu, H. Zhang, H.H. Hng, and Q. Yan, *Nanohybridization of ferrocene clusters and reduced graphene oxides with enhanced lithium storage capability.* Chemical Communications, 2011. **47**(37): p. 10383-10385.
223. J.X. Zhu, T. Zhu, X.Z. Zhou, Y.Y. Zhang, X.W. Lou, X.D. Chen, H. Zhang, H.H. Hng, and Q.Y. Yan, *Facile synthesis of metal oxide/reduced graphene oxide hybrids with high lithium storage capacity and stable cyclability.* Nanoscale, 2011. **3**(3): p. 1084-1089.
224. X.J. Zhu, Y.W. Zhu, S. Murali, M.D. Stollers, and R.S. Ruoff, *Nanostructured Reduced Graphene Oxide/Fe(2)O(3) Composite As a High-Performance Anode Material for Lithium Ion Batteries.* ACS Nano, 2011. **5**(4): p. 3333-3338.
225. M. Qian, T. Feng, H. Ding, L.F. Lin, H.B. Li, Y.W. Chen, and Z. Sun, *Electron field emission from screen-printed graphene films.* Nanotechnology, 2009. **20**(42).
226. B.G. Choi, J. Hong, W.H. Hong, P.T. Hammond, and H. Park, *Facilitated Ion Transport in All-Solid-State Flexible Supercapacitors.* ACS Nano, 2011. **5**(9): p. 7205-7213.
227. W. Gao, N. Singh, L. Song, Z. Liu, A.L.M. Reddy, L.J. Ci, R. Vajtai, Q. Zhang, B.Q. Wei, and P.M. Ajayan, *Direct laser writing of micro-supercapacitors on hydrated graphite oxide films.* Nature Nanotechnology, 2011. **6**(8): p. 496-500.
228. S. Konwer, R. Boruah, and S.K. Dolui, *Studies on Conducting Polypyrrole/Graphene Oxide Composites as Supercapacitor Electrode.* Journal of Electronic Materials, 2011. **40**(11): p. 2248-2255.
229. M.A. Pope, C. Punckt, and I.A. Aksay, *Intrinsic Capacitance and Redox Activity of Functionalized Graphene Sheets.* Journal of Physical Chemistry C, 2011. **115**(41): p. 20326-20334.
230. R.B. Rakhi and H.N. Alshareef, *Enhancement of the energy storage properties of supercapacitors using graphene nanosheets dispersed with metal oxide-loaded carbon nanotubes.* Journal of Power Sources, 2011. **196**(20): p. 8858-8865.
231. Y. Sun, Q. Wu, and G. Shi, *Supercapacitors based on self-assembled graphene organogel.* Physical Chemistry Chemical Physics, 2011. **13**(38): p. 17249-17254.
232. C.P. Tien and H.S. Teng, *Polymer/graphite oxide composites as high-performance materials for electric double layer capacitors.* Journal of Power Sources, 2010. **195**(8): p. 2414-2418.
233. Y. Wang, Z.Q. Shi, Y. Huang, Y.F. Ma, C.Y. Wang, M.M. Chen, and Y.S. Chen, *Supercapacitor Devices Based on Graphene Materials.* Journal of Physical Chemistry C, 2009. **113**(30): p. 13103-13107.

234. Z. Weng, Y. Su, D.-W. Wang, F. Li, J. Du, and H.-M. Cheng, *Graphene-Cellulose Paper Flexible Supercapacitors.* Advanced Energy Materials, 2011. **1**(5): p. 917-922.
235. G. Yu, L. Hu, N. Liu, H. Wang, M. Vosgueritchian, Y. Yang, Y. Cui, and Z. Bao, *Enhancing the Supercapacitor Performance of Graphene/MnO(2) Nanostructured Electrodes by Conductive Wrapping.* Nano Letters, 2011. **11**(10): p. 4438-4442.
236. J. Zhang, J. Jiang, H. Li, and X.S. Zhao, *A high-performance asymmetric supercapacitor fabricated with graphene-based electrodes.* Energy & Environmental Science, 2011. **4**(10): p. 4009-4015.
237. K. Zhang, L. Mao, L.L. Zhang, H.S.O. Chan, X.S. Zhao, and J.S. Wu, *Surfactant-intercalated, chemically reduced graphene oxide for high performance supercapacitor electrodes.* Journal of Materials Chemistry, 2011. **21**(20): p. 7302-7307.
238. K. Zhang, L.L. Zhang, X.S. Zhao, and J.S. Wu, *Graphene/Polyaniline Nanoriber Composites as Supercapacitor Electrodes.* Chemistry of Materials, 2010. **22**(4): p. 1392-1401.
239. L. Zhang and G.Q. Shi, *Preparation of Highly Conductive Graphene Hydrogels for Fabricating Supercapacitors with High Rate Capability.* Journal of Physical Chemistry C, 2011. **115**(34): p. 17206-17212.
240. Y.P. Zhang, H.B. Li, L.K. Pan, T. Lu, and Z. Sun, *Capacitive behavior of graphene-ZnO composite film for supercapacitors.* Journal of Electroanalytical Chemistry, 2009. **634**(1): p. 68-71.
241. G. Zhao, L. Jiang, Y. He, J. Li, H. Dong, X. Wang, and W. Hu, *Sulfonated Graphene for Persistent Aromatic Pollutant Management.* Advanced Materials, 2011. **23**(34): p. 3959-+.
242. B.J. Kim, M.S. Kang, V.H. Pham, T.V. Cuong, E.J. Kim, J.S. Chung, S.H. Hur, and J.H. Cho, *Low-voltage solution-processed graphene transistors based on chemically and solvothermally reduced graphene oxide.* Journal of Materials Chemistry, 2011. **21**(34): p. 13068-13073.
243. L. Zhou, W. Wang, J. Tang, J.-H. Zhou, H.-J. Jiang, and J. Shen, *Graphene oxide noncovalent photosensitizer and its anticancer activity in vitro.* Chemistry (Weinheim an der Bergstrasse, Germany), 2011. **17**(43): p. 12084-91.
244. S. Zhang, Z. Du, and G. Li, *Layer-by-Layer Fabrication of Chemical-Bonded Graphene Coating for Solid-Phase Microextraction.* Analytical Chemistry, 2011. **83**(19): p. 7531-7541.
245. W. Gao, M. Majumder, L.B. Alemany, T.N. Narayanan, M.A. Ibarra, B.K. Pradhan, and P.M. Ajayan, *Engineered Graphite Oxide Materials for Application in Water Purification.* Acs Applied Materials & Interfaces, 2011. **3**(6): p. 1821-1826.
246. J. Kysilka, M. Rubes, L. Grajciar, P. Nachtigall, and O. Bludsky, *Accurate Description of Argon and Water Adsorption on Surfaces of Graphene-Based Carbon Allotropes.* Journal of Physical Chemistry A, 2011. **115**(41): p. 11387-11393.

247. S. Liu, T.H. Zeng, M. Hofmann, E. Burcombe, J. Wei, R. Jiang, J. Kong, and Y. Chen, *Antibacterial Activity of Graphite, Graphite Oxide, Graphene Oxide, and Reduced Graphene Oxide: Membrane and Oxidative Stress.* ACS Nano, 2011. **5**(9): p. 6971-6980.
248. Q. Min, X. Zhang, H. Zhang, F. Zhou, and J.-J. Zhu, *Synthesis of Fe(3)O(4)-graphene-TiO(2) ternary composite networks for enhanced capture of phosphopeptides.* Chemical communications (Cambridge, England), 2011. **47**(42): p. 11709-11.
249. H. Pang, Q. Lu, and F. Gao, *Graphene oxide induced growth of one-dimensional fusiform zirconia nanostructures for highly selective capture of phosphopeptides.* Chemical communications (Cambridge, England), 2011. **47**(42): p. 11772-4.
250. Q. Wu, G. Zhao, C. Feng, C. Wang, and Z. Wang, *Preparation of a graphene-based magnetic nanocomposite for the extraction of carbamate pesticides from environmental water samples.* Journal of chromatography. A, 2011. **1218**(44): p. 7936-42.
251. S. Zhang, Y. Shao, J. Liu, I.A. Aksay, and Y. Lin, *Graphene-Polypyrrole Nanocomposite as a Highly Efficient and Low Cost Electrically Switched Ion Exchanger for Removing ClO(4)(-) from Wastewater.* Acs Applied Materials & Interfaces, 2011. **3**(9): p. 3633-7.
252. G. Zhao, X. Ren, X. Gao, X. Tan, J. Li, C. Chen, Y. Huang, and X. Wang, *Removal of Pb(II) ions from aqueous solutions on few-layered graphene oxide nanosheets.* Dalton Transactions, 2011. **40**(41): p. 10945-10952.
253. Q. Liu, Z.F. Liu, X.Y. Zhong, L.Y. Yang, N. Zhang, G.L. Pan, S.G. Yin, Y. Chen, and J. Wei, *Polymer Photovoltaic Cells Based on Solution-Processable Graphene and P3HT.* Advanced Functional Materials, 2009. **19**(6): p. 894-904.
254. Z. Liu, Q. Liu, Y. Huang, Y. Ma, S. Yin, X. Zhang, W. Sun, and Y. Chen, *Organic Photovoltaic Devices Based on a Novel Acceptor Material: Graphene.* Advanced Materials, 2008. **20**(20): p. 3924-3930.
255. M.S. Ryu and J. Jang, *Effect of solution processed graphene oxide/nickel oxide bi-layer on cell performance of bulk-heterojunction organic photovoltaic.* Solar Energy Materials and Solar Cells, 2011. **95**(10): p. 2893-2896.
256. K. Yang, C. Xu, L. Huang, L. Zou, and H. Wang, *Hybrid nanostructure heterojunction solar cells fabricated using vertically aligned ZnO nanotubes grown on reduced graphene oxide.* Nanotechnology, 2011. **22**(40).
257. Y. Zang, D. Xie, X. Wu, Y. Chen, Y. Lin, M. Li, H. Tian, X. Li, Z. Li, H. Zhu, T. Ren, and D. Plant, *Enhanced photovoltaic properties in graphene/polycrystalline BiFeO(3)/Pt heterojunction structure.* Applied Physics Letters, 2011. **99**(13): p. 32904-32904.
258. J. Liang, Y. Huang, J. Oh, M. Kozlov, D. Sui, S. Fang, R.H. Baughman, Y. Ma, and Y. Chen, *Electromechanical Actuators Based on Graphene and Graphene/Fe(3)O(4) Hybrid Paper.* Advanced Functional Materials, 2011. **21**(19): p. 3778-3784.

259. K.P. Loh, Q. Bao, G. Eda, and M. Chhowalla, *Graphene oxide as a chemically tunable platform for optical applications.* Nature Chemistry, 2010. **2**(12): p. 1015-1024.
260. Z.B. Liu, Y.F. Xu, X.Y. Zhang, X.L. Zhang, Y.S. Chen, and J.G. Tian, *Porphyrin and Fullerene Covalently Functionalized Graphene Hybrid Materials with Large Nonlinear Optical Properties.* Journal of Physical Chemistry B, 2009. **113**(29): p. 9681-9686.
261. S. Niyogi, E. Bekyarova, M.E. Itkis, J.L. McWilliams, M.A. Hamon, and R.C. Haddon, *Solution properties of graphite and graphene.* Journal of the American Chemical Society, 2006. **128**(24): p. 7720-7721.
262. Y.F. Xu, Z.B. Liu, X.L. Zhang, Y. Wang, J.G. Tian, Y. Huang, Y.F. Ma, X.Y. Zhang, and Y.S. Chen, *A Graphene Hybrid Material Covalently Functionalized with Porphyrin: Synthesis and Optical Limiting Property.* Advanced Materials, 2009. **21**(12): p. 1275-+.
263. L.M. Veca, F.S. Lu, M.J. Meziani, L. Cao, P.Y. Zhang, G. Qi, L.W. Qu, M. Shrestha, and Y.P. Sun, *Polymer functionalization and solubilization of carbon nanosheets.* Chemical Communications, 2009(18): p. 2565-2567.
264. N. Mohanty and V. Berry, *Graphene-Based Single-Bacterium Resolution Biodevice and DNA Transistor: Interfacing Graphene Derivatives with Nanoscale and Microscale Biocomponents.* Nano Letters, 2008. **8**(12): p. 4469-4476.
265. Y.J. Zhang, W.B. Hu, B. Li, C. Peng, C.H. Fan, and Q. Huang, *Synthesis of polymer-protected graphene by solvent-assisted thermal reduction process.* Nanotechnology, 2011. **22**(34).
266. Y.F. Yang, J. Wang, J. Zhang, J.C. Liu, X.L. Yang, and H.Y. Zhao, *Exfoliated Graphite Oxide Decorated by PDMAEMA Chains and Polymer Particles.* Langmuir, 2009. **25**(19): p. 11808-11814.
267. M. Fang, K.G. Wang, H.B. Lu, Y.L. Yang, and S. Nutt, *Covalent polymer functionalization of graphene nanosheets and mechanical properties of composites.* Journal of Materials Chemistry, 2009. **19**(38): p. 7098-7105.
268. S.H. Lee, D.R. Dreyer, J.H. An, A. Velamakanni, R.D. Piner, S. Park, Y.W. Zhu, S.O. Kim, C.W. Bielawski, and R.S. Ruoff, *Polymer Brushes via Controlled, Surface-Initiated Atom Transfer Radical Polymerization (ATRP) from Graphene Oxide.* Macromolecular Rapid Communications, 2010. **31**(3): p. 281-288.
269. S. Stankovich, R.D. Piner, S.T. Nguyen, and R.S. Ruoff, *Synthesis and exfoliation of isocyanate-treated graphene oxide nanoplatelets.* Carbon, 2006. **44**(15): p. 3342-3347.
270. H.T. Hu, X.B. Wang, J.C. Wang, F.M. Liu, M. Zhang, and C.H. Xu, *Microwave-assisted covalent modification of graphene nanosheets with chitosan and its electrorheological characteristics.* Applied Surface Science, 2011. **257**(7): p. 2637-2642.
271. S. Wang, P.J. Chia, L.L. Chua, L.H. Zhao, R.Q. Png, S. Sivaramakrishnan, M. Zhou, R.G.S. Goh, R.H. Friend, A.T.S. Wee, and P.K.H. Ho, *Band-like transport in*

surface-functionalized highly solution-processable graphene nanosheets. Advanced Materials, 2008. **20**(18): p. 3440-+.

272. O.C. Compton, D.A. Dikin, K.W. Putz, L.C. Brinson, and S.T. Nguyen, *Electrically Conductive "Alkylated" Graphene Paper via Chemical Reduction of Amine-Functionalized Graphene Oxide Paper.* Advanced Materials, 2010. **22**(8): p. 892-+.
273. H.F. Yang, C.S. Shan, F.H. Li, D.X. Han, Q.X. Zhang, and L. Niu, *Covalent functionalization of polydisperse chemically-converted graphene sheets with amine-terminated ionic liquid.* Chemical Communications, 2009(26): p. 3880-3882.
274. H.F. Yang, F.H. Li, C.S. Shan, D.X. Han, Q.X. Zhang, L. Niu, and A. Ivaska, *Covalent functionalization of chemically converted graphene sheets via silane and its reinforcement.* Journal of Materials Chemistry, 2009. **19**(26): p. 4632-4638.
275. S. Park, D.A. Dikin, S.T. Nguyen, and R.S. Ruoff, *Graphene Oxide Sheets Chemically Cross-Linked by Polyallylamine.* Journal of Physical Chemistry C, 2009. **113**(36): p. 15801-15804.
276. R.K. Layek, S. Samanta, D.P. Chatterjee, and A.K. Nandi, *Physical and mechanical properties of poly(methyl methacrylate) -functionalized graphene/poly(vinylidine fluoride) nanocomposites Piezoelectric beta polymorph formation.* Polymer, 2010. **51**(24): p. 5846-5856.
277. S. Kamada, H. Nomoto, K. Fukuda, T. Fukawa, H. Shirai, and M. Kimura, *Noncovalent wrapping of chemically modified graphene with pi-conjugated disk-like molecules.* Colloid and Polymer Science, 2011. **289**(8): p. 925-932.
278. X.Y. Chen, L. Yuan, P.Y. Yang, J.H. Hu, and D. Yang, *Covalent Polymeric Modification of Graphene Nanosheets Via Surface-Initiated Single-Electron-Transfer Living Radical Polymerization.* Journal of Polymer Science Part a-Polymer Chemistry, 2011. **49**(23): p. 4977-4986.
279. X.Y. Yang, X.Y. Zhang, Z.F. Liu, Y.F. Ma, Y. Huang, and Y. Chen, *High-Efficiency Loading and Controlled Release of Doxorubicin Hydrochloride on Graphene Oxide.* Journal of Physical Chemistry C, 2008. **112**(45): p. 17554-17558.
280. Y.-C. Cao, C. Xu, X. Wu, X. Wang, L. Xing, and K. Scott, *A poly (ethylene oxide)/graphene oxide electrolyte membrane for low temperature polymer fuel cells.* Journal of Power Sources, 2011. **196**(20): p. 8377-8382.
281. S.-S. Li, K.-H. Tu, C.-C. Lin, C.-W. Chen, and M. Chhowalla, *Solution-Processable Graphene Oxide as an Efficient Hole Transport Layer in Polymer Solar Cells.* Acs Nano, 2010. **4**(6): p. 3169-3174.
282. I.P. Murray, S.J. Lou, L.J. Cote, S. Loser, C.J. Kadleck, T. Xu, J.M. Szarko, B.S. Rolczynski, J.E. Johns, J. Huang, L. Yu, L.X. Chen, T.J. Marks, and M.C. Hersam, *Graphene Oxide Interlayers for Robust, High-Efficiency Organic Photovoltaics.* The Journal of Physical Chemistry Letters, 2011. **2**(24): p. 3006-3012.
283. D.R. Dreyer, K.A. Jarvis, P.J. Ferreira, and C.W. Bielawski, *Graphite Oxide as a Dehydrative Polymerization Catalyst: A One-Step Synthesis of Carbon-*

Reinforced Poly(phenylene methylene) Composites. Macromolecules, 2011. **44**(19): p. 7659-7667.
284. A.V. Kumar and K.R. Rao, *Recyclable graphite oxide catalyzed Friedel-Crafts addition of indoles to alpha,beta-unsaturated ketones.* Tetrahedron Letters, 2011. **52**(40): p. 5188-5191.
285. A. Kolmakov, D.A. Dikin, L.J. Cote, J. Huang, M.K. Abyaneh, M. Amati, L. Gregoratti, S. Guenther, and M. Kiskinova, *Graphene oxide windows for in situ environmental cell photoelectron spectroscopy.* Nature Nanotechnology, 2011. **6**(10): p. 651-657.
286. M. Krueger, S. Berg, D.A. Stone, E. Strelcov, D.A. Dikin, J. Kim, L.J. Cote, J. Huang, and A. Kolmakov, *Drop-Casted Self-Assembling Graphene Oxide Membranes for Scanning Electron Microscopy on Wet and Dense Gaseous Samples.* Acs Nano, 2011. **5**(12): p. 10047-10054.
287. X.L. Li, G.Y. Zhang, X.D. Bai, X.M. Sun, X.R. Wang, E. Wang, and H.J. Dai, *Highly conducting graphene sheets and Langmuir-Blodgett films.* Nature Nanotechnology, 2008. **3**(9): p. 538-542.
288. A. Mukherjee, L.B. Alemany, J. Chattopadhyay, S. Chakraborty, W.H. Guo, S.M. Yates, and W.E. Billups, *Dodecylated large fullerenes: An unusual class of solids.* Chemistry of Materials, 2008. **20**(17): p. 5513-5521.
289. A.L.M. Blumenfeld, V.E. Shumilova, I.B. Parnes, Z.N. Novikov, Yu. N. , *Investigation of graphite oxide by means of ^{13}C nmr and ^{1}H spin-lattice relaxation.* Materials Science Forum, 1992. **613**: p. 91-93.
290. H.P. Boehm, *SOME ASPECTS OF THE SURFACE-CHEMISTRY OF CARBON-BLACKS AND OTHER CARBONS.* Carbon, 1994. **32**(5): p. 759-769.
291. H.P. Boehm, W. Heck, R. Sappok, and E. Diehl, *SURFACE OXIDES OF CARBON.* Angewandte Chemie-International Edition, 1964. **3**(10): p. 669-&.
292. E. Fuente, J.A. Menendez, M.A. Diez, D. Suarez, and M.A. Montes-Moran, *Infrared spectroscopy of carbon materials: A quantum chemical study of model compounds.* Journal of Physical Chemistry B, 2003. **107**(26): p. 6350-6359.
293. Z.M. Wang, K. Hohsinoo, K. Shishibori, H. Kanoh, and K. Ooi, *Surfactant-mediated synthesis of a novel nanoporous carbon-silica composite.* Chemistry of Materials, 2003. **15**(15): p. 2926-2935.
294. R.G. Gillis and Q.N. Porter, *5-METHOXYPHENANTHRENE-4-CARBOXYLIC ACID.* Australian Journal of Chemistry, 1989. **42**(6): p. 1007-1010.
295. S.W. Pelletier, Z. Djarmati, and C. Pape, *SUBSTITUENT EFFECTS IN C-13 NMR-SPECTROSCOPY - METHYL, ETHYL, 2-PROPYL AND 2-METHYL-2-PROPYL CARBOXYLATES.* Tetrahedron, 1976. **32**(9): p. 995-996.
296. T. Mukaiyama, T. Shintou, and K. Fukumoto, *A convenient method for the preparation of inverted tert-alkyl carboxylates from chiral tert-alcohols by a new type of oxidation-reduction, condensation using 2,6-dimethyl-1,4-benzoquinone.* Journal of the American Chemical Society, 2003. **125**(35): p. 10538-10539.
297. L.M. Sweeting, A.L. Rheingold, J.M. Gingerich, A.W. Rutter, R.A. Spence, C.D. Cox, and T.J. Kim, *Crystal structure and triboluminescence .2. 9-*

anthracenecarboxylic acid and its esters. Chemistry of Materials, 1997. **9**(5): p. 1103-1115.
298. I.B. Rubin and M.V. Buchanan, *C-13 NMR-SPECTRA OF ANTHRAQUINONE-DERIVED DYES.* Magnetic Resonance in Chemistry, 1985. **23**(3): p. 161-165.
299. Y. Sakamoto, Y. Nakamura, T. Aoki, S. Ohshima, M. Takekawa, and S. Fujisawa, *Structure-reactivity studies by NMR spectroscopy and molecular orbital calculation: Nitration of polycyclic aromatic ketones.* Polycyclic Aromatic Compounds, 1999. **14**: p. 77-86.
300. O. Exner, P. Fiedler, M. Budesinsky, and J. Kulhanek, *Conformation and steric effects in mono- and dimethoxybenzoic acids.* Journal of Organic Chemistry, 1999. **64**(10): p. 3513-3518.
301. P.E. Hansen, O.K. Poulsen, and A. Berg, *C-13,C-13 COUPLING-CONSTANTS AND C-13 CHEMICAL-SHIFTS OF AROMATIC CARBONYL-COMPOUNDS - EFFECTS OF ORTHO-INTERACTIONS AND PERI-INTERACTIONS INVOLVING CARBONYL SUBSTITUENT.* Organic Magnetic Resonance, 1977. **9**(11): p. 649-658.
302. S.W. Chaikin and W.G. Brown, *REDUCTION OF ALDEHYDES, KETONES AND ACID CHLORIDES BY SODIUM BOROHYDRIDE.* Journal of the American Chemical Society, 1949. **71**(1): p. 122-125.
303. L.B. Alemany, D.M. Grant, R.J. Pugmire, T.D. Alger, and K.W. Zilm, *CROSS POLARIZATION AND MAGIC ANGLE SAMPLE SPINNING NMR-SPECTRA OF MODEL ORGANIC-COMPOUNDS .1. HIGHLY PROTONATED MOLECULES.* Journal of the American Chemical Society, 1983. **105**(8): p. 2133-2141.
304. H.C. Schniepp, J.L. Li, M.J. McAllister, H. Sai, M. Herrera-Alonso, D.H. Adamson, R.K. Prud'homme, R. Car, D.A. Saville, and I.A. Aksay, *Functionalized single graphene sheets derived from splitting graphite oxide.* Journal of Physical Chemistry B, 2006. **110**(17): p. 8535-8539.
305. D. Yang, A. Velamakanni, G. Bozoklu, S. Park, M. Stoller, R.D. Piner, S. Stankovich, I. Jung, D.A. Field, C.A. Ventrice, and R.S. Ruoff, *Chemical analysis of graphene oxide films after heat and chemical treatments by X-ray photoelectron and Micro-Raman spectroscopy.* Carbon, 2009. **47**(1): p. 145-152.
306. S. Cadars, J. Sein, L. Duma, A. Lesage, T.N. Pham, J.H. Baltisberger, S.P. Brown, and L. Emsley, *The refocused INADEQUATE MAS NMR experiment in multiple spin-systems: Interpreting observed correlation peaks and optimising lineshapes.* Journal of Magnetic Resonance, 2007. **188**(1): p. 24-34.
307. G.P. Holland, J.E. Jenkins, M.S. Creager, R.V. Lewis, and J.L. Yarger, *Quantifying the fraction of glycine and alanine in beta-sheet and helical conformations in spider dragline silk using solid-state NMR.* Chemical Communications, 2008(43): p. 5568-5570.
308. T. Miyoshi, W. Hu, and H. Hagihara, *Local packing disorders in a polymer crystal by two dimensional solid-state NMR.* Macromolecules, 2007. **40**(19): p. 6789-6792.

309. R. Verel, T. Manolikas, A.B. Siemer, and B.H. Meier, *Improved resolution in C-13 solid-state spectra through spin-state-selection.* Journal of Magnetic Resonance, 2007. **184**(2): p. 322-329.
310. R. Witter, U. Sternberg, S. Hesse, T. Kondo, F.T. Koch, and A.S. Ulrich, *C-13 chemical shift constrained crystal structure refinement of cellulose I-alpha and its verification by NMR anisotropy experiments.* Macromolecules, 2006. **39**(18): p. 6125-6132.
311. S. Park and R.S. Ruoff, *Chemical methods for the production of graphenes.* Nature Nanotechnology, 2009. **4**(4): p. 217-224.
312. M.D. Stoller, S. Park, Y. Zhu, J. An, and R.S. Ruoff, *Graphene-Based Ultracapacitors.* Nano Letters, 2008. **8**(10): p. 3498-3502.
313. G.K. Dimitrakakis, E. Tylianakis, and G.E. Froudakis, *Pillared Graphene: A New 3-D Network Nanostructure for Enhanced Hydrogen Storage.* Nano Letters, 2008. **8**(10): p. 3166-3170.
314. D.R. Dreyer, H.P. Jia, and C.W. Bielawski, *Graphene Oxide: A Convenient Carbocatalyst for Facilitating Oxidation and Hydration Reactions.* Angewandte Chemie International Edition, 2010: p. n/a-n/a.
315. A. Santos, P. Yustos, S. Rodríguez, F. Garcia-Ochoa, and M. de Gracia, *Decolorization of Textile Dyes by Wet Oxidation Using Activated Carbon as Catalyst.* Industrial & Engineering Chemistry Research, 2007. **46**(8): p. 2423-2427.
316. D. Mohan, V.K. Gupta, S.K. Srivastava, and S. Chander, *Kinetics of mercury adsorption from wastewater using activated carbon derived from fertilizer waste.* Colloids and Surfaces A: Physicochemical and Engineering Aspects, 2000. **177**(2-3): p. 169-181.
317. V. Chandra, J. Park, Y. Chun, J.W. Lee, I.-C. Hwang, and K.S. Kim, *Water-Dispersible Magnetite-Reduced Graphene Oxide Composites for Arsenic Removal.* ACS Nano, 2010. **4**(7): p. 3979-3986.
318. J.R. Lomeda, C.D. Doyle, D.V. Kosynkin, W.-F. Hwang, and J.M. Tour, *Diazonium Functionalization of Surfactant-Wrapped Chemically Converted Graphene Sheets.* Journal of the American Chemical Society, 2008. **130**(48): p. 16201-16206.
319. H.E. Inc, *Criteria and Standards for Improved Potable Water Quality*. 2nd ed. 2001, New York: John Wiley & Sons. 1.
320. F.B. Brikke, M., *Linking technology choice with operation and maintenance in the context of community water supply and sanitation*. Vol. pp72-73. 2003.
321. A.A. Zagordini, *Ion Exchange Materials: Properties and Applications*. 2007.
322. N.K. Wilson, R.D. Zehr, and P.D. Ellis, *Carbon-13 nuclear magnetic resonance.13C chemical shifts and13C199Hg coupling constants for some organomercury compounds.* Journal of Magnetic Resonance (1969), 1976. **21**(3): p. 437-443.
323. V. Nummert, M. Piirsalu, V. Mäemets, S. Vahur, and I.A. Koppel, *Effect of ortho substituents on carbonyl carbon 13C NMR chemical shifts in substituted phenyl*

benzoates. Journal of Physical Organic Chemistry, 2009. **22**(12): p. 1155-1165.
324. P.F. Barron, *Solid state 13C NMR of mercuric(II) acetate: scalar 13c---199Hg coupling and crystal structure.* Journal of Organometallic Chemistry, 1982. **236**(2): p. 157-161.
325. P.F. Barron, D. Doddrell, and W. Kitching, *Oxythallation and oxymercuration. Carbon-13 NMR examination of some norbornene derivatives.* Journal of Organometallic Chemistry, 1977. **132**(3): p. 351-358.
326. H.-O.B. Kalinowski, S.; and S. Braun, *Carbon-13 NMR Spectroscopy.* 1988. 199.
327. V. Smuleac, D.A. Butterfield, S.K. Sikdar, R.S. Varma, and D. Bhattacharyya, *Polythiol-functionalized alumina membranes for mercury capture.* Journal of Membrane Science, 2005. **251**(1-2): p. 169-178.
328. Y. Zhu, A.L. Higginbotham, and J.M. Tour, *Covalent Functionalization of Surfactant-Wrapped Graphene Nanoribbons.* Chemistry of Materials, 2009. **21**(21): p. 5284-5291.
329. X. Feng, G.E. Fryxell, L.-Q. Wang, A.Y. Kim, J. Liu, and K.M. Kemner, *Functionalized Monolayers on Ordered Mesoporous Supports.* Science, 1997. **276**(5314): p. 923-926.
330. E.L. Cussler, *Diffusion: Mass Transfer in Fluid Systems.* 2003: Cambridge University Press.
331. G.a.S. Balco, J.O. (2003) *Measuring the density of rock, sand, till, etc.* UW Cosmogenic Nuclide Laboratory, methods and procedures. **Volume**,
332. S.W. Martin and F.L. Shea, *Microstructures of Carbon Products.* Industrial and Engineering Chemistry, 1958. **50**(1): p. 41-46.
333. J. Chmiola, C. Largeot, P.L. Taberna, P. Simon, and Y. Gogotsi, *Monolithic Carbide-Derived Carbon Films for Micro-Supercapacitors.* Science, 2010. **328**(5977): p. 480-483.
334. D. Pech, M. Brunet, H. Durou, P.H. Huang, V. Mochalin, Y. Gogotsi, P.L. Taberna, and P. Simon, *Ultrahigh-power micrometre-sized supercapacitors based on onion-like carbon.* Nature Nanotechnology, 2010. **5**(9): p. 651-654.
335. D. Pech, M. Brunet, P.L. Taberna, P. Simon, N. Fabre, F. Mesnilgrente, V. Conedera, and H. Durou, *Elaboration of a microstructured inkjet-printed carbon electrochemical capacitor.* Journal of Power Sources, 2010. **APL calculation 195**(4): p. 1266-1269.
336. S. Cerveny, F. Barroso-Bujans, A. Alegria, and J. Colmenero, *Dynamics of Water Intercalated in Graphite Oxide.* Journal of Physical Chemistry C, 2010. **114**(6): p. 2604-2612.
337. X.J. Liu and T. Osaka, *All-solid-state electric double-layer capacitor with isotropic high-density graphite electrode and polyethylene oxide/LiClO4 polymer electrolyte.* Journal of the Electrochemical Society, 1996. **143**(12): p. 3982-3986.
338. M. Rikukawa and K. Sanui, *Proton-conducting polymer electrolyte membranes based on hydrocarbon polymers.* Progress in Polymer Science, 2000. **25**(10): p. 1463-1502.

339. K.W. Park, H.J. Ahn, and Y.E. Sung, *All-solid-state supercapacitor using a Nafion (R) polymer membrane and its hybridization with a direct methanol fuel cell.* Journal of Power Sources, 2002. **109**(2): p. 500-506.
340. T. Thampan, S. Malhotra, H. Tang, and R. Datta, *Modeling of conductive transport in proton-exchange membranes for fuel cells.* Journal of the Electrochemical Society, 2000. **147**(9): p. 3242-3250.
341. G. Eda and M. Chhowalla, *Chemically Derived Graphene Oxide: Towards Large-Area Thin-Film Electronics and Optoelectronics.* Advanced Materials, 2010. **22**(22): p. 2392-2415.
342. G. Eda, G. Fanchini, and M. Chhowalla, *Large-area ultrathin films of reduced graphene oxide as a transparent and flexible electronic material.* Nature Nanotechnology, 2008. **3**(5): p. 270-274.
343. L.B. Casablanca, M.A. Shaibat, W. Cai, S. Park, R. Piner, R.S. Ruoff, and Y. Ishii, *NMR-Based Structural Modeling of Graphite Oxide Using Multidimensional (13)C Solid-State NMR and ab Initio Chemical Shift Calculations.* Journal of the American Chemical Society, 2010. **132**(16): p. 5672-5676.
344. Z.Q. Wei, D.B. Wang, S. Kim, S.Y. Kim, Y.K. Hu, M.K. Yakes, A.R. Laracuente, Z.T. Dai, S.R. Marder, C. Berger, W.P. King, W.A. de Heer, P.E. Sheehan, and E. Riedo, *Nanoscale Tunable Reduction of Graphene Oxide for Graphene Electronics.* Science, 2010. **328**(5984): p. 1373-1376.
345. Y.L. Zhang, L. Guo, S. Wei, Y.Y. He, H. Xia, Q.D. Chen, H.B. Sun, and F.S. Xiao, *Direct imprinting of microcircuits on graphene oxides film by femtosecond laser reduction.* Nano Today, 2009. **5**(1): p. 15-20.
346. K.M. Abraham, Z. Jiang, and B. Carroll, *Highly conductive PEO-like polymer electrolytes.* Chemistry of Materials, 1997. **9**(9): p. 1978-1988.
347. J.R. Macdonald and E. Barsoukov, *Impedance Spectroscopy Theory, Experiment, And Applications.* second ed. 2005, New Jersey: John Wiley & Sons, Inc.
348. M. Hirata, T. Gotou, and M. Ohba, *Thin-film particles of graphite oxide. 2: Preliminary studies for internal micro fabrication of single particle and carbonaceous electronic circuits.* Carbon, 2005. **43**(3): p. 503-510.
349. C. Petit, M. Seredych, and T.J. Bandosz, *Revisiting the chemistry of graphite oxides and its effect on ammonia adsorption.* Journal of Materials Chemistry, 2009. **19**(48): p. 9176-9185.
350. N. Agmon, *The Grotthuss Mechanism.* Chemical Physics Letters, 1995. **244**(5-6): p. 456-462.
351. M. Saito, N. Arimura, K. Hayamizu, and T. Okada, *Mechanisms of ion and water transport in perfluorosulfonated ionomer membranes for fuel cells.* Journal of Physical Chemistry B, 2004. **108**(41): p. 16064-16070.
352. K.A. Mauritz and R.B. Moore, *State of understanding of Nafion.* Chemical Reviews, 2004. **104**(10): p. 4535-4585.
353. C. Punckt, M.A. Pope, J. Liu, Y.H. Lin, and I.A. Aksay, *Electrochemical Performance of Graphene as Effected by Electrode Porosity and Graphene Functionalization.* Electroanalysis, 2010. **22**(23): p. 2834-2841.

354. P.L. Taberna, C. Portet, and P. Simon, *Electrode surface treatment and electrochemical impedance spectroscopy study on carbon/carbon supercapacitors.* Applied Physics a-Materials Science & Processing, 2006. **82**(4): p. 639-646.
355. A. Balducci, W.A. Henderson, M. Mastragostino, S. Passerini, P. Simon, and F. Soavi, *Cycling stability of a hybrid activated carbon//poly(3-methylthiophene) supercapacitor with N-butyl-N-methylpyrrolidinium bis(trifluoromethanesulfonyl)imide ionic liquid as electrolyte.* Electrochimica Acta, 2005. **50**(11): p. 2233-2237.
356. Y. Chen, X.O. Zhang, D.C. Zhang, P. Yu, and Y.W. Ma, *High performance supercapacitors based on reduced graphene oxide in aqueous and ionic liquid electrolytes.* Carbon, 2011. **49**(2): p. 573-580.
357. M.D. Stoller, S.J. Park, Y.W. Zhu, J.H. An, and R.S. Ruoff, *Graphene-Based Ultracapacitors.* Nano Letters, 2008. **8**(10): p. 3498-3502.